

# Indirect Signatures of Gravitino Dark Matter in Models with $R$ -Parity Violation

**Diplomarbeit**

David Tran  
DESY, Theory Group

Universität Hamburg  
Juni 2008

# Contents

<b>1</b>	<b>Introduction</b>	<b>1</b>
<b>2</b>	<b>Supersymmetry, Supergravity and the Gravitino</b>	<b>3</b>
2.1	Supersymmetry . . . . .	3
2.1.1	Motivations for Supersymmetry . . . . .	3
2.1.2	The Supersymmetry Algebra . . . . .	4
2.1.3	Chiral and Vector Superfields . . . . .	5
2.1.4	Constructing Supersymmetric Theories . . . . .	6
2.1.5	Soft Supersymmetry Breaking . . . . .	8
2.2	The Minimal Supersymmetric Standard Model . . . . .	8
2.2.1	Specifying the MSSM . . . . .	9
2.2.2	Electroweak Symmetry Breaking and Sparticle Mixing . . . . .	10
2.3	Supergravity and the Gravitino . . . . .	11
2.3.1	Supergravity . . . . .	11
2.3.2	Supersymmetry Breaking and the Super-Higgs Mechanism . . . . .	12
2.3.3	The Massive Gravitino Field . . . . .	13
<b>3</b>	<b>Gravitino Cosmology</b>	<b>15</b>
3.1	Basic Concepts of Cosmology . . . . .	15
3.2	Thermal Leptogenesis . . . . .	17
3.2.1	The Seesaw Mechanism . . . . .	18
3.2.2	Generation of the CP Asymmetry . . . . .	19
3.2.3	Relating Lepton Asymmetry and Baryon Asymmetry . . . . .	20
3.2.4	Bounds on Neutrino Masses from Leptogenesis . . . . .	22
3.3	Thermal Production of Gravitinos . . . . .	23
3.4	The Gravitino Problem . . . . .	24
3.4.1	Constraints from Overclosure . . . . .	24
3.4.2	Constraints from Big Bang Nucleosynthesis . . . . .	24
3.4.3	Possible Solutions to the Gravitino Problem . . . . .	25
<b>4</b>	<b><math>R</math>-Parity Violation</b>	<b>27</b>
4.1	$R$ -Invariance and $R$ -Parity . . . . .	27
4.2	Gaugino-Lepton Mixing via $R$ -parity Violation . . . . .	29
4.3	Cosmological Implications . . . . .	30
4.3.1	Primordial Nucleosynthesis . . . . .	30
4.3.2	Baryogenesis without $R$ -Parity . . . . .	30

4.3.3	Gravitino Dark Matter with Broken $R$ -Parity . . . . .	31
4.4	A Model for $R$ -Parity Violation . . . . .	32
<b>5</b>	<b>The Source Term for Gravitino Decay Products</b>	<b>36</b>
5.1	Distribution of Dark Matter in the Galaxy . . . . .	37
5.2	Decay Rates and Branching Ratios . . . . .	38
5.3	Energy Spectra from Fragmentation . . . . .	43
<b>6</b>	<b>Gamma Rays from Gravitino Dark Matter Decay</b>	<b>47</b>
6.1	The Diffuse Extragalactic Gamma-Ray Spectrum . . . . .	47
6.2	Gamma Rays from Gravitino Dark Matter . . . . .	48
6.3	Experimental Prospects . . . . .	54
<b>7</b>	<b>Propagation of Charged Particles in the Galaxy</b>	<b>55</b>
7.1	Lessons from Observations of Cosmic Rays . . . . .	55
7.2	The Diffusion Model . . . . .	55
7.3	Determination of the Propagation Model Parameters . . . . .	57
7.4	Solar Modulation . . . . .	58
<b>8</b>	<b>Positrons from Gravitino Dark Matter Decay</b>	<b>60</b>
8.1	The Experimental Status . . . . .	60
8.2	Solution of the Transport Equation . . . . .	61
8.3	Positrons from Gravitino Decay . . . . .	63
8.4	Experimental Prospects . . . . .	67
<b>9</b>	<b>Antiprotons from Gravitino Dark Matter Decay</b>	<b>68</b>
9.1	The Experimental Status . . . . .	68
9.2	Solution of the Transport Equation . . . . .	68
9.3	Antiprotons from Gravitino Decay . . . . .	71
<b>10</b>	<b>Conclusions and Outlook</b>	<b>75</b>
<b>A</b>	<b>Calculation of Gravitino Decay Rates</b>	<b>77</b>
<b>B</b>	<b>Derivation of the Gamma-Ray Flux Equations</b>	<b>80</b>
B.1	The Halo Contribution . . . . .	80
B.2	The Extragalactic Contribution . . . . .	81
<b>C</b>	<b>Solution of the Transport Equation</b>	<b>84</b>
C.1	Solution for Positrons . . . . .	84
C.2	Solution for Antiprotons . . . . .	86

## Abstract

The scenario of gravitino dark matter in supersymmetric theories with broken  $R$ -parity is investigated. After arguing that this scenario is strongly favored in the combined picture of thermal leptogenesis, Big Bang nucleosynthesis and supersymmetric dark matter, the possible signatures for indirect detection of gravitino dark matter in the spectra of extragalactic gamma rays, as well as cosmic-ray positrons and antiprotons are calculated. We show that the late-time decay of gravitino dark matter with a mass of  $\sim 150$  GeV and a lifetime of  $\sim 10^{26}$  s, or late-decaying dark matter generally, may provide a simultaneous qualitative explanation for cosmic-ray anomalies in the diffuse extragalactic gamma-ray spectrum and the positron fraction, whose origin is presently unclear. At the same time, we find that the accompanying antiproton flux tends to be too large, although it may be compatible with observations for certain sets of propagation parameters.

## Zusammenfassung

Das Szenario dunkler Materie in Form von Gravitinos in supersymmetrischen Theorien mit verletzter  $R$ -Parität wird untersucht. Nachdem argumentiert wurde, dass dieses Szenario im kombinierten Bild von thermischer Leptogenese, primordialer Nukleosynthese und supersymmetrischer dunkler Materie stark bevorzugt ist, werden die möglichen Signaturen für den indirekten Nachweis von dunkler Gravitino-Materie berechnet. Wir zeigen, daß der Zerfall von dunkler Gravitino-Materie mit einer Masse von  $\sim 150$  GeV und einer Lebensdauer von  $\sim 10^{26}$  s, oder allgemeiner der Zerfall von dunkler Materie zu späten kosmologischen Zeiten, eine simultane qualitative Erklärung zweier Anomalien in der kosmischen Strahlung, nämlich in der diffusen extragalaktischen Gamma-Strahlung und in der Positronen-Fraktion, liefern kann, deren Ursprung derzeit ungeklärt ist. Auf der anderen Seite wird gezeigt, dass der zugleich resultierende Fluß von kosmischen Antiprotonen tendenziell zu hoch ist, obwohl er für bestimmte Werte der Propagationsparameter kompatibel mit den Beobachtungen sein könnte.

# Chapter 1

## Introduction

There is massive evidence from various kinds of observations, ranging from the dynamics of galactic clusters over rotation curves of spiral galaxies, gravitational lensing, measurements of the cosmic microwave background (CMB) anisotropies to simulations of structure formation and more, implying that most of the matter in the Universe is in the form of non-luminous, so-called dark matter [1, 2]. While its existence is almost conclusively proven, the nature of this elusive dark matter is still a mystery and has been one of the outstanding puzzles in cosmology and astrophysics for a long time. Since no particle in the Standard Model of particle physics can account for the observed dark matter density, the astronomical observations provide impressive evidence for physics beyond the Standard Model. There are many viable non-Standard Model candidates for the dark matter of the Universe, of which supersymmetry provides some of the most interesting examples. In this thesis, one particularly intriguing dark matter candidate is studied in detail, namely the gravitino in  $R$ -parity breaking vacua. This scenario is motivated by an apparent conflict between three paradigms that are separately very attractive and well-motivated, namely thermal leptogenesis, standard Big Bang nucleosynthesis and supersymmetric dark matter. Gravitino dark matter together with a small violation of  $R$ -parity provides an attractive way to reconcile these paradigms while retaining all their virtues [3].

The gravitino is a hypothetical particle that arises in theories with local supersymmetry, so-called supergravity theories. It has all the right properties for a dark matter particle, being non-baryonic, electrically neutral, colorless and cold (i.e. non-relativistic at the time of structure formation). In fact, the gravitino was the first supersymmetric particle proposed as a dark matter candidate [4]. Due to its extremely weak interactions with the Standard Model particles, the gravitino mass can lie in a wide range without conflicting with any experimental bounds. This also means that the gravitino interacts far too weakly with Standard Model particles to be accessible in direct detection experiments. However, if the gravitino is unstable, as would be the case if  $R$ -parity is broken, its decay products might be detectable in present and future experiments. This opens the possibility of indirect detection of gravitino dark matter. Indeed, as we show in this thesis, the decay of gravitino dark matter can lead to striking signatures and may naturally account for anomalous excesses observed in both the diffuse extragalactic gamma-ray spectrum and the positron fraction in cosmic-ray measurements.

This thesis is organized as follows. We first present a brief introduction to supersym-

metry and supergravity, as well as a summary of some important facts about the gravitino. A review of some relevant concepts of gravitino cosmology follows, including a discussion of the baryogenesis scenario of thermal leptogenesis and its implications for dark matter. The so-called gravitino problem of cosmology is discussed, which essentially consists of conflicting bounds on the reheating temperature after inflation stemming from thermal leptogenesis on the one side and primordial nucleosynthesis with supersymmetric dark matter on the other side. We explain why the scenario of gravitino dark matter in combination with a small violation of  $R$ -parity can resolve this conflict between supersymmetric dark matter, primordial nucleosynthesis and leptogenesis. An introduction to  $R$ -parity violation is given, including an exposition of a sample model that can yield the required small couplings and gravitino dark matter. Following this exposition, in the main part of the thesis we investigate the astrophysical signatures of having an unstable gravitino as the dominant component of the dark matter. The source term for possible decay products of gravitino dark matter is presented. We then calculate the gamma-ray spectrum from gravitino decay. After that, we discuss a model for propagation of charged particles in the Galaxy that allows for semi-analytical solutions. The antimatter signatures of gravitino decay in the positron and antiproton spectra are then computed. Some calculations that are too unwieldy for the main text have been relegated to the appendices, namely the calculation of gravitino decay rates, the derivation of the gamma-ray flux equations and the solution of the transport equation for the positrons and antiprotons. Results presented in this thesis have already been published in [5, 6].

## Chapter 2

# Supersymmetry, Supergravity and the Gravitino

One of the most popular extensions of physics beyond the Standard Model is supersymmetry (SUSY). This hypothetical spacetime symmetry relates particles of different spin and thus provides a unifying link between fermions and bosons. The local version of supersymmetry automatically includes gravity and is therefore known as supergravity. The gauge field of local supersymmetry transformations, the gravitino, will be our dark matter candidate of choice. In this chapter, we first discuss the basics of global supersymmetry and the minimal supersymmetric Standard Model, which is the common basis of all realistic supersymmetric particle physics models, roughly following [7]. After that, we briefly summarize some basic ideas of supergravity and interesting properties of the gravitino.

## 2.1 Supersymmetry

### 2.1.1 Motivations for Supersymmetry

There are many good reasons to believe that supersymmetry may be realized in Nature. Apart from the purely conceptual appeal, there are convincing practical reasons. Supersymmetry is an integral part of string theory, where it is required for consistency of the theory. Furthermore, one can show that supersymmetry is the only possible extension of the Lorentz symmetries of the  $S$ -matrix of an interacting relativistic quantum field theory. The theoretical prejudice is that it would be strange if Nature stopped one step short of the maximally allowed symmetry. On a more pedestrian level, supersymmetry provides a solution to the hierarchy problem in the Standard Model, as the new symmetry adds additional interactions that cancel the quadratically divergent radiative corrections to scalar masses. This is the main motivation for introducing weak-scale supersymmetry. In addition, the different gauge couplings seem to unify at a very high energy scale, the grand unification scale  $M_X = 2 \times 10^{16}$  GeV, in the supersymmetric extension of the Standard Model if one assumes that superpartner masses lie at the TeV scale. The most interesting feature for the present discussion is that supersymmetry naturally provides an excellent dark matter candidate, namely the lightest supersymmetric particle (LSP). Despite all these virtues, no direct experimental evidence for supersymmetry has been found to date. However, it is hoped that this situation will change in the near future with the commissioning of the Large Hadron Collider (LHC).

### 2.1.2 The Supersymmetry Algebra

Supersymmetry generalizes the conventional Poincaré algebra of relativistic spacetime symmetries to include transformations that relate particles of different spin. The Coleman-Mandula theorem is evaded by including anticommutators in addition to commutators in the algebra. The famous supersymmetry algebra is

$$\{Q_\alpha, \bar{Q}_{\dot{\beta}}\} = 2\sigma_{\alpha\dot{\beta}}^\mu P_\mu, \quad (2.1)$$

$$\{Q_\alpha, Q_\beta\} = \{\bar{Q}_{\dot{\alpha}}, \bar{Q}_{\dot{\beta}}\} = 0, \quad (2.2)$$

$$[P_\mu, Q_\alpha] = [P_\mu, \bar{Q}_{\dot{\alpha}}] = 0. \quad (2.3)$$

The supersymmetry generators  $Q_\alpha$  are two-component Weyl spinors carrying the spinor indices  $\alpha, \beta$  and  $\dot{\alpha}, \dot{\beta}$ . The  $\sigma^\mu$  denote the Pauli matrices, and  $P_\mu$  is the four-momentum operator. Since the anticommutator of the supersymmetry algebra is proportional to the momentum operator, supersymmetry must be a spacetime symmetry. In principle, one could have more than only one supersymmetry generator. However, we are regarding only theories with one supercharge, since the low-energy theory can be  $N = 1$  supersymmetric at most as extended supersymmetries can not accommodate chiral fermions. It is noteworthy that the squared momentum operator  $P^2$  commutes with the supersymmetry generators, implying that particles and their superpartners in the same multiplet must have the same mass. Since this mass degeneracy is not even approximately observed, supersymmetry, if it is realized in Nature, must be a badly broken symmetry.

The supersymmetry algebra can be rewritten purely in terms of commutators if one introduces infinitesimal anticommuting Grassman variables  $\xi, \eta$  which satisfy  $\xi\bar{\eta} = -\bar{\eta}\xi$ . Eq. (2.1) then becomes

$$[\xi Q_\alpha, \bar{\eta} \bar{Q}_{\dot{\beta}}] = 2\xi\sigma_{\alpha\dot{\beta}}^\mu \bar{\eta} P_\mu. \quad (2.4)$$

The supersymmetry generators can be explicitly expressed in terms of derivatives as

$$Q_\alpha = \frac{\partial}{\partial\theta^\alpha} - i\sigma_{\alpha\dot{\beta}}^\mu \bar{\theta}^{\dot{\beta}} \partial_\mu, \quad (2.5)$$

$$\bar{Q}_{\dot{\alpha}} = -\frac{\partial}{\partial\bar{\theta}^{\dot{\alpha}}} + i\sigma_{\beta\dot{\alpha}}^\mu \theta^\beta \partial_\mu, \quad (2.6)$$

It is also useful to introduce the supercovariant derivatives

$$D_\alpha = \frac{\partial}{\partial\theta^\alpha} + i\sigma_{\alpha\dot{\beta}}^\mu \bar{\theta}^{\dot{\beta}} \partial_\mu, \quad (2.7)$$

$$\bar{D}_{\dot{\alpha}} = -\frac{\partial}{\partial\bar{\theta}^{\dot{\alpha}}} - i\sigma_{\beta\dot{\alpha}}^\mu \theta^\beta \partial_\mu, \quad (2.8)$$

which anticommute with the supersymmetry operators. One can give a geometric interpretation to the supersymmetry transformations by employing the superspace formalism. Superspace coordinates  $z = (x_\mu, \theta, \bar{\theta})$  contain both conventional four-dimensional spacetime coordinates and two anticommuting fermionic Grassmann coordinates  $\theta, \bar{\theta}$  which satisfy

$$\{\theta, \theta\} = \{\theta, \bar{\theta}\} = \{\bar{\theta}, \bar{\theta}\} = 0. \quad (2.9)$$

Supersymmetry transformations then generate translations in superspace. Fields on superspace are, of course, called superfields, in line with the rest of the super-nomenclature. One can understand superfields in terms of power series expansions in the anticommuting Grassmann variables as the coefficients of component fields on ordinary spacetime. These expansions terminate after the quadratic term due to  $\theta\theta\theta = \bar{\theta}\bar{\theta}\bar{\theta} = 0$ . The most general expansion of a superfield in terms of the Grassmann parameters is given by

$$F(x, \theta, \bar{\theta}) = f(x) + \theta\phi(x) + \bar{\theta}\bar{\xi}(x) + \theta\theta m(x) + \bar{\theta}\bar{\theta}n(x) + \theta\sigma^\mu\bar{\theta}v_\mu(x) + \theta\theta\bar{\theta}\bar{\lambda}(x) + \bar{\theta}\bar{\theta}\theta\psi(x) + \theta\theta\bar{\theta}\bar{\theta}d(x), \quad (2.10)$$

where all the different components will be related by the actions of the generators  $Q, \bar{Q}$ . We will now examine two special kinds of superfields which will be used to describe matter and gauge fields and are therefore called chiral and vector superfields, respectively.

### 2.1.3 Chiral and Vector Superfields

When working out the representation theory of the supersymmetry algebra, one finds that the simplest irreducible representations are given by chiral and vector superfields. These have the right particle content to describe matter and gauge fields, as well as their respective superpartners.

Left-chiral superfields are defined by the property of being annihilated by the supercovariant derivatives,

$$\bar{D}_{\dot{\alpha}}\Phi(x, \theta, \bar{\theta}) = 0. \quad (2.11)$$

Correspondingly, right-chiral superfields are characterized by the conjugate condition

$$D_{\alpha}\Phi^{\dagger}(x, \theta, \bar{\theta}) = 0. \quad (2.12)$$

The expansion of a left-chiral superfield in component fields is, with  $y^\mu = x^\mu + i\theta\sigma^\mu\bar{\theta}$ ,

$$\begin{aligned} \Phi(x, \theta, \bar{\theta}) &= \phi(x)\sqrt{2}\theta\psi(y) + \theta\theta F(y) \\ &= \phi(x) + \sqrt{2}\theta\psi(x) + \theta\theta F(x) - i\theta\sigma^\mu\bar{\theta}\partial_\mu\phi(x) - \frac{1}{\sqrt{2}}i\theta\theta\bar{\theta}\bar{\sigma}^\mu\partial_\mu\psi(x) \\ &\quad + \frac{1}{4}\theta\theta\bar{\theta}\bar{\theta}\square\phi(x). \end{aligned} \quad (2.13)$$

A chiral superfield contains a complex scalar  $\phi$ , a Weyl fermion  $\psi$  and an auxiliary complex scalar field  $F$ . The individual component fields of a chiral superfield transform under an infinitesimal supersymmetry transformation as

$$\begin{aligned} \delta_\xi\phi &= \sqrt{2}\xi\psi, \\ \delta_\xi\psi &= \sqrt{2}\xi F + i\sqrt{2}\sigma^\mu\bar{\xi}\partial_\mu\phi, \\ \delta_\xi F &= -i\sqrt{2}\partial_\mu\psi\sigma^\mu\bar{\xi}. \end{aligned} \quad (2.14)$$

A supersymmetry transformation therefore maps a scalar into a spinor, a spinor into a scalar and the  $F$ -term into a total derivative. Products of chiral superfields are also chiral superfields, however the product  $\Phi^\dagger\Phi$  is not. However, this combination represents another important

type of superfield, the vector superfield.

In addition to the matter fields contained in chiral multiplets, we also need gauge fields, which will be part of the vector multiplets. Vector superfields are characterized by the reality condition

$$V^\dagger(x, \theta, \bar{\theta}) = V(x, \theta, \bar{\theta}). \quad (2.15)$$

The Taylor expansion of vector superfields is given by

$$\begin{aligned} V(x, \theta, \bar{\theta}) = & C(x) + i\theta\chi(x) - i\bar{\theta}\bar{\chi}(x) + \frac{i}{2}\theta\theta(M(x) + iN(x)) \\ & - \frac{i}{2}\bar{\theta}\bar{\theta}(M(x) - iN(x)) - \theta\sigma^\mu\bar{\theta}v_\mu(x) + i\theta\theta\bar{\theta}\left(\bar{\lambda}(x) + \frac{i}{2}\bar{\sigma}^\mu\partial_\mu\chi(x)\right) \\ & - i\bar{\theta}\bar{\theta}\bar{\theta}\left(\lambda(x) + \frac{i}{2}\bar{\sigma}^\mu\partial_\mu\bar{\chi}(x)\right) + \frac{1}{2}\theta\theta\bar{\theta}\bar{\theta}\left(D(x) + \frac{1}{2}\square C(x)\right). \end{aligned} \quad (2.16)$$

$C$ ,  $D$ ,  $M$  and  $N$  are real scalars,  $\chi$  and  $\lambda$  are Weyl spinors and  $v^\mu$  is a vector field. This expansion is rather bulky, but one can eliminate many unphysical degrees of freedom by choosing Wess-Zumino gauge, which allows us to set

$$\chi(x) = C(x) = M(x) = N(x) = 0. \quad (2.17)$$

This corresponds to a partial gauge fixing that still allows for the usual gauge transformations. We will not list the transformation properties of all components of a vector multiplet. However, we note that the highest component of a vector multiplet transforms under an infinitesimal supersymmetry transformation into a total derivative,

$$\delta_\xi D = \xi\sigma^\mu\partial_\mu\bar{\lambda} + \bar{\xi}\bar{\sigma}^\mu\partial_\mu\lambda. \quad (2.18)$$

This will prove crucial to the construction of supersymmetric Lagrangians.

### 2.1.4 Constructing Supersymmetric Theories

We now want to use the superfields discussed above to construct actions that are invariant under supersymmetry transformations,

$$\delta_\xi \left( \int d^4x \mathcal{L}(x) \right) = 0. \quad (2.19)$$

We have seen that the highest components of the supermultiplets, the  $D$ - and  $F$ -terms, respectively, transform as total derivatives. Using this fact, we can construct a Lagrangian from these components, writing schematically

$$\mathcal{L} = \mathcal{L}_D + \mathcal{L}_F. \quad (2.20)$$

We use the Berezin rules of integration over Grassman variables,

$$\int d\theta_\alpha = 0, \quad \int \theta_\alpha d\theta_\beta = \delta_{\alpha\beta}, \quad (2.21)$$

to express invariant Lagrangians as an integration of chiral and vector superfields over the anticommuting superspace coordinates, leaving us with the  $F$ -terms from the chiral superfields and the  $D$ -terms from vector superfields. We can therefore use these to construct invariant actions. The most general renormalizable supersymmetric Lagrangian with canonical kinetic terms containing only chiral superfields is

$$\mathcal{L} = \sum_i \int d^2\theta d^2\bar{\theta} \Phi_i^\dagger \Phi_i + \left[ \int d^2\theta W(\Phi_i) + \text{h.c.} \right]. \quad (2.22)$$

We have introduced the superpotential  $W$ , which is a holomorphic function of any number of chiral superfields. The most general form of the superpotential allowed by renormalizability and gauge-invariance is

$$W = L^i \Phi_i + \frac{1}{2} M^{ij} \Phi_i \Phi_j + \frac{1}{6} y^{ijk} \Phi_i \Phi_j \Phi_k, \quad (2.23)$$

where renormalizability demands that no terms higher than cubic terms appear, and supersymmetry requires the superpotential to be holomorphic. The first term is of course only gauge-invariant for a singlet field. We can now expand the general Lagrangian in terms of component fields,

$$\begin{aligned} \mathcal{L} &= \sum_i \int d^2\theta d^2\bar{\theta} \Phi_i \Phi_i^\dagger + \left[ \int d^2\theta W(\Phi_i) + \text{h.c.} \right] \\ &= \sum_i (F_i F_i^* + |\partial_\mu \phi|^2 - i\bar{\psi}_i \sigma_\mu \partial^\mu \psi_i) \\ &\quad + \left[ \sum_j \frac{\partial W(\phi_i)}{\partial \phi_j} F_j - \frac{1}{2} \sum_{j,k} \frac{\partial^2 W(\phi_i)}{\partial \phi_j \partial \phi_k} \psi_j \psi_k + \text{h.c.} \right]. \end{aligned} \quad (2.24)$$

We find no kinetic term for the fields  $F_i$ , which are therefore auxiliary fields with no dynamics. From their equation of motion, one finds

$$F_j = - \left[ \frac{\partial W(\phi_i)}{\partial \phi_j} \right]^*. \quad (2.25)$$

The coupling between matter and gauge fields is achieved by the minimal prescription

$$\int d^2\theta d^2\bar{\theta} \Phi^\dagger \Phi \rightarrow \int d^2\theta d^2\bar{\theta} \Phi^\dagger e^{2gV} \Phi, \quad (2.26)$$

for which in Wess-Zumino gauge we get the component-field expression

$$\int d^2\theta d^2\bar{\theta} \Phi^\dagger e^{2gV} \Phi = |D_\mu \phi|^2 - i\bar{\psi} \sigma_\mu D^\mu \psi + g\phi^* D_\alpha T^a \phi + ig\sqrt{2} (\phi^* \lambda \psi - \bar{\lambda} \bar{\psi} \phi) + |F|^2, \quad (2.27)$$

where  $D_\mu = \partial_\mu + igA_\mu^a T_a$  is the usual gauge-covariant derivative. We still need kinetic terms for the gauge fields. We can form a chiral superfield  $W_\alpha$  from the combination

$$W_\alpha = \bar{D} \bar{D} e^{-gV} D_\alpha e^{gV}, \quad (2.28)$$

where the  $\bar{D}$  are supercovariant derivatives. The product  $W_\alpha W^\alpha$  is a gauge-invariant left-chiral superfield, so its  $F$ -term may constitute a part of the Lagrangian,

$$\begin{aligned} \frac{1}{32g^2} W_\alpha W^\alpha &= -\frac{1}{4} F_{\mu\nu}^a F_a^{\mu\nu} + \frac{1}{2} D_a D^a \\ &+ \left( -\frac{i}{2} \lambda^a \sigma_\mu \partial^\mu \bar{\lambda}_a + \frac{1}{2} g f^{abc} \lambda_a \sigma_\mu A_b^\mu \bar{\lambda}_c + \text{h.c.} \right). \end{aligned} \quad (2.29)$$

This gives us the familiar kinetic term for the gauge fields as well as a kinetic term for the gauginos and a gaugino-gauge field coupling that is fixed by the structure constants  $f^{abc}$  of the gauge group. There is no kinetic term for the  $D_a$  fields, which are therefore also auxiliary fields that can be integrated out using their equation of motion, yielding

$$D_a = -g \sum_{i,j} \phi_i^* T_a^{ij} \phi_j. \quad (2.30)$$

Together with the third term on the right-hand side of Eq.(2.27), we get the following  $D$ -term contribution to the scalar potential:

$$-V_D = -\frac{1}{2} \sum_a \left| \sum_{i,j} g \phi_i^* T_{ij}^a \phi_j \right|^2. \quad (2.31)$$

This gives us all the pieces we need to construct Lagrangians for supersymmetric theories.

### 2.1.5 Soft Supersymmetry Breaking

We already know that supersymmetry must be a broken symmetry. While we do not know the mechanism by which supersymmetry is broken, we can simply accept the fact that it is broken and cast the effect of this breaking in the form of additional mass terms which are added to the supersymmetric Lagrangian. These mass terms break supersymmetry explicitly, but in a way that still allows the quadratic divergences to cancel. For this reason, they are called soft mass terms. The most general soft mass terms allowed include gaugino mass terms, scalar mass terms and scalar quadratic and trilinear terms. The general form of the soft terms is therefore given by

$$\mathcal{L}_{\text{soft}} = - \left( \frac{1}{2} M_a \lambda^a \lambda^a + \frac{1}{6} a^{ijk} \phi_i \phi_j \phi_k + \frac{1}{2} b^{ij} \phi_i \phi_j + t^i \phi_i \right) + \text{c.c.} - (m^2)_i^j \phi^j \phi_i^*. \quad (2.32)$$

In summary, we find that a softly broken supersymmetric theory can be specified by the gauge group, superpotential and soft mass terms. We will illustrate this for the minimal supersymmetric Standard Model.

## 2.2 The Minimal Supersymmetric Standard Model

Realistic supersymmetric particle physics models certainly have to include at least the Standard Model field content. The most economic supersymmetric theory that contains the Standard Model as a subset is the Minimal Supersymmetric Standard Model (MSSM). We take the MSSM as a direct application of the basic concepts of supersymmetry discussed so far.

### 2.2.1 Specifying the MSSM

The gauge group of the MSSM is of course the same as in the Standard Model,  $SU(3)_C \times SU(2)_L \times U(1)_Y$ , where the subscripts denote color, left chirality and weak hypercharge, respectively. To supersymmetrize the model, we need to introduce for each Standard Model fermion a chiral superfield and for each gauge field a vector superfield. The matter fields of the MSSM are given by  $Q$ , which contains the (s)quark doublets,  $U^c$  and  $D^c$  the (s)quark singlets,  $L$  the (s)lepton doublets and  $E^c$  the (s)lepton singlets. Each of these superfields comes in three generations. For the gauge part, one has to introduce eight gluinos  $\tilde{g}$ , three Winos  $\tilde{W}$  and a Bino  $\tilde{B}$ . In addition, one needs at least two Higgs doublets, denoted by  $H_u$  with hypercharge  $Y = 1/2$  and  $H_d$  with hypercharge  $Y = -1/2$ , as a single Higgs doublet introduces gauge anomalies that have to be canceled by another Higgs doublet with opposite hypercharge.

In terms of the matter superfields given above, the MSSM superpotential is chosen as

$$W_{\text{MSSM}} = \mu H_u H_d + \lambda_{ij}^e H_d L_i E_j^c + \lambda_{ij}^d H_d Q_i D_j^c - \lambda_{ij}^u H_u Q_i U_j^c. \quad (2.33)$$

The generation indices  $i$  and  $j$  are summed over, and contractions over gauge indices are understood. Gauge invariance restricts the form of the superpotential, but does not completely fix it. There are additional renormalizable terms that are allowed by gauge invariance, and which could thus in principle be part of the superpotential. These terms violate lepton and baryon number, however, leading to problems such as rapid proton decay. To avoid these difficulties from the beginning, as well as to keep the possible interactions to a minimum, in the MSSM the conservation of a discrete symmetry called  $R$ -parity is imposed on the superpotential. It is a multiplicative symmetry, where  $R$ -parity, or  $R_p$ , is assigned to the various component fields according to

$$R_p = (-1)^{3B-L+2S}, \quad (2.34)$$

where  $B$ ,  $L$  and  $S$  denote baryon number, lepton number, and spin, respectively. This way, Standard Model particles are assigned  $R$ -parity  $+1$  and their superpartners  $R$ -parity  $-1$ . Imposing conservation of this symmetry has the immediate consequence that baryon number and lepton number are conserved at tree level, and that supersymmetric particles can only be produced in pairs. It also means that the lightest supersymmetric particle is absolutely stable, which yields an excellent dark matter candidate in supersymmetric theories: the lightest supersymmetric particle, which may very well constitute the dark matter if it is color- and electrically neutral.

We will return to the issue of  $R$ -parity and its role for dark matter in more detail in 4. We will just note here that demanding  $R$ -parity conservation is an ad hoc procedure, and that exact conservation of  $R$ -parity may be an excessive measure, since e.g. forbidding only either lepton number violation or baryon number violation is also sufficient to prevent rapid proton decay.

In order to account for supersymmetry breaking, we have to introduce the following soft

mass terms in the MSSM:

$$\begin{aligned}
 -\mathcal{L}_{\text{soft}} = & m_{\tilde{q}}^2 |\tilde{q}_L|^2 + m_{\tilde{u}}^2 |\tilde{u}_R^c|^2 + m_{\tilde{d}}^2 |\tilde{d}_R^c|^2 + m_{\tilde{l}}^2 |\tilde{l}_L|^2 + m_{\tilde{e}}^2 |\tilde{e}_R^c|^2 \\
 & + \left( \lambda_e A_e H_d \tilde{l}_L \tilde{e}_R^c + \lambda_d A_d H_d \tilde{q}_L \tilde{d}_R^c + \lambda_u A_u H_u \tilde{q}_L \tilde{u}_R^c + B\mu H_d H_u + \text{h.c.} \right) \\
 & + m_{H_u}^2 |H_u|^2 + m_{H_d}^2 |H_d|^2 + \frac{1}{2} M_1 \tilde{B} \tilde{B} + \frac{1}{2} M_2 \tilde{W} \tilde{W} + \frac{1}{2} M_3 \tilde{g} \tilde{g}, \quad (2.35)
 \end{aligned}$$

which determine the supersymmetric particle spectrum. The soft masses introduce a huge number of free parameters into the theory, over a hundred total, which limits its predictivity considerably.

## 2.2.2 Electroweak Symmetry Breaking and Sparticle Mixing

We now regard only a single phenomenological aspect of the MSSM which will be of interest later, namely the mixing between gauginos and Higgsinos arising from electroweak symmetry breaking. The Higgs potential responsible for electroweak breaking in the MSSM is completely determined by the superpotential and the soft terms. After the Higgs fields acquire vacuum expectation values (VEVs), this will induce mixings between various particles. It is convenient to express quantities in terms of the ratio between the two Higgs VEVs, which we call

$$\tan \beta = \frac{\langle H_u^0 \rangle}{\langle H_d^0 \rangle} \equiv \frac{v_u}{v_d}. \quad (2.36)$$

The breakdown of  $SU(2) \times U(1)_Y \rightarrow SU(2) \times U(1)_{\text{em}}$  will cause particles with the same  $SU(3)_C \times U(1)_{\text{em}}$  quantum numbers to mix. Mixing of particles is indeed ubiquitous in supersymmetric models. Except for the gluinos, which are color octets and therefore do not mix with any other particles, none of the superpartners of the Standard Model particles will in general be mass eigenstates. In particular, we will be interested in a mixing between electroweak gauginos and Higgsinos, which will prove to be important later. After electroweak symmetry breaking, the Higgs VEV induces off-diagonal terms in the mass matrices via the interaction described by the second-to-last term in Eq. (2.27). The neutralino mass matrix,  $\mathcal{L}_{\text{mass}} = -\frac{1}{2} \psi^{0T} M_N \psi^0 + \text{h.c.}$ , in the  $\psi^0 = (\tilde{B}, \tilde{W}, \tilde{H}_u^0, \tilde{H}_d^0)$  basis is then given by

$$M_N = \begin{pmatrix} M_1 & 0 & -M_Z c_\beta s_W & M_Z s_\beta s_W \\ 0 & M_2 & M_Z c_\beta c_W & -M_Z s_\beta c_W \\ -M_Z c_\beta s_W & M_Z c_\beta c_W & 0 & -\mu \\ M_Z s_\beta s_W & -M_Z s_\beta c_W & -\mu & 0 \end{pmatrix} \quad (2.37)$$

$$= \begin{pmatrix} M_1 & 0 & -g' v_d / \sqrt{2} & g' v_u / \sqrt{2} \\ 0 & M_2 & g v_d / \sqrt{2} & g v_u / \sqrt{2} \\ -g' v_d / \sqrt{2} & g v_d / \sqrt{2} & 0 & -\mu \\ g' v_u / \sqrt{2} & -g v_u / \sqrt{2} & -\mu & 0 \end{pmatrix}, \quad (2.38)$$

where  $M_1$  and  $M_2$  are the  $U(1)_Y$  and  $SU(2)_L$  gaugino masses, and  $g, g'$  are the corresponding gauge couplings.  $c_W \equiv \cos \theta_W / s_W \equiv \sin \theta_W$  is the sine/cosine of the weak mixing angle  $\theta_W$  and  $c_\beta \equiv \cos \beta$ ,  $s_\beta = \sin \beta$ . The mass eigenstates of the mass matrix are called neutralinos and denoted by  $\chi_i^0$ . The lightest neutralino  $\chi_1^0$  is usually taken to be the lightest supersymmetric particle and is the most widely studied dark matter candidate.

In the charged sector, we find an analogous mixing. The chargino mass matrix  $\mathcal{L}_{\text{mass}} = \psi^{-T} M_C \psi^+ + \text{h.c.}$  in the basis  $\psi^- = (\widetilde{W}^-, \widetilde{H}_d^-)$ ,  $\psi^+ = (\widetilde{W}^+, \widetilde{H}_u^+)$  is

$$M_C = \begin{pmatrix} M_2 & \sqrt{2} M_W s_\beta \\ \sqrt{2} M_W c_\beta & \mu \end{pmatrix} \quad (2.39)$$

$$= \begin{pmatrix} M_2 & g v_u \\ g v_d & \mu \end{pmatrix}. \quad (2.40)$$

This mass matrix will not be symmetric unless  $\tan \beta = 1$ . The mass eigenstates of the mass matrix are called charginos, which will be mixtures of the charged gauginos and charged Higgsinos. This wraps up our rather sketchy discussion of the MSSM. We now turn to the local version of supersymmetry, supergravity.

## 2.3 Supergravity and the Gravitino

### 2.3.1 Supergravity

If we want supersymmetry to play a fundamental physical role and not just be an accidental global symmetry, it should be a spontaneously broken local symmetry. One therefore promotes the rigid supersymmetry transformations (2.4) to local, spacetime-dependent transformations,

$$\xi, \eta \rightarrow \xi(x), \eta(x). \quad (2.41)$$

Since the supersymmetry algebra involves the four-momentum operator, these transformations will correspond to general coordinate transformations. Invariance under such coordinate transformations is the hallmark of gravity theories. One is thus led from flat to curved superspace and supergravity as a generalization of General Relativity. The technical details of supergravity are way beyond the scope of this thesis (and my intellectual Hubble radius, for that matter), so we just summarize some supergravity factoids here.

Theories with local supersymmetry necessarily include gravity and predict the existence of the gravitino  $\psi_\mu$ , the superpartner of the graviton in the supergravity multiplet. The gravitino is the gauge field of local supersymmetry transformations. It is a spin-3/2 Majorana vector-spinor that couples to the Noether current associated with the gauged supersymmetry transformations. Since the gravitational coupling constant has mass-dimension  $-2$ , supergravity is a manifestly non-renormalizable theory. Gravitino interactions involve higher-order operators suppressed by powers of the reduced Planck mass

$$M_{\text{P}} \equiv \frac{1}{\sqrt{8\pi G}} = 2.4 \times 10^{18} \text{ GeV}, \quad (2.42)$$

where  $G$  is Newton's constant. Thus, the gravitino interactions are extremely weak. As the graviton's superpartner, the gravitino is massless as long as supersymmetry is unbroken. We can expect that the spontaneous breaking of local supersymmetry is accompanied by a Nambu-Goldstone fermion, the Goldstino. Once supersymmetry gets spontaneously broken, the gravitino absorbs the spin-1/2 Goldstino, thereby acquiring a mass via the super-Higgs mechanism and absorbing the helicity  $\pm 1/2$  components of the Goldstino as well as the Gold-

stino interactions.

For phenomenological studies, one can simply take the four-dimensional  $N = 1$  supergravity Lagrangian as the starting point. The full Lagrangian for supergravity coupled to chiral matter and Yang-Mills fields is rather long and will not be reproduced here for budgetary reasons. It can be found e.g. in [8]. Interestingly enough, one finds that the supergravity Lagrangian depends on only two (arbitrary) functions, the Kähler function  $G$  and the gauge kinetic function  $f_{ab}$ . The Kähler function is defined as

$$G(\phi^*, \phi) = \frac{K(\phi^*, \phi)}{M_{\text{P}}^2} + \ln \frac{|W(\phi)|^2}{M_{\text{P}}^6}. \quad (2.43)$$

It is a real function of the real, gauge-invariant Kähler potential  $K$  and the analytic superpotential  $W$ . We denote differentiation of the Kähler function with respect to the scalar fields by

$$G_i \equiv \frac{\partial G}{\partial \phi_i}, \quad G_{ij^*} \equiv \frac{\partial^2 G}{\partial \phi_i \partial \phi_j^*}. \quad (2.44)$$

### 2.3.2 Supersymmetry Breaking and the Super-Higgs Mechanism

It is believed that supersymmetry breaking originates in a hidden sector of fields that are Standard Model gauge singlets, where at least one field acquires a vacuum expectation value. The breaking is then communicated to the visible sector via gravitational or otherwise extremely weak interactions. The necessary condition for supersymmetry breaking is

$$\langle G_i \rangle \equiv \left\langle \frac{\partial G}{\partial \phi_i} \right\rangle \neq 0 \quad (2.45)$$

for some  $i$ , which reduces in the flat superspace limit  $M_{\text{P}} \rightarrow \infty$  to  $\langle \partial W / \partial \phi_i \rangle \neq 0$ , the condition for  $F$ -term breaking in global supersymmetry.

One finds that the only break supersymmetry spontaneously through a non-vanishing VEV in a Lorentz-invariant fashion are  $F$ -term breaking,

$$\langle \delta_\xi \chi^i \rangle \propto \langle F^i \rangle \xi \neq 0 \quad (2.46)$$

and/or  $D$ -term breaking,

$$\langle \delta_\xi \lambda^a \rangle \propto \langle D^a \rangle \xi \neq 0. \quad (2.47)$$

Once supersymmetry is spontaneously broken, the gravitino absorbs the Goldstino and becomes massive, in a manner analogous to the standard Higgs mechanism. For instance, in the case of a minimal Kähler potential  $K = \phi_i \phi^{*i}$  and pure  $F$ -term breaking, the possible mass terms from the part of the Lagrangian describing the fermionic fields  $\chi_i$  are given by [9]

$$e^{-1} \mathcal{L}_{\text{mass}} = \frac{i}{2} e^{G/2} \bar{\psi}_\mu \sigma^{\mu\nu} \psi_\nu + \frac{1}{\sqrt{2}} e^{G/2} G_i \bar{\psi}_\mu \gamma^\mu \chi_i - \frac{1}{2} e^{G/2} (G_{ij} + G_i G_j) \bar{\chi}^i \chi^j, \quad (2.48)$$

with  $M_{\text{P}} = 1$  here. We can identify

$$\eta = G_i \chi^i \quad (2.49)$$

as the Goldstone fermion. The second term then represents a mixing between Goldstino and gravitino. Upon a field redefinition

$$\psi'_\mu = \psi_\mu - \frac{i}{3\sqrt{2}}\gamma_\mu\eta - \frac{\sqrt{2}}{3}e^{-G/2}\partial_\mu\eta, \quad (2.50)$$

the mixing term is eliminated, and the gravitino acquires a mass

$$m_{3/2} = e^{G/2}M_{\text{P}} = e^{K/2M_{\text{P}}^2}\frac{|W|}{M_{\text{P}}^2}. \quad (2.51)$$

where we have restored units of  $M_{\text{P}}$ .

The gravitino mass is highly dependent on the mechanism of supersymmetry breaking. A number of viable mechanisms for spontaneous breaking of local supersymmetry have been proposed. Here we just list the most-discussed ones together with the corresponding gravitino masses: In gauge mediation, one expects gravitino masses of order 10 eV – 10 GeV while in gravity mediation, one gets gravitino masses of 100 GeV – 1 TeV. In anomaly mediation one would expect rather heavy gravitino masses of 10 TeV – 100 TeV, and in gaugino mediation one gets masses of 10 GeV – 100 GeV. Thus, the gravitino mass can vary over many orders of magnitude depending on the mechanism of supersymmetry breaking, altogether yielding masses in the range  $10 \text{ eV} < m_{3/2} < 100 \text{ TeV}$  in the most common scenarios.

We also note that the breaking of local supersymmetry can naturally generate universal soft terms, and that one can break supersymmetry with a vanishing vacuum energy, corresponding to a vanishing cosmological constant, which can be problematic in global supersymmetry, where the spontaneous symmetry breaking necessarily introduces a positive vacuum energy.

### 2.3.3 The Massive Gravitino Field

One can obtain the equations of motion for the massive gravitino field by variation of the action corresponding to the sum of the usual Einstein-Hilbert Lagrangian and the Rarita-Schwinger Lagrangian

$$\mathcal{L} = -\frac{1}{2M_{\text{P}}^2}\sqrt{-g}R - \frac{1}{2}\epsilon^{\mu\nu\rho\sigma}\bar{\psi}_\mu\gamma_5\gamma_\nu D_\rho\psi_\sigma, \quad (2.52)$$

where the covariant derivative is given by  $D_\mu = \partial_\mu + \frac{1}{2}\omega_\mu^{mn}\sigma_{mn}$  with  $\sigma_{mn} = \frac{1}{4}[\gamma_m, \gamma_n]$  and the spin connection  $\omega_\mu^{mn}$ . One finds that the free gravitino field satisfies the Rarita-Schwinger equation

$$-\frac{1}{2}\epsilon^{\mu\nu\rho\sigma}\bar{\psi}_\mu\gamma_5\gamma_\nu\partial_\rho\psi_\sigma - \frac{1}{4}m_{3/2}\bar{\psi}_\mu[\gamma^\mu, \gamma^\nu]\psi_\nu = 0. \quad (2.53)$$

The interactions of the massive gravitino are then described by the Lagrangian

$$\mathcal{L} = -\frac{1}{2}\epsilon^{\mu\nu\rho\sigma}\bar{\psi}_\mu\gamma_5\gamma_\nu\partial_\rho\psi_\sigma - \frac{1}{4}m_{3/2}\bar{\psi}_\mu[\gamma^\mu, \gamma^\nu]\psi_\nu - \frac{1}{2M_{\text{P}}}\bar{\psi}_\mu S^\mu, \quad (2.54)$$

where  $S^\mu$  denotes the supercurrent associated with supersymmetry transformations. In addition, the gravitino satisfies the constraints

$$\gamma^\mu \psi_\mu(x) = 0, \tag{2.55}$$

as well as

$$\partial^\mu \psi_\mu(x) = 0, \tag{2.56}$$

which together with the Rarita-Schwinger equation imply that the gravitino satisfies the Dirac equation component-wise,

$$(i\not{\partial} - m_{3/2})\psi_\mu = 0. \tag{2.57}$$

Calculations of gravitino decay rates will require summing over the four gravitino polarizations in squared matrix elements. We therefore need the polarization tensor for a gravitino with momentum  $p$ , which is given by [10]

$$\begin{aligned} \Pi_{\mu\nu}(p) &\equiv \sum_s \psi_\mu^s(p) \bar{\psi}_\nu^s(p) \\ &= -(\not{p} + m_{3/2}) \left[ \eta_{\mu\nu} - \frac{p_\mu p_\nu}{m_{3/2}^2} - \frac{1}{3} \left( \eta_{\mu\rho} - \frac{p_\mu p_\rho}{m_{3/2}^2} \right) \left( \eta_{\nu\sigma} - \frac{p_\nu p_\sigma}{m_{3/2}^2} \right) \gamma^\rho \gamma^\sigma \right]. \end{aligned} \tag{2.58}$$

This object satisfies the relations

$$\gamma^\mu \Pi_{\mu\nu}(p) = 0, \tag{2.59}$$

$$p^\mu \Pi_{\mu\nu}(p) = 0, \tag{2.60}$$

$$(\not{p} - m_{3/2})\Pi_{\mu\nu}(p) = 0. \tag{2.61}$$

This brief discussion of gravitino properties will be sufficient for the present purpose. We now turn to more phenomenological matters, namely the cosmology of gravitinos.

## Chapter 3

# Gravitino Cosmology

In this chapter, we discuss some aspects of the cosmology of gravitinos. Indeed, gravitinos will play a crucial role in cosmology if they exist. After a short review of some basic concepts of cosmology that will be useful later, we discuss the baryogenesis mechanism of thermal leptogenesis. We will see that the high reheating temperature required by leptogenesis can potentially create a host of problems due to a possible overproduction of gravitinos in the early Universe. We discuss the so-called gravitino problem and then present the solution that we adopt as the scenario for the remaining discussion.

### 3.1 Basic Concepts of Cosmology

Cosmology starts from the observation that the Universe is highly symmetric in space on very large scales, but not in time, as the Universe is clearly expanding. The theoretical framework is General Relativity, which is taken to govern the geometry of spacetime of the Universe as a whole. The assumption of homogeneity and isotropy simplifies cosmological considerations significantly. Cosmology is conventionally done in the framework of Robertson-Walker metrics, which are the maximally spatially symmetric solutions to the field equations of General Relativity,

$$R_{\mu\nu} - \frac{1}{2}Rg_{\mu\nu} = 8\pi GT_{\mu\nu} + \Lambda g_{\mu\nu}, \quad (3.1)$$

where  $R_{\mu\nu}$  is the Ricci tensor, obtained by contraction of the Riemann curvature tensor.  $R$  is the Ricci curvature scalar,  $R = g^{\mu\nu}R_{\mu\nu}$ . On the right-hand side we have the energy-momentum tensor  $T_{\mu\nu}$  and the cosmological constant  $\Lambda$ . The Robertson-Walker line element is given by

$$ds^2 = dt^2 - a(t)^2 \left( \frac{dr^2}{1 - kr^2} + r^2 d\theta^2 + r^2 \sin^2 \theta d\phi^2 \right), \quad (3.2)$$

where  $ds^2 = g_{\mu\nu}dx^\mu dx^\nu$ . The constant  $k$  can always be scaled to be either  $k = +1, -1$  or  $0$  by setting  $r \rightarrow |k|^{1/2}r$  and  $a \rightarrow |k|^{-1/2}a$ . The geometry of the Universe is characterized by  $k$ , where  $k = +1, -1$  or  $0$  corresponds to a closed, open or flat Universe, respectively. Observations suggest that the Universe is flat to a high degree. In the line element, the factor  $a(t)$  that scales the space-like components of the metric is called the cosmic scale factor. It depends on the time-like coordinate  $t$ , the cosmological time. By the assumptions of homogeneity and isotropy, the energy-momentum tensor is restricted to be of the perfect

fluid form,

$$T_{\mu\nu} = pg_{\mu\nu} + (p + \rho)u_\mu u_\nu, \quad (3.3)$$

with the pressure  $p$ , the energy density  $\rho$  and the four-velocity  $u_\mu = dx_\mu/ds$ . The rate of change in the scale factor, which corresponds to the expansion rate of the Universe, is called the Hubble rate,

$$H(t) \equiv \frac{\dot{a}(t)}{a(t)}. \quad (3.4)$$

The present value of the Hubble parameter  $H_0 = H(t_0)$  is often expressed in a rather strange way as

$$H_0 = 100h \text{ km s}^{-1} \text{ Mpc}^{-1}, \quad (3.5)$$

with the dimensionless factor  $h \simeq 73$ . The evolution of the scale factor is governed by the Friedmann equation, which one obtains from plugging the Robertson-Walker metric into Einstein's equation and evaluating the 00-component,

$$H^2(t) \equiv \left(\frac{\dot{a}}{a}\right)^2 = \frac{8\pi G}{3}\rho - \frac{k}{a^2}. \quad (3.6)$$

We also have the following equation for the acceleration of the scale factor,

$$\ddot{a} = -\frac{4\pi G\rho}{3}(\rho + 3p)a. \quad (3.7)$$

The critical density is defined as

$$\rho_c = \frac{3H^2}{8\pi G}. \quad (3.8)$$

The dimensionless density parameters  $\Omega_i$  are then defined as the ratios of the energy densities  $\rho_i$  to the critical density,

$$\Omega_i = \frac{\rho_i}{\rho_c}. \quad (3.9)$$

By rearranging the Friedmann equation, one can see that the critical density determines the geometry of the Universe, since

$$\frac{k}{H^2 a^2} = \Omega_{\text{tot}} - 1. \quad (3.10)$$

If the total energy density equals the critical density, the Universe is flat. If the energy density is higher or lower than the critical density, the Universe is closed or open, respectively. The observed flatness of the Universe is thus equivalent to the statement that the actual energy density of the Universe is extremely close to the critical density. The density parameters  $\Omega_i$  are then a direct measure of the ratio of the individual energy densities to the total energy density of the Universe.

Another widely used concept in cosmology is the redshift  $z$ , which is defined as the relative change of wavelength of light between emission at time  $t$  and absorption today, or equivalently ratio of the present scale factor  $a_0 = a(t_0)$  to the scale factor at cosmological time  $a(t)$ ,

$$z + 1 = \frac{a_0}{a(t)} = \frac{\lambda(t_0) - \lambda(t)}{\lambda(t)}. \quad (3.11)$$

A useful cosmological distance measure is the comoving distance  $\chi$ , which is defined as the coordinate distance between two points on the same spacelike hypersurface. It remains constant for any two objects moving with the Hubble flow. If a photon is emitted at some point at time  $t_e$  and absorbed at another point at time  $t$ , the comoving distance between the points is given by

$$\chi = \int_{t_e}^t \frac{dt'}{a(t')}. \quad (3.12)$$

We now devote some space to an introduction to leptogenesis, since leptogenesis will have some profound implications for the nature of possible dark matter candidates.

### 3.2 Thermal Leptogenesis

It is a striking (and, from a human point of view, very agreeable) fact that there is an extreme asymmetry between the matter and antimatter abundances in the Universe. To obtain a dimensionless number, one can divide the baryon number density  $n_B$  by the photon number density  $n_\gamma$ ,

$$\eta_B = \frac{n_B}{n_\gamma} \sim 10^{-10}. \quad (3.13)$$

While other cosmological abundances can be understood in terms of standard hot Big Bang cosmology, this is an exception. If matter and antimatter had been in equilibrium at temperatures  $\mathcal{O}(1 \text{ GeV})$ , one would expect to find a residual matter abundance today that is smaller by a factor  $\sim 10^8$  and equal to the antimatter abundance. Therefore, a primordial baryon asymmetry must have existed already at temperatures  $\mathcal{O}(1 \text{ GeV})$  because otherwise there would not be appreciable amounts of matter left in the Universe today. Thus, the baryon-to-photon ratio  $\eta_B$  is really a measure of the matter-antimatter asymmetry,

$$\eta_B = \frac{n_B}{n_\gamma} = \frac{n_B - n_{\bar{B}}}{n_\gamma}. \quad (3.14)$$

We thus find ourselves confronted with two related puzzles here, namely why the baryon-to-photon ratio is so high, and why the antimatter-to-matter ratio is so low.

There are two main reasons to believe that the baryon asymmetry was not an initial condition of the Universe, but was generated dynamically. The first is that such an initial condition would correspond to extreme fine-tuning to the level of  $10^{-7}$ , which seems highly implausible. Even more importantly, there are very good reasons, namely the horizon problem and the flatness problem among others, to believe that the Universe underwent an inflationary period of exponential expansion in its early history. Inflation very efficiently erases any initial conditions and dilutes the abundances of particles and sets the curvature of the Universe to zero. Any pre-existing baryon asymmetry would therefore be erased during inflation. We conclude that the asymmetry must be generated dynamically at some time after the inflationary period. This physical process responsible for the generation of the primordial baryon asymmetry is usually referred to as baryogenesis.

Indeed, it has been found that the baryon asymmetry can be dynamically generated if Sakharov's conditions [11] are fulfilled:

- Baryon number violation
- C and CP violation
- Departure from thermal equilibrium

The reason for requiring (sufficiently large) baryon number violation should be obvious. If C and CP violation are not present, processes and inverse processes proceed at the same rate, preventing the generation of an asymmetry. The departure from thermal equilibrium is needed because in thermal equilibrium, the expectation value for the baryon number is always zero, as one can quickly demonstrate:

$$\begin{aligned}\langle B \rangle_T &= \text{tr}[e^{-\beta H} B] = \text{tr}[(\text{CPT})(\text{CPT})^{-1} e^{-\beta H} B] \\ &= \text{tr}[e^{-\beta H} (\text{CPT})^{-1} B (\text{CPT})] = -\text{tr}[e^{-\beta H} B],\end{aligned}\tag{3.15}$$

where we have used the fact that  $B$  is odd under CP and that the Hamiltonian commutes with CPT.

Interestingly, all of Sakharov's conditions are qualitatively fulfilled in the Standard Model. Quantitatively, baryogenesis does not work in the Standard Model, however. Nevertheless, there is a number of different viable baryogenesis mechanisms, which differ in their ways of extending the Standard Model in order to implement Sakharov's conditions. Prominent examples include electroweak baryogenesis and Affleck-Dine baryogenesis.

One particularly compelling scenario for baryogenesis is the leptogenesis mechanism proposed by Fukugita and Yanagida [12], which connects the seesaw mechanism for light neutrino masses with baryogenesis. Leptogenesis was motivated by two important discoveries, namely the finiteness of neutrino masses established by neutrino oscillation experiments and the discovery of non-perturbative solutions of the electroweak field equations, the so-called sphaleron configurations. In leptogenesis, the baryon asymmetry is generated indirectly by first generating a lepton asymmetry via the out-of-equilibrium decays of heavy sterile neutrinos, which is subsequently converted into a baryon asymmetry by sphaleron processes. In this section, we roughly follow [13].

### 3.2.1 The Seesaw Mechanism

There are quite a number of different mechanisms for explaining the smallness of the neutrino masses. However, the most natural one seems to be the seesaw mechanism. There, the Standard Model is augmented by right-handed neutrinos which are singlets under the Standard Model gauge group. Such right-handed neutrinos arise naturally in  $SO(10)$  grand unified theories (GUTs). Furthermore, the right-handed neutrinos are actually necessary for anomaly cancelation in such grand unified theories.

With these additional right-handed neutrinos, it becomes possible to have gauge invariant Dirac and Majorana mass terms for the neutrinos. If we denote the left-handed Standard Model neutrinos by  $\nu_L$  and the right-handed Majorana neutrinos by  $N_R$ , we can write

$$\mathcal{L}_{m_\nu} = (\bar{\nu}_L, \bar{N}_L^c) \begin{pmatrix} 0 & m_D \\ m_D^T & M_R \end{pmatrix} \begin{pmatrix} \nu_R^c \\ N_R \end{pmatrix},\tag{3.16}$$

where  $m_D$  is the Dirac mass matrix between the left-handed and right-handed neutrinos, and  $M_R$  is the right-handed neutrino mass matrix. Since the right-handed neutrinos are gauge singlets, they are not protected by symmetries from acquiring large Majorana masses. If we denote the matrix of left-handed neutrino Yukawa couplings by  $h$ , we have

$$M_R \gg m_D = hv. \quad (3.17)$$

When diagonalizing the mass matrix, the seesaw mechanism yields the light neutrino mass eigenstates

$$\nu \simeq V_\nu^T \nu_L + \nu_L^c V_\nu^*, \quad (3.18)$$

where  $V_\nu$  is the mixing matrix in the leptonic charged current, as well as the heavy neutrino eigenstates

$$N \simeq N_R + N_R^c. \quad (3.19)$$

The corresponding mass matrices are given by

$$m_\nu \simeq -V_\nu^T m_D^T \frac{1}{M_R} m_D V_\nu, \quad m_N \simeq M_R. \quad (3.20)$$

The light neutrino masses are therefore suppressed by the large scale of the right-handed neutrinos. One thus ends up with a set of very light and a set of very heavy neutrino mass eigenstates. The idea in leptogenesis is that the ultra-heavy right-handed neutrinos may create a lepton asymmetry in their decays in the very early Universe if these decays occur out of thermal equilibrium.

### 3.2.2 Generation of the CP Asymmetry

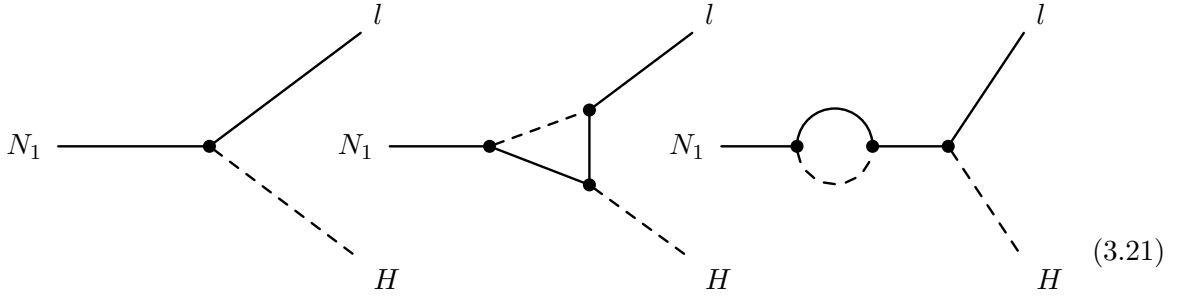


Figure 3.1: Tree level and one-loop diagrams for the decay of the lightest right-handed neutrino into Higgs and lepton doublets. The interference of these diagrams generates a CP asymmetry.

In leptogenesis, the out-of-equilibrium condition is provided by the expansion of the Universe. The idea is that the number density of heavy neutrinos falls out of thermal equilibrium when their decay rate drops below the Hubble rate,

$$\Gamma_{N_1}(T) < H(T), \quad (3.22)$$

since the decays will then be too slow to follow the rapid expansion of the Universe and retain the equilibrium number density value. The CP asymmetry is generated in the decays of  $N_1 \rightarrow Hl$ ,  $N_1 \rightarrow \bar{H}\bar{l}$  by the interference between tree-level and one-loop graphs. The decay

width of the heavy neutrinos  $N_i$  at tree level is given by

$$\Gamma_{Di} = \Gamma(N_i \rightarrow Hl) + \Gamma(N_i \rightarrow \bar{H}\bar{l}) \simeq \frac{1}{8\pi} \left( hh^\dagger \right)_{ii} M_i. \quad (3.23)$$

The CP asymmetry from  $N_1$  decays is defined as

$$\varepsilon_1 = \sum_{\alpha} \frac{\Gamma(N_1 \rightarrow l_{\alpha}H) - \Gamma(N_1 \rightarrow \bar{l}_{\alpha}\bar{H})}{\Gamma(N_1 \rightarrow l_{\alpha}H) + \Gamma(N_1 \rightarrow \bar{l}_{\alpha}\bar{H})}, \quad (3.24)$$

where the sum is over flavors  $\alpha$ . We will work here in a simplified picture, where we assume that the generation of the CP asymmetry occurs solely through the decays of the lightest right-handed neutrino  $N_1$ , and where we ignore flavor effects. The CP asymmetry is then given by

$$\varepsilon_1 \simeq \frac{3}{16\pi} \frac{1}{(hh^\dagger)_{11}} \sum_{i=2,3} \text{Im} \left[ \left( hh^\dagger \right)_{i1}^2 \right] \frac{M_1}{M_i} \quad (3.25)$$

for hierarchical heavy neutrino masses in a basis where the right-handed neutrino mass matrix is diagonal. The amount of generated CP asymmetry is thus determined by the hierarchy of heavy neutrino masses.

### 3.2.3 Relating Lepton Asymmetry and Baryon Asymmetry

Another crucial ingredient in baryogenesis is the relationship between lepton and baryon asymmetries at high temperatures. Non-abelian gauge theories possess an infinite number of degenerate vacua with different topological charge, which are separated by a potential barrier whose height is given by the so-called sphaleron energy. The transition probability is given by instanton configurations representing tunneling between neighboring vacua. The  $SU(2)$  instantons induce at lowest order effective interactions of all left-handed fermions

$$\mathcal{O}_{B+L} = \prod_i (q_{Li} q_{Li} q_{Li} l_{Li}), \quad (3.26)$$

which violate baryon and lepton number by  $\Delta B = \Delta L = 3$  units each. In the vacuum, these  $B + L$  violating transition rates are given by  $\Gamma \sim e^{-4\pi/\alpha} = \mathcal{O}(10^{-165})$  and are therefore completely negligible due to the smallness of the weak coupling. However, at higher temperatures, transitions by thermal fluctuations over the barrier become possible, and the Boltzmann suppression disappears for temperatures exceeding the barrier height. The sphalerons configurations correspond to saddle points of the field energy. Analyses show that sphaleron transition rates increase rapidly with temperature, roughly  $\propto T^4$ . At very high temperatures, the sphaleron processes will therefore become crucial, and they are in thermal equilibrium for  $10^2 \text{ GeV} < T < 10^{12} \text{ GeV}$ . Any  $B + L$  asymmetry generated at high temperatures will eventually get erased by sphaleron processes, implying that such an asymmetry cannot be responsible for the generation of the observed baryon asymmetry.

One now needs to determine the relationship between lepton asymmetry and baryon asymmetry at high temperatures as determined by the sphalerons and other processes in thermal equilibrium. In a weakly coupled plasma, one can assign a chemical potential to each Higgs, quark and lepton field in the thermal bath. From the equilibrium conditions of the  $SU(2)$

electroweak instantons, as well as the  $SU(3)$  QCD instantons, the vanishing of the total hypercharge of the plasma and the Yukawa and gauge interactions, one can then relate the chemical potentials in the thermal bath to each other to find that they can all be expressed in terms of a single chemical potential. The corresponding baryon and lepton asymmetries are proportional to this chemical potential. The baryon asymmetry is therefore related to the lepton asymmetry and the  $B - L$  asymmetry by a simple proportionality relation,

$$\langle B \rangle_T = c_S \langle B - L \rangle_T = \frac{c_S}{c_S - 1} \langle L \rangle_T, \quad (3.27)$$

where  $c_S = (8N_f + 4)/(22N_f + 13)$  is a number  $\mathcal{O}(1)$  and  $N_f$  is the number of fermion generations. One can see from this relation that a  $B - L$  asymmetry at high temperatures is necessary to achieve a non-vanishing baryon asymmetry.

The final baryon asymmetry generated by leptogenesis is

$$Y_B \equiv \frac{n_B}{s} = \kappa c_S \frac{\varepsilon_1}{g_*}, \quad (3.28)$$

where  $g_*$  is the number of relativistic degrees of freedom. The efficiency factor  $\kappa$  describes the effect of the competition between the different out-of-equilibrium production and washout processes. In order to determine the efficiency factor, one has to solve the Boltzmann equations for leptogenesis, which are given by

$$\frac{dN_{N_1}}{dz} = -(D + S)(N_{N_1} - N_{N_1}^{\text{eq}}), \quad (3.29)$$

$$\frac{dN_{B-L}}{dz} = -\varepsilon_1 D(N_{N_1} - N_{N_1}^{\text{eq}}) - W N_{B-L}. \quad (3.30)$$

where  $z = M_1/T$ . The processes contributing to the different terms in the Boltzmann equations include decays, inverse decays,  $\Delta L = 1$  scatterings and  $\Delta L = 2$  scatterings involving heavy neutrino exchange. In the first Boltzmann equation, which describes the evolution of the  $N_1$  abundance, the term  $D = \Gamma_D/Hz$  describes the effects of decays and inverse decays, while  $S = \Gamma_S/Hz$  accounts for  $\Delta L = 1$  scatterings. The second Boltzmann equation describes the evolution of the  $B - L$  asymmetry, which is the result of a competition between the source term  $D$  that accounts for decays and the washout term  $W = \Gamma_W/Hz$  to which all other processes contribute.

One can regard the behavior of the Boltzmann equations in the different regimes of so-called strong and weak washout. The borderline between the strong and weak washout regimes is determined by the decay parameter

$$K = \frac{\Gamma_D(z = \infty)}{H(z = 1)} = \frac{\tilde{m}_1}{m_*}. \quad (3.31)$$

The effective neutrino mass  $\tilde{m}_1$  is defined as

$$\tilde{m}_1 = \frac{(m_D m_D^\dagger)_{11}}{M_1}, \quad (3.32)$$

while the equilibrium neutrino mass  $m_*$  is given by

$$m_* = \frac{16\pi^{5/2}\sqrt{g_*}}{3\sqrt{5}} \frac{v_F^2}{M_{\text{P}}} \simeq 1.08 \times 10^{-3} \text{ eV}. \quad (3.33)$$

where  $v_F$  is the finite-temperature Higgs VEV. The condition  $K = 1$ , or the equality of  $\tilde{m}_1$  and  $m_*$  is equivalent to  $\Gamma_1 = H|_{T=M_1}$ . For  $K \ll 1$  one speaks of weak washout, and for  $K \gg 1$  of strong washout.

In the case of weak washout, the decays happen far out of equilibrium, and the final efficiency factor depends on the initial  $N_1$  abundance. In addition, an initial  $B-L$  asymmetry is not erased, thus limiting the predictivity of leptogenesis. In the case of strong washout, on the other hand, calculations yield a result that is essentially independent of the initial conditions. Remarkably, solar and atmospheric oscillation experiments suggest that the light neutrino mass scale is larger than the equilibrium mass  $m_*$ , implying that leptogenesis is indeed in the strong washout regime, where the final efficiency factor is independent of any initial  $B-L$  asymmetry and  $N_1$  abundance. From detailed analyses of the leptogenesis Boltzmann equations, Buchmüller, di Bari and Plümacher found a power law behavior [14]

$$\kappa_f = \kappa(z = \infty) = (2 \pm 1) \times 10^{-2} \left( \frac{0.01 \text{ eV}}{\tilde{m}_1} \right) \quad (3.34)$$

for the case that  $\tilde{m}_1 > 10^{-3} \text{ eV}$ .

### 3.2.4 Bounds on Neutrino Masses from Leptogenesis

One can derive both an upper bound on the light neutrino masses and a lower bound on the heavy neutrino masses from the requirement of successful leptogenesis. The washout term  $W$  receives a contribution from  $\Delta L = 2$  scatterings that depends on the absolute neutrino mass scale

$$\bar{m}^2 = m_1^2 + m_2^3 + m_3^2, \quad (3.35)$$

where the contribution is given by

$$\Delta W \propto \frac{M_{\text{P}} M_1 \bar{m}^2}{v_F^4}. \quad (3.36)$$

When the absolute neutrino mass scale becomes sufficiently large, the growing contribution from the washout rate  $\Delta W$  renders leptogenesis inefficient. The upper bound one finds in this way is  $\bar{m} < 0.1 \text{ eV}$ . Successful leptogenesis thus favors the light neutrino mass range

$$10^{-3} \text{ eV} < m_i < 0.1 \text{ eV}. \quad (3.37)$$

More important from the point of view of dark matter is the lower bound on the lightest right-handed neutrino mass. It was found that the CP asymmetry and the lightest right-handed neutrino mass are not completely independent parameters. For hierarchical right-handed neutrino masses, there is an upper bound on the CP asymmetry generated in the

decays of the Majorana neutrinos, the so-called Davidson-Ibarra bound [15]:

$$|\varepsilon_1| < \frac{3}{8\pi} \frac{M_1}{\langle H_u^0 \rangle^2} (m_3 - m_1), \quad (3.38)$$

where  $m_3$  and  $m_1$  denote light neutrino masses. Combining the upper bound on the light neutrino masses from neutrino oscillation experiments, e.g.  $m_3 = \sqrt{\Delta m_{\text{atm}}^2}$  for hierarchical light neutrino masses, with typical efficiency factors,  $\kappa \sim 0.01$ , leptogenesis can only be effective if the lightest right-handed neutrino mass is heavier than  $\sim 2 \times 10^9$  GeV. Therefore, if the heavy neutrinos were thermally produced, the reheating temperature of the Universe after inflation must have been at least roughly as large as  $M_1$ . The bound on the CP asymmetry then translates into a lower bound on the reheating temperature from leptogenesis,

$$T_R \gtrsim 2 \times 10^9 \text{ GeV}. \quad (3.39)$$

This bound establishes a crucial connection between baryogenesis and dark matter, since it severely constrains the nature of the dark matter if thermal leptogenesis is indeed the mechanism responsible for baryogenesis. The high reheating temperatures required by leptogenesis can lead to various problems with gravitino overproduction and disruption of primordial nucleosynthesis, as we shall discuss shortly. This will lead us to the conclusion that leptogenesis favors the gravitino as the most plausible candidate for the dark matter of the Universe.

### 3.3 Thermal Production of Gravitinos

Any initial gravitino abundance is greatly diluted during the exponential expansion of the Universe during the slow-roll phase of inflation. After inflation, however, the Universe reheats to a temperature  $T_R$  due to coherent oscillations of the inflaton field around the potential minimum. During the reheating phase, gravitinos regenerated as they are produced by supersymmetric QCD scattering processes in the thermal plasma. The QCD processes give the dominant contribution due to the large strong coupling constant. The production rate of gravitinos in the hot supersymmetric plasma has been calculated to leading order in all gauge couplings. The QCD contribution was calculated in [10] and electroweak contributions in [16, 17]. The resulting gravitino density resulting from the QCD contributions depends on only three unknown parameters, namely the reheating temperature, the gravitino mass and the gluino mass,

$$\Omega_{3/2} h^2 \simeq 0.27 \left( \frac{T_R}{10^{10} \text{ GeV}} \right) \left( \frac{100 \text{ GeV}}{m_{3/2}} \right) \left( \frac{m_{\tilde{g}}}{1 \text{ TeV}} \right)^2. \quad (3.40)$$

The gravitino abundance is therefore proportional to the reheating temperature. Compared to the dark matter abundance inferred from WMAP measurements [18],

$$\Omega_{\text{CDM}} h^2 = 0.101_{-0.010}^{+0.007}, \quad (3.41)$$

we see that gravitinos are copiously produced during the high-temperature phase of the Universe. Remarkably, for high reheating temperatures  $\sim 10^{10}$  GeV, the gravitino abundance is naturally of the same order as the dark matter abundance in the Universe, implying that

the gravitino may indeed be the dominant component of the dark matter if it is the lightest supersymmetric particle.

## 3.4 The Gravitino Problem

### 3.4.1 Constraints from Overclosure

From Eq. (3.40), we see that the high reheating temperatures required by thermal leptogenesis, combined with typical values for the gluino and gravitino mass, lead to large gravitino abundances of the same order as the dark matter relic density. If the gravitino is stable (i.e. the lightest supersymmetric particle), this can potentially lead to overclosure of the Universe. In the case of a stable gravitino LSP, for each value of the gluino mass, one therefore gets a corresponding upper bound on the reheating temperature from overclosure constraints, since the gravitino abundance must not exceed the observed dark matter abundance. If we assume a typical gluino mass of  $m_{\tilde{g}} = 500$  GeV and a high reheating temperature  $T_R = 10^9$  GeV, we find that the gravitino cannot be too light,  $m_{3/2} \gtrsim 10$  GeV.

### 3.4.2 Constraints from Big Bang Nucleosynthesis

The abundances of light elements in the Universe today can be understood quantitatively well if one assumes that they were thermally produced in an early high-temperature phase. This process is known by the name of Big Bang nucleosynthesis (BBN) or primordial nucleosynthesis. Nucleosynthesis takes place at temperatures  $\sim 1$  MeV, corresponding to timescales of  $\sim 100$  s after the Big Bang. Essentially the only free parameter in the complex network of primordial nucleosynthesis reactions is the baryon-to-photon ratio  $\eta_B$ . Remarkably, one finds that BBN reproduces the observed primordial abundances very well for  $\eta_B \sim 10^{-10}$ . The fact that this number agrees with the one inferred from WMAP measurements of the CMB anisotropies is one of the triumphs of hot Big Bang cosmology. Furthermore, the fact that BBN works so well within the standard picture puts severe constraints on the addition of new exotic particles which tend to easily upset the delicate predictions.

Late-decaying particles can substantially change the BBN predictions in two ways: both electromagnetic showers and hadronic showers triggered by the decay of the exotic particle will dissociate the light elements formed by BBN, thus altering their primordial abundances. The gravitino is the prime example of such an exotic late-decaying particle. If the gravitino is not the LSP, it will, due to its long lifetime, decay during and after BBN into the LSP and generally release electromagnetic energy in the form of photons. If these photons have energies above a certain threshold, they can photo-dissociate light elements in reactions like  $D + \gamma \rightarrow n + p$ . An even worse situation arises if the gravitino is heavier than the gluino, in which case it can decay into gluon-gluino pairs which will produce energetic hadrons that can hadro-dissociate the primordial elements. The BBN bounds on late-decaying particles have been analyzed in detail, in particular for the case of the gravitino, and typical bounds on the reheating temperature of  $T_R \lesssim 10^7$  GeV for  $m_{3/2} \sim 100$  GeV have been found [19]. These upper bounds on the reheating temperature are very difficult to reconcile with the lower bounds  $T_R \gtrsim 10^9$  GeV required by thermal leptogenesis. Thus, the hadronic decay modes of the gravitino put severe constraints on the standard scenario of leptogenesis with neutralino dark matter. If the gravitino is not the LSP, leptogenesis and the often favored

picture with the lightest neutralino as the dominant component of the cold dark matter seem to be incompatible. Indeed, we can say that the high reheating temperature from leptogenesis seems to favor the scenario that the gravitino itself is the lightest supersymmetric particle.

If the gravitino is the LSP and  $R$ -parity is conserved, the NLSP is generally very long-lived because it must always decay into a final state containing a gravitino. The corresponding interactions between NLSPs, gravitinos and Standard Model particles have only gravitational strength, yielding a decay rate that is suppressed by the Planck scale. The BBN constraints then essentially apply to the NLSP, whose nature will determine the phenomenological viability of the scenario. In models with a gravitino LSP, the most likely candidates for the NLSP are the lightest neutralino  $\chi_1^0$  and the right-handed scalar tau  $\tilde{\tau}_R^-$ . Both of these possibilities are problematic. The NLSP will predominantly decay via  $\tilde{\tau}_R \rightarrow \tau\psi_{3/2}$  or  $\chi_1^0 \rightarrow \gamma\psi_{3/2}$ , respectively. The decay rates in both cases are given by

$$\Gamma_{\chi_1^0, \tilde{\tau}} = \frac{m_{\chi_1^0, \tilde{\tau}}^5}{48\pi m_{3/2}^2 M_{\text{P}}^2}. \quad (3.42)$$

The corresponding lifetimes are then very long,

$$\tau_{\chi_1^0, \tilde{\tau}} \simeq 9 \text{ days} \left( \frac{m_{3/2}}{10 \text{ GeV}} \right)^2 \left( \frac{150 \text{ GeV}}{m_{\chi_1^0, \tilde{\tau}}} \right)^5. \quad (3.43)$$

This will again generally lead to problems with primordial nucleosynthesis, since this time the NLSP is present during and after BBN. A right-handed stau decaying via  $\tilde{\tau}_R \rightarrow \tau\psi_{3/2}$  will only release electromagnetic energy, which may be marginally acceptable. However, it was recently realized that scalar taus can form bound states with Helium [20], catalyzing the production of Lithium by a factor 300 – 600 [21], in stark conflict with observations. A neutralino NLSP, on the other hand, can dissociate the primordial elements via photo-dissociation due to photons from  $\chi_1^0 \rightarrow \gamma\psi_{3/2}$ . If the neutralino is heavy enough to decay via  $\chi_1^0 \rightarrow Z^0\psi_{3/2}$ , its hadronic decay modes may have disastrous consequences [19]. In view of these difficulties, thermal leptogenesis and supersymmetric dark matter seem, at least naively, to be incompatible.

### 3.4.3 Possible Solutions to the Gravitino Problem

The obvious way to avoid the gravitino problem is to abandon leptogenesis, either completely or at least its standard form, in favor of a baryogenesis mechanism that does not require a very large reheating temperature. There are alternative leptogenesis scenarios in which the lower bound on the reheating temperature is avoided, such as resonant leptogenesis with quasi-degenerate right-handed neutrino masses, which can generate very large CP asymmetries, or non-thermal leptogenesis from inflaton decay.

We should also mention that the gravitino problem disappears if the gravitino is either very light,  $m_{3/2} \lesssim 16 \text{ eV}$ , or very heavy,  $m_{3/2} \gtrsim 100 \text{ TeV}$ . If it is very heavy, the gravitino will decay before the beginning of nucleosynthesis. In the case of a very light gravitino, on the other hand, one cannot have supersymmetric dark matter, so some other particle like the axion would have to constitute the dark matter. Such very light or very heavy gravitino masses seem disfavored, so we will not regard this possibility further.

We will adopt here the viewpoint that giving up thermal leptogenesis is unacceptable, so we look for ways to arrive at a consistent thermal history of the Universe within the standard scenario. If we want to keep the standard scenario, one way out is to assume a late-time entropy production after NLSP decoupling and before the onset of primordial nucleosynthesis [22]. This will both dilute the gravitino abundance and the NLSP abundance to weaken the BBN constraints. Another possibility is a scenario with a sneutrino NLSP [23] or a stop NLSP [24] whose late decays do not pose a substantial threat to the BBN predictions. A detailed analysis of the impact of charged massive particles on the standard BBN scenario can be found in [25].

The simplest, although somewhat radical, way to avoid all the above-mentioned problems is to assume a small amount of  $R$ -parity violation. This has the effect that the NLSP does not necessarily have to decay into a gravitino anymore. Instead, additional decay channels into Standard Model-only particles become accessible. These decays will generally proceed at a much higher rate than the decays into gravitinos, thus allowing the NLSP to decay well before the onset of BBN. The NLSP abundance is therefore reduced to harmless levels, and the BBN predictions are completely unaffected. The other important consequence of  $R$ -parity violation is that it makes the lightest supersymmetric particle unstable, also allowing it to decay into Standard Model particles. In the case of a gravitino LSP, this may open the possibility of indirect detection of gravitino dark matter and thus potentially make the scenario testable via indirect detection experiments. Indeed, the scenario with gravitino dark matter and a slight violation of  $R$ -parity is the one that we will adopt for the remaining discussion. In the next chapter, we will study  $R$ -parity violation and some of its consequences in regard to dark matter.

## Chapter 4

# *R*-Parity Violation

In this chapter, we examine some of the phenomenological consequences of *R*-parity violation and discuss a model that yields *R*-parity breaking Yukawa couplings in the range required by cosmology, as discussed in the previous chapter.

### 4.1 *R*-Invariance and *R*-Parity

The supersymmetry algebra (2.1) is invariant under  $U(1)_R$  phase rotations of the Grassmann coordinates,  $\theta \rightarrow e^{i\varphi}\theta$  and  $\bar{\theta} \rightarrow e^{-i\varphi}\bar{\theta}$ , a property known as *R*-invariance. The supersymmetry generators transform under such *R*-transformations as

$$\begin{aligned} Q_\alpha &\rightarrow e^{i\varphi R} Q_\alpha e^{-i\varphi R} = e^{-i\varphi} Q_\alpha, \\ \bar{Q}_{\dot{\alpha}} &\rightarrow e^{i\varphi R} \bar{Q}_{\dot{\alpha}} e^{-i\varphi R} = e^{i\varphi} \bar{Q}_{\dot{\alpha}}. \end{aligned} \quad (4.1)$$

Therefore,  $\theta$ ,  $\bar{\theta}$ ,  $Q$  and  $\bar{Q}$  carry *R*-charges +1, -1, -1 and +1, respectively. One can define an *R*-transformation acting on left-chiral superfields as

$$R\Phi(x, \theta, \bar{\theta}) = e^{i\varphi R_\Phi} \Phi(x, \theta, \bar{\theta}) = \Phi'(x, e^{i\varphi}\theta, e^{-i\varphi}\bar{\theta}), \quad (4.2)$$

so that  $\Phi$  has *R*-charge  $R_\Phi$ . However, there are severe problems with exact  $U(1)_R$  symmetry, both theoretical and phenomenological. Problematic is that gaugino masses break  $U(1)_R$ . In the case of an unbroken  $U(1)_R$ , both the gravitino and the gluinos would have to stay massless. Massless or light gluinos are not observed, and the masslessness of the gravitino would mean that local supersymmetry cannot be broken spontaneously, which is clearly unacceptable. Continuous *R*-invariance must therefore be given up, but one can retain a discrete  $Z_2$  subgroup of  $U(1)_R$  by taking  $\varphi = \pi$ . Then  $e^{i\pi R} = (-1)^R$  is the so-called matter parity  $M_p$  of a superfield, whereas the same quantity for the component fields is called *R*-parity or  $R_p$ . Vector superfields are restricted by the reality condition to have *R*-charge 0. From the component-field expansion Eq. (2.16) one can then see that the component fields must have *R*-charges  $R(v^\mu) = 0$ ,  $R(\lambda) = -R(\bar{\lambda}) = 1$ . One usually assigns matter parity  $\pm 1$  or 0 to a chiral superfield, depending on whether its scalar component is a Standard Model particle (i.e. a Higgs boson) or the scalar superpartner of a Standard Model fermion. The component fields then have *R*-charge  $R(\phi) = R_\Phi$  and  $R(\psi) = -R(\bar{\psi}) = R_\Phi - 1$ . This has the effect that Standard Model particles always have positive *R*-parity and superpartners have negative *R*-parity. As a matter of fact, this assignment is equivalent with identifying *R* with  $3(B - L)$ .

We can thus say that the matter parity of a superfield is given by  $(-1)^{3(B-L)}$ . The *R*-parity of a component field with spin  $S$  is then given by

$$R_p = (-1)^{3(B-L)}(-1)^{2S}, \quad (4.3)$$

which is nothing but the definition of *R*-parity that we introduced in the discussion of the MSSM superpotential, Eq. (2.34). We see that *R*-parity is conserved even when  $B$  and  $L$  are separately broken, but  $B - L$  is conserved. The conservation of *R*-parity is often believed to be an exact symmetry of Nature and is imposed from the start in the MSSM, where it can be used very effectively to forbid unwanted interactions mediated by the direct exchange of spin-0 squarks and sleptons. We can already see that *R*-parity is intimately related to the conservation of baryon and lepton number. Namely, imposing *R*-parity essentially amounts to lepton and baryon number conservation. Conversely, *R*-parity violation is always accompanied by a breaking of lepton and baryon number. However, it does not necessarily have to be the case that *R*-parity is indeed an exact symmetry. However, the non-conservation of *R*-parity has some dramatic effects: Single supersymmetric particles can be created, and the lightest supersymmetric particle is no longer stable and can decay into Standard Model particles.

We now turn to the question of how *R*-parity can be broken. *R*-parity violation can originate either from the superpotential or from the soft mass terms. While in the standard Standard Model there are no renormalizable gauge-invariant interactions that violate baryon or lepton number ( $B$  and  $L$  are accidental symmetries in the Standard Model), such interactions are in principle present in supersymmetric extensions of the Standard Model. When we discussed the MSSM superpotential in Chapter 2, we mentioned that it is not the most general gauge invariant, renormalizable superpotential. There are additional dimension-four operators that could appear in the MSSM superpotential, which we can find by examining quantum numbers. The additional lepton number violating terms can be found by observing that the lepton superfields  $L_i$  and the  $Y = -1/2$  Higgs superfield  $H_d$  have the same gauge quantum numbers, allowing us to replace  $H_d$  by  $L_i$  in the terms appearing in the MSSM superpotential, Eq. (2.33). In addition, one has the baryon-number violating term  $U_i^c D_j^c D_k^c$ . The most general gauge invariant, renormalizable *R*-odd superpotential with the MSSM field content is therefore

$$\mathcal{W}_{R_p} = \mu_i H_u L_i + \frac{1}{2} \lambda_{ijk} L_i L_j E_k^c + \lambda'_{ijk} L_i Q_j D_k^c + \frac{1}{2} \lambda''_{ijk} U_i^c D_j^c D_k^c. \quad (4.4)$$

The first three terms violate lepton number conservation, while the fourth term violates baryon number conservation. Since these new interactions are renormalizable, they are not expected to be suppressed by a large mass scale. Therefore, the lepton- and baryon-number breaking interactions stemming from *R*-parity violation are fraught with phenomenological difficulties such as rapid proton decay or too large neutrino masses arising from the lepton-number violating mixing of neutrinos with neutral Higgsinos and gauginos, unless the interactions are strongly suppressed by very small or vanishing couplings. In general, the new couplings introduce 48 additional free parameters, which is of course a rather undesirable feature. However, experiments put very severe bounds on the *R*-parity violating couplings. For instance, for soft masses  $\sim 100$  GeV, proton stability yields the bound  $\lambda'_{11k} \lambda''_{11k} \lesssim 10^{-27}$ , and the non-observation of the flavor-violating process  $\mu\text{Ti} \rightarrow e\text{Ti}$  sets the limits  $\lambda_{1k2} \lambda'_{k11} \lesssim 4 \times 10^{-8}$

for  $k = 1, 2, 3$ . For more details on the constraints on *R*-parity violation, see [26].

A remark about the choice of weak eigenstate basis is in order. Since the superfields  $L_i$  and  $H_u$  have the same gauge quantum numbers, we can always redefine the fields by a unitary transformation in such a way that the bilinear  $\mu_i$  couplings vanish. Such a transformation will change the values of the lepton number violating trilinear couplings  $\lambda_{ijk}$  and  $\lambda'_{ijk}$ , but leave the baryon number violating coupling  $\lambda''_{ijk}$  invariant. This means that the values of the lepton number violating couplings are basis-dependent. When one speaks about the size of these couplings, one therefore always needs to specify the corresponding basis. In the following, we will always refer to the case where the bilinear terms are rotated away. This also means that there is a redundancy between the bilinear and trilinear couplings.

In addition to the *R*-parity violating interactions arising from the superpotential (4.4) *R*-parity violation also introduces a number of additional soft mass terms which correspond to another 51 free parameters.

## 4.2 Gaugino-Lepton Mixing via *R*-parity Violation

*R*-parity violation has a rich phenomenology. Here we restrict ourselves to one particular feature that will be important in the following: The effect of bilinear *R*-parity violation via the first term in Eq. (4.4) is a physical mixing between scalar leptons and Higgs bosons, and between leptons and neutralinos/charginos. Once *R*-parity is broken, the only quantum number distinguishing between the neutral down-type Higgsinos and the neutrinos, namely lepton number, is lifted. These particles are then free to mix with each other, and the  $4 \times 4$  neutralino mass matrix gets extended to a  $7 \times 7$  neutralino-neutrino mass matrix. Since we expect the *R*-parity violation to be dominant for the third generation, we disregard the other two generations and just write a  $5 \times 5$  matrix. In the basis  $\psi^0 = (-i\tilde{\gamma}, -i\tilde{Z}, \tilde{H}_u^0, \tilde{H}_d^0, \nu_\tau)$ , with  $\mathcal{L}_{\text{mass}} = -\frac{1}{2}\psi^{0T} M_N \psi^0 + \text{h.c.}$ , the neutralino-neutrino mass matrix reads

$$M_N = \begin{pmatrix} M_1 c_W^2 + M_2 s_W^2 & (M_2 - M_1) s_W c_W & 0 & 0 & 0 \\ (M_2 - M_1) s_W c_W & M_1 s_W^2 + M_2 c_W^2 & g v_u / 2 c_W & -g v_d / 2 c_W & -g v_3 / 2 c_W \\ 0 & g v_u / 2 c_W & 0 & -\mu & -\mu_3 \\ 0 & -g v_d / 2 c_W & -\mu & 0 & 0 \\ 0 & -g v_3 / 2 c_W & -\mu_3 & 0 & 0 \end{pmatrix}. \quad (4.5)$$

The off-diagonal terms involving the bilinear  $\mu_3$  parameter as well as the ones containing the sneutrino VEV  $\langle \tilde{\nu} \rangle = v_3$  therefore induce a mixing between Zinos/Higgsinos and neutrinos.

Likewise, in the charged sector the violation of lepton number causes a mixing between the charged Higgsinos and charged leptons. As a consequence, the  $2 \times 2$  chargino mass matrix gets enlarged to a  $5 \times 5$  chargino-charged lepton mass matrix with  $\mathcal{L}_{\text{mass}} = -\psi^{-T} M_C \psi^+ + \text{h.c.}$ . Again, we write this extended mass matrix as a  $3 \times 3$  matrix due to a dominant third-generation coupling. In the  $\psi^- = (-i\tilde{W}, \tilde{H}_d^-, \tau^-)$ ,  $\psi^+ = (-i\tilde{W}^+, \tilde{H}_u^+, \tau^+)$  basis, it is given

by

$$M_C = \begin{pmatrix} M_2 & gv_u/\sqrt{2} & 0 \\ gv_d/\sqrt{2} & \mu & h_\tau v_3 \\ gv_3/\sqrt{2} & \mu_3 & h_\tau v_d \end{pmatrix}, \quad (4.6)$$

where  $h_\tau$  is the  $\tau$  Yukawa coupling. Again, the *R*-parity violation introduces a mixing between charginos and charged leptons. If *R*-parity is conserved, one can choose a  $(H_d, L_i)$  basis where these matrices reduce to the  $4 \times 4$  and  $2 \times 2$  neutralino/chargino mass matrices (2.38), (2.40). The reason we are interested in these mixings is that they will give rise to gravitino decay modes into Standard Model particles when the gravitino is the lightest supersymmetric particle.

### 4.3 Cosmological Implications

*R*-parity violation has important consequences in cosmology. It may influence baryogenesis if the couplings are large enough. Furthermore, the lightest supersymmetric particle becomes unstable, potentially jeopardizing its role as a possible dark matter particle. In the context of gravitino dark matter, however, it provides an interesting solution to the gravitino problem.

#### 4.3.1 Primordial Nucleosynthesis

If *R*-parity is broken, the NLSP does not necessarily have to decay into a gravitino anymore. Instead, the *R*-parity violating couplings will open new decay channels to pure Standard Model final states. If these decays proceed fast enough, the NLSP can decay into Standard Model particles before the onset of BBN, thus evading the BBN constraints altogether. Big Bang nucleosynthesis will be unaffected if the NLSP lifetime is shorter than  $\sim 100$  s. This can be used to give a lower bound on the *R*-parity violating couplings. For example, if the NLSP is a right-handed stau, it can decay via  $\tilde{\tau}_R \rightarrow \mu\nu_\tau$  through the operator  $\lambda_{323} L_3 L_2 E_3^c$ , where the corresponding lifetime is given by

$$\tau_{\tilde{\tau}} \simeq 10^3 \text{ s} \left( \frac{\lambda_{323}}{10^{-14}} \right)^{-2} \left( \frac{m_{\tilde{\tau}}}{100 \text{ GeV}} \right)^{-1}. \quad (4.7)$$

Therefore, *R*-parity violating couplings as tiny as  $10^{-14}$  are sufficient to deplete the NLSP abundance to harmless levels before the onset of BBN. For a neutralino NLSP, a very similar argument applies. Therefore, the assumption of a very mild violation of *R*-parity can completely avoid all problems with primordial nucleosynthesis introduced by the additional supersymmetric particles.

#### 4.3.2 Baryogenesis without *R*-Parity

A possible non-conservation of *R*-parity also has interesting consequences for baryogenesis. On the one hand, the new baryon and lepton number violating interactions provide a potential source of baryon asymmetry. On the other hand, since the *R*-parity violating operators contain lepton doublets, they contribute to the washout processes, potentially rendering the baryogenesis process ineffective. The *R*-parity violating interactions must therefore not be too strong, which yields an upper bound on the corresponding couplings from cosmology. The

requirement that an existing baryon asymmetry is not erased before the electroweak phase transition typically implies an upper limit on the couplings given by [27, 28, 29]

$$\lambda_{ijk}, \lambda'_{ijk} < 10^{-7}. \quad (4.8)$$

This bound can be slightly relaxed for certain flavor structures. Together with the lower bound on *R*-parity violation from the BBN requirement of having a sufficiently short NLSP lifetime, we therefore find a preferred window for the couplings of

$$10^{-14} < \lambda_{ijk}, \lambda'_{ijk} < 10^{-7}. \quad (4.9)$$

While this window spans several orders of magnitude, the questions whether this breaking, which necessarily leads to LSP decay, is compatible with gravitino dark matter, and whether such small *R*-parity violating couplings can naturally arise, must be addressed.

### 4.3.3 Gravitino Dark Matter with Broken *R*-Parity

The most immediate consequence of *R*-parity violation in the context of dark matter is that it renders the lightest supersymmetric particle unstable, enabling it to decay into final states containing only Standard Model particles. For the neutralino dark matter scenario, this is lethal as it makes the neutralinos decay too fast to still constitute the dark matter. In general, however, the LSP can still constitute the dark matter as long as its lifetime is longer than the age of the Universe. The primordial LSP abundance is then not reduced significantly in the time between its creation in the early Universe and the present day. This generally restricts the *R*-parity violating couplings to be very small.

We now entertain the possibility that the gravitino itself may constitute the dark matter of the Universe. As we have seen from Eq. (3.40), the correct relic density can be achieved for typical supersymmetric parameters if the high reheating temperature is rather large,  $T_R > 10^9$  GeV, which is nicely compatible with thermal leptogenesis [30]. The question is if the gravitino lifetime is sufficiently long in the presence of *R*-parity violation for gravitinos to still constitute the dominant component of the dark matter. This is indeed the case; as it turns out, the gravitino does in fact remain a viable dark matter candidate even if *R*-parity is broken [31]. The gravitino lifetime in terms of the *R*-parity violating couplings is given by [32, 33]

$$\tau_{3/2} \simeq 10^{23} \text{ s} \left( \frac{\lambda}{10^{-7}} \right)^{-2} \left( \frac{m_{3/2}}{100 \text{ GeV}} \right)^{-3}. \quad (4.10)$$

The long lifetime is a result of the fact that the gravitino decay rate is doubly suppressed both by the Planck scale and the smallness of the *R*-parity violating couplings. For  $m_{3/2} = 100$  GeV, the range of *R*-parity violating Yukawa couplings given above therefore corresponds to gravitino lifetimes of

$$10^{23} \text{ s} < \tau_{3/2} < 10^{37} \text{ s}, \quad (4.11)$$

which is easily compatible with gravitino dark matter, since such lifetimes exceed the age of the Universe,  $T \sim 4 \times 10^{17}$  s, by many orders of magnitude.

In summary, we find that the assumption of a high reheating temperature  $T_R \gtrsim 10^{10}$  GeV, *R*-parity violating couplings in the range  $10^{-14} < \lambda, \lambda' < 10^{-7}$  and gravitino dark matter

	$\mathbf{10}_i$	$\bar{\mathbf{5}}_i$	$\mathbf{1}_i$	$H_u$	$H_d$	$N$	$N^c$	$\Phi$	$X$	$Z$
$R$	1	1	1	0	0	0	-2	-1	4	0

Table 4.1: *R*-charges of matter fields, Higgs fields and  $SO(10)$  singlets

with a mass  $m_{3/2} \gtrsim 10$  GeV can reconcile the seemingly incompatible paradigms of thermal leptogenesis, Big Bang nucleosynthesis and supersymmetric dark matter. This is the scenario that we will adopt for the remaining discussion and whose phenomenological signatures we will work out.

#### 4.4 A Model for *R*-Parity Violation

After having found that thermal leptogenesis, Big Bang nucleosynthesis and supersymmetric dark matter are compatible for small *R*-parity violating couplings,  $10^{-14} < \lambda, \lambda' < 10^{-7}$ , the question is if such small couplings in this range can be naturally generated. We present a sample model proposed by Buchmüller, Covi, Hamaguchi, Ibarra and Yanagida [3] that accomplishes this by tying *R*-parity violation to spontaneous breaking of  $B - L$ .

The model contains the usual three generations of quarks and leptons in the  $SU(5)$  representations  $\mathbf{10}_i = (Q, U^c, E^c)_i$ ,  $\bar{\mathbf{5}}_i = (D^c, L)_i$  and  $\mathbf{1}_i = \nu_i^c$ , as well as the two Higgs doublets  $H_u$  and  $H_d$ . In addition, we have two Standard Model singlets  $N^c$  and  $N$ , as well as three  $SO(10)$  singlets  $X$ ,  $\Phi$  and  $Z$ . Since  $N$  and  $N^c$  are contained in a  $\mathbf{16}$  and a  $\bar{\mathbf{16}}$  of  $SO(10)$ , their  $B - L$  charges must be +1 and -1, respectively. The  $SO(10)$  singlets  $X$ ,  $\Phi$  and  $Z$  have  $B - L$  charge 0.  $\Phi$  will eventually be replaced by its expectation value,  $\langle \Phi \rangle = v_{B-L}$ . Furthermore, the spectator field  $Z$  will acquire a non-vanishing *F*-term,  $\langle Z \rangle = F_Z \theta \theta$ , which breaks supersymmetry and  $U(1)_R$ .

The symmetry group of the model is the Standard Model gauge group times a  $U(1)_{B-L}$  and a  $U(1)_R$  symmetry,

$$G = SU(3)_C \times SU(2)_L \times U(1)_Y \times U(1)_{B-L} \times U(1)_R. \quad (4.12)$$

The superpotential for the matter fields is the sum of the usual MSSM part plus a seesaw part and a term to generate the right-handed neutrino mass matrix,

$$W_M = h_{ij}^u \mathbf{10}_i \mathbf{10}_j H_u + h_{ij}^d \bar{\mathbf{5}}_i \mathbf{10}_j H_d + h_{ij}^\nu \bar{\mathbf{5}}_i \mathbf{1}_j H_d + \frac{1}{M_P} h_{ij}^n \mathbf{1}_i \mathbf{1}_j N^2, \quad (4.13)$$

The vacuum expectation values of the Higgs doublets will generate the Dirac masses for the quark and lepton fields, while the vacuum expectation value of the Higgs field  $N$  generates Majorana masses for the right-handed neutrinos  $\mathbf{1}_i$ . In addition, we assume another part of the superpotential that will eventually break  $B - L$ ,

$$W_{B-L} = X(NN^c - \Phi^2), \quad (4.14)$$

where the Yukawa couplings have been set to one. The dangerous superpotential terms

$$\bar{\mathbf{5}}_i H_d N^c, \quad \bar{\mathbf{5}}_i \bar{\mathbf{5}}_j \mathbf{10}_k N^c \quad (4.15)$$

would induce after  $B - L$  breaking a bilinear  $R$ -parity violating mixing leading to too large neutrino masses on the one hand, and  $R$ -parity violating trilinear terms leading to rapid proton decay on the other hand. One gets rid of these terms by introducing a global  $U(1)_R$  symmetry and by assigning  $R$ -charge  $-2$  to  $N^c$ . The dangerous terms are then forbidden by  $R$ -invariance.

When  $\Phi$  develops a VEV  $\langle \Phi \rangle = v_{B-L}$ ,  $B - L$  is broken by the superpotential  $W_{B-L}$ , and a Majorana mass matrix  $M$  for the right-handed neutrinos is generated by the VEV  $\langle N \rangle$ , since the expectation values satisfy the relation

$$\langle N \rangle = \langle N^c \rangle = \langle \Phi \rangle = v_{B-L}. \quad (4.16)$$

To make contact with the low-energy world, one can integrate out the heavy right-handed Majorana neutrinos to obtain an effective superpotential. After doing so, the superpotential reads

$$W_M = h_{ij}^u \mathbf{10}_i \mathbf{10}_j H_u + h_{ij}^d \bar{\mathbf{5}}_i \mathbf{10}_j H_d - \frac{1}{2} \left( h^\nu \frac{1}{M} h^{\nu T} \right)_{ij} (\bar{\mathbf{5}}_i H_u) (\bar{\mathbf{5}}_j H_u), \quad (4.17)$$

where the last term is the dimension-5 seesaw operator responsible for generating light neutrino masses.

Since  $\Phi$  carries  $R$ -charge  $-1$ , the VEV  $\langle \Phi \rangle = v_{B-L}$  also breaks  $R$ -parity, in contrast to the VEV  $\langle Z \rangle$  which is  $R$ -parity conserving. The breaking of  $R$ -parity is therefore coupled to  $B - L$  breaking. This does not immediately affect the matter fields, since they have no coupling to  $\Phi$  at lowest order. However, the breaking is transmitted to the low-energy degrees of freedom via higher-dimensional operators in the superpotential and the Kähler potential.

Since the superpotential is holomorphic, no  $R$ -parity violating terms can arise from the superpotential at any order in perturbation theory. However, the Kähler potential is not restricted by holomorphicity and can be a source of  $R$ -parity violation. The leading correction to the Kähler potential that leads to the breaking of  $R$ -parity is

$$\delta K_1 = \frac{1}{M_{\text{P}}^3} (a_i Z^\dagger + a'_i Z) \Phi^\dagger N^c \bar{\mathbf{5}}_i H_u + \frac{1}{M_{\text{P}}^3} (c_i Z^\dagger + c'_i Z) \Phi N^\dagger \bar{\mathbf{5}}_i H_u + \text{h.c.} \quad (4.18)$$

We can replace the spectator fields  $Z$ ,  $N^c$  and  $\Phi$  by their VEVs. This yields the following correction to the superpotential:

$$\delta W_1 = \mu_i \Theta \bar{\mathbf{5}}_i H_u, \quad (4.19)$$

with  $\mu_i = \mathcal{O}(m_{3/2})$ . This is just the bilinear  $R$ -parity violating operator from Eq. (4.4). In this equation,

$$\Theta = \frac{v_{B-L}^2}{M_{\text{P}}^2} \simeq \frac{M_3}{M_{\text{P}}}, \quad (4.20)$$

where  $M_3 \simeq v_{B-L}^2 / M_{\text{P}}$  if the largest eigenvalue of  $h^n$  is of order 1. The gravitino mass is

given by

$$m_{3/2} = \frac{F_Z}{\sqrt{3}M_{\text{P}}}. \quad (4.21)$$

We also have the correction to the Kähler potential

$$\delta K_0 = \frac{k}{M_{\text{P}}} Z^\dagger H_d H_u + \text{h.c.}, \quad (4.22)$$

which yields an *R*-parity conserving superpotential mass term for the Higgs doublets,

$$\delta W_0 = \mu H_d H_u, \quad (4.23)$$

with  $\mu = \mathcal{O}(m_{3/2})$ . Since the operators that generate  $\mu$  and  $\mu_i$  have different mass-dimension, we can have  $\mu > \mu_i, m_{3/2}$  and a gravitino LSP. Before analyzing the resulting superpotential in terms of superfields, one can redefine the Higgs and lepton fields in order to rotate away the bilinear terms,

$$H_d = H'_d - \varepsilon_i L'_i, \quad L_i = L'_i + \varepsilon_i H'_d, \quad (4.24)$$

where  $\varepsilon_i = \mu_i \Theta / \mu$ . This leads to a superpotential with trilinear *R*-parity violation. Expressed in terms of superfields, we get the superpotential

$$\begin{aligned} W &= W_M + \delta W_0 + \delta W_1 \\ &= \mu H'_d H_u + h_{ij}^u Q_i U_j^c H_u + h_{ij}^d D_i^c Q_j H'_d + h_{ij}^e L'_i E_j^c H'_d \\ &\quad - \varepsilon_k h_{ij}^d D_i^c Q_j L'_k - \frac{1}{2} \left( h^\nu \frac{1}{M} h^{\nu T} \right)_{ij} (L'_i H_u)(L'_j H_u) + \mathcal{O}(\varepsilon^2, \varepsilon m_\nu). \end{aligned} \quad (4.25)$$

The bilinear mixing of Higgs and lepton superfields induces after the field redefinition trilinear *R*-parity breaking terms of order  $\mathcal{O}(\varepsilon)$ , so that all the *R*-parity violation is now encoded in the trilinears. Interestingly, the operators leading to proton decay are suppressed by higher orders of the Planck scale. The leading operator is

$$\delta W_2 = \frac{1}{M_{\text{P}}^5} U^c D^c D^c N^c \Phi^3 X. \quad (4.26)$$

Replacing the fields by their VEVs, one then gets

$$\delta W_2 \propto \frac{m_{3/2} v_{B-L}^4}{M_{\text{P}}^5} U^c D^c D^c + \dots \quad (4.27)$$

For any *B* – *L* breaking scale that yields couplings in the range  $10^{-14} < \lambda, \lambda' < 10^{-7}$ , the contribution to proton decay from this operator is completely negligible. The size of the couplings and therefore the phenomenological viability of the model depends on the *B* – *L* breaking scale  $v_{B-L}$ .

Since the trilinear *R*-parity violating couplings are generated as

$$\lambda_{ijk} = \varepsilon_k h_{ij}, \quad (4.28)$$

they are suppressed by a factor  $v_{B-L}^2 / M_{\text{P}}^2$  and a factor  $\mathcal{O}(0.01 \dots 1)$  that depends on the

flavor structure of the Kähler potential. We can expect the couplings to be hierarchical in the same way as the Yukawa couplings  $h_{ij}$  and thus to be largest for the third generation. For the flavor model proposed in [34], one obtains couplings of order  $\lambda_{3ij}, \lambda'_{3ij} \sim 10^{-8}$  and  $\lambda'' \sim 10^{-28}$ . For an appropriate choice of flavor structure, this model can therefore indeed yield a gravitino LSP with *R*-parity violating couplings in the required range.

## Chapter 5

# The Source Term for Gravitino Decay Products

Having set the stage in the previous chapters, we are now ready to begin our analysis of possible indirect signatures of gravitino dark matter decay. The annihilation or decay of dark matter in the Milky Way halo and at cosmological distances potentially offers the exciting possibility of indirect dark matter searches. Indirect dark matter detection aims to detect secondary particles created in dark matter annihilations or decays, not the dark matter itself. These particles, if existent, will reach us in the form of gamma rays and high-energy cosmic rays. For gravitino dark matter, the possibility of indirect detection is especially crucial, since gravitinos are undetectable in direct dark matter searches due to their extremely weak interactions.

In order for the indirect approach to work, the respective primary fluxes must in principle be distinguishable against the background from ordinary astrophysical processes. Therefore, one should ideally have low, well-understood backgrounds that can be accurately measured, so that possible exotic contributions can be more or less reliably identified. There are four main channels that meet these requirements at least partially, and which are therefore suitable targets to look for potential indirect dark matter signatures. These include gamma rays, neutrinos, positrons and antiprotons. In this thesis we will cover the gamma-ray and anti-matter signatures. Interestingly enough, as we shall see, even for gravitino lifetimes far in excess of the age of the Universe, the decay products may be observable in present and future experiments due to the sheer amount of dark matter present in the Universe.

Calculating indirect dark matter signatures is done in two steps. First, the spectra of secondary particles produced in dark matter annihilations or decays must be determined at the time of injection. Then, these spectra have to be propagated to our position in the Galaxy, where measurements are made. In this chapter, we derive the source term for gamma rays, positrons and antiprotons from gravitino decay. The three ingredients in the source term are the dark matter halo profile, the branching ratios into the different decay channels that produce these particles, and the differential energy spectra of the secondary particles produced in gravitino decays.

## 5.1 Distribution of Dark Matter in the Galaxy

Due to the extremely weak gravitational-strength interactions, self-annihilations do not play any significant role for gravitino dark matter. Instead, only the  $R$ -parity violating decay of gravitinos will produce secondary particles. In the case of decaying dark matter, the amount of decay products is simply proportional to the dark matter mass density  $\rho_{\text{DM}}(\vec{r})$ .

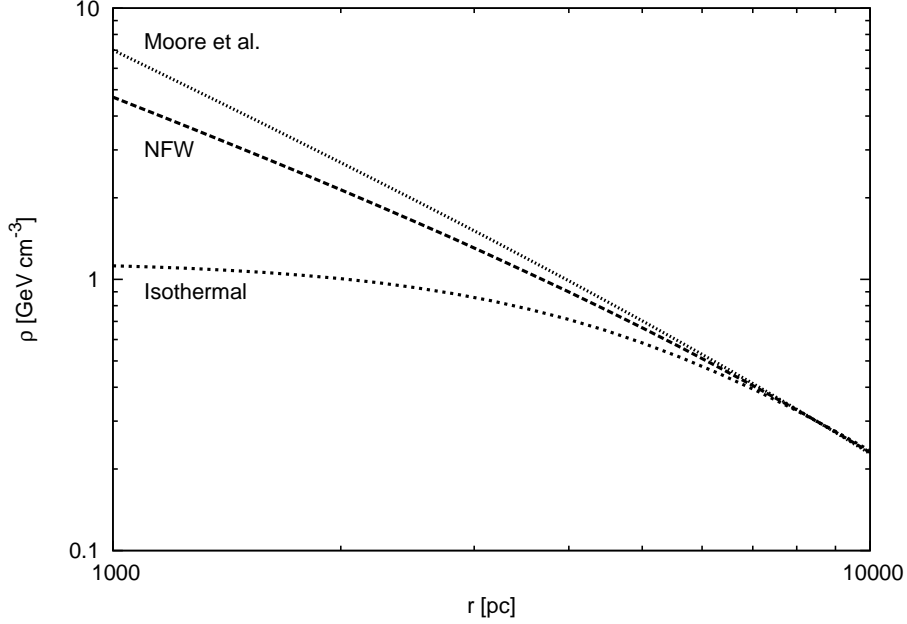


Figure 5.1: Comparison of different dark matter halo profiles. Within a few kiloparsecs around the Sun at  $r_{\odot} = 8.5$  kpc, the different profiles are rather similar, while they differ drastically towards the Galactic center.

For a quantitative analysis of dark matter signatures, it is therefore necessary to know how the dark matter is distributed in our Galaxy. What is known from the flat Galactic rotation curve is that the dark matter density should fall off at large distances as  $r^{-2}$ . The distribution in the inner regions of the Milky Way is much more uncertain. Numerical  $N$ -body simulations tend to produce dark matter halo profiles with a central cusp, while observations favor a halo profile that is flat in the inner region of the Galaxy, a so-called cored profile. The halo density profiles are usually parametrized as a spherically symmetric mass density in one of two equivalent ways. One can either use the parametrization

$$\rho_{\text{DM}}(r) = \rho_{\odot} \left( \frac{r_{\odot}}{r} \right)^{\gamma} \left( \frac{1 + (r_{\odot}/r_c)^{\alpha}}{1 + (r/r_c)^{\alpha}} \right)^{(\beta-\gamma)/\alpha}, \quad (5.1)$$

with  $r_{\odot} = 8.5$  kpc being the distance of the Sun from the center of the Galaxy and  $\rho_{\odot}$  being the local dark matter density. An alternative way to express the halo density is to write

$$\rho_{\text{DM}}(r) = \frac{\rho_0}{(r/r_c)^{\gamma} [1 + (r/r_c)^{\alpha}]^{(\beta-\gamma)/\alpha}}, \quad (5.2)$$

where the density parameter  $\rho_0$  is different for each halo profile and chosen such that  $\rho(r_{\odot}) =$

Halo Model	$\alpha$	$\beta$	$\gamma$	$r_c$ [kpc]
Isothermal	2	2	0	5
Navarro, Frenk and White [36]	1	3	1	20
Moore et al. [37]	1.5	3	1.3	30

Table 5.1: Parameters for different dark matter halo profiles

$\rho_\odot$ . The parameters  $\alpha, \beta$  and  $\gamma$  are listed in Table 5.1 for three commonly used halo profiles, namely the cored isothermal profile, the Navarro, Frenk and White (NFW) profile, and the Moore et al. profile. The local halo density is known only within a factor of two or so and is assumed to be  $\rho_\odot = 0.3 \text{ GeV cm}^{-3}$  [35] in the following. The different profiles are plotted in Fig. 5.1 for comparison. There we see that the Moore et al. profile has the highest dark matter density throughout, while the isothermal profile has the lowest. Since the abundances of decay products are proportional to the dark matter density, we can expect to see this reflected in the halo-dependence of the cosmic-ray fluxes. Numerical simulations also indicate that dark matter tends to form substructures. This does not enhance the signals from decaying dark matter, in contrast to the case of annihilating dark matter, where the dependence on the square of the dark matter density can lead to significant enhancements by so-called boost factors. The independence of boost factors makes predictions for decaying dark matter more robust than those for annihilating dark matter.

We define the source term  $Q_X(E, \vec{r})$  as the number of particles created in a volume element at  $\vec{r}$  per unit energy and time. For some particle species  $X$  it is simply proportional to the gravitino decay width, the gravitino number density and the differential energy spectrum,

$$Q_X(E, \vec{r}) = \frac{1}{m_{3/2}\tau_{3/2}} \rho_{\text{DM}}(\vec{r}) \frac{dN_X}{dE}. \quad (5.3)$$

where  $m_{3/2}$  and  $\tau_{3/2}$  denote the gravitino mass and lifetime, and  $dN_X/dE$  is the differential energy spectrum of particle  $X$  produced in the decays of gravitinos.

## 5.2 Decay Rates and Branching Ratios

We now turn to the determination of gravitino decay rates and branching ratios. Since in our scenario the gravitino is the lightest supersymmetric particle, it can only decay via  $R$ -parity violating interactions into pure Standard Model final states. The relevant decay processes, which will potentially produce indirect signatures are

$$\psi_{3/2} \rightarrow \gamma\nu, \quad (5.4)$$

$$\psi_{3/2} \rightarrow Z^0\nu, \quad (5.5)$$

$$\psi_{3/2} \rightarrow W^\pm l^\mp, \quad (5.6)$$

where the latter two are only accessible if the gravitino is heavier than the respective gauge boson. These decay channels arise due to the bilinear gaugino-lepton mixing discussed in Chapter 4. The corresponding diagrams are shown in Fig. 5.2. We neglect three-body decays here, which will be suppressed by a phase space factor and coupling factors. From the direct

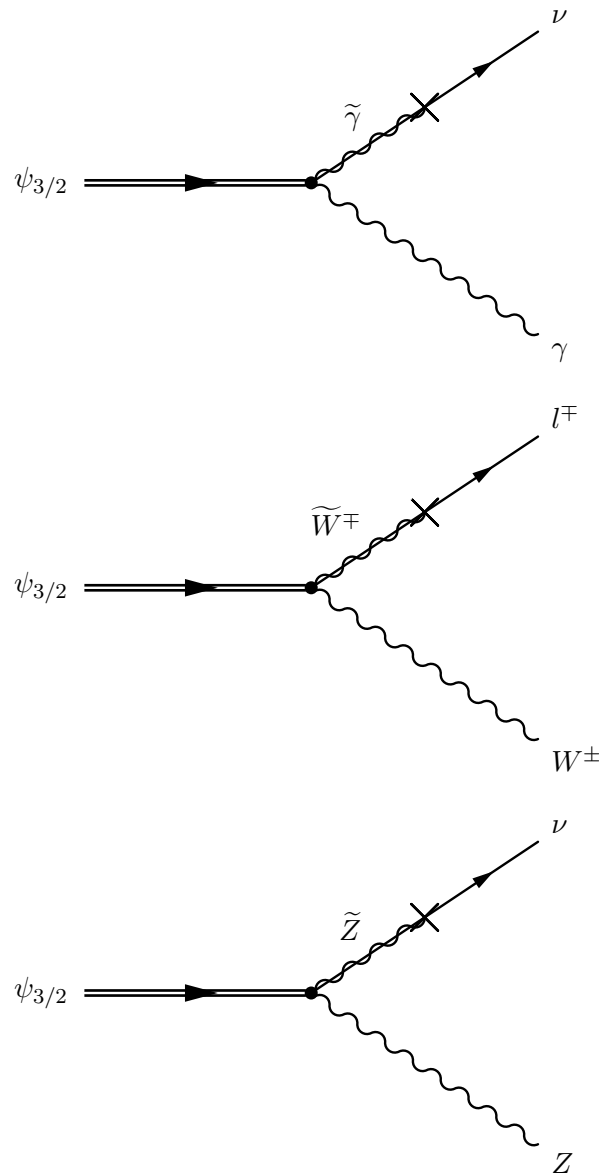


Figure 5.2:  $R$ -parity violating gravitino decay modes. The crosses denote the gaugino-lepton mixing arising from a non-vanishing sneutrino VEV.

production of photons, neutrinos and charged leptons in the two-body decays one gets hard monochromatic lines in the respective spectra. If the decay channels containing the gauge bosons are kinematically open, the fragmentation of the gauge bosons will produce a continuous spectrum of all kinds of particles.

The decay rates can be calculated from the gravitino-gaugino-gauge boson interaction

part of the supergravity Lagrangian [8]. We get for the decay rates in the different channels

$$\Gamma(\psi_{3/2} \rightarrow \gamma\nu) \simeq \frac{1}{32\pi} |U_{\tilde{\gamma}\nu}|^2 \frac{m_{3/2}^2}{M_{\text{P}}^2}, \quad (5.7)$$

$$\Gamma(\psi_{3/2} \rightarrow W^\pm l^\mp) \simeq \frac{1}{16\pi} |U_{\tilde{W}\tau}|^2 \frac{m_{3/2}^3}{M_{\text{P}}^2} f\left(\frac{M_W}{m_{3/2}}\right), \quad (5.8)$$

$$\Gamma(\psi_{3/2} \rightarrow Z^0\nu) \simeq \frac{1}{32\pi} |U_{\tilde{Z}\nu}|^2 \frac{m_{3/2}^3}{M_{\text{P}}^2} f\left(\frac{M_Z}{m_{3/2}}\right), \quad (5.9)$$

where the kinematical function  $f$  is defined as

$$f(x) := 1 - \frac{4}{3}x^2 + \frac{1}{3}x^8. \quad (5.10)$$

These decay rates are derived in Appendix A.

The decay rates are proportional to the  $R$ -parity violating mixing parameters  $|U_{ij}|^2$  which stem from the diagonalization of the neutralino-neutrino mass matrix. The values of these parameters are determined by the structure of the  $R$ -parity violation and are thus model-dependent. However, we do not need to know the absolute value of these parameters if we can find model-independent relations between the mixing parameters.

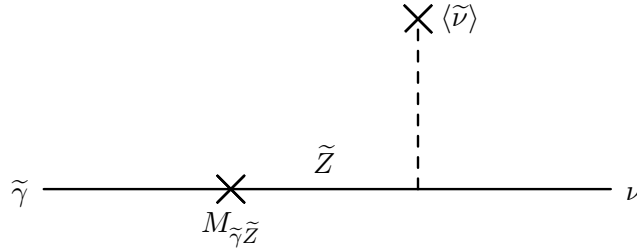


Figure 5.3: Effective photino–neutrino mixing induced by photino–Zino mixing

As explained in Chapter 4, we can choose to work in a basis where the  $\mu_i$  are zero, so that the only source of  $R$ -parity violation is the sneutrino VEV  $\langle \tilde{\nu} \rangle = v_3$ . This  $R$ -parity violation will induce mixings leading to the extended neutralino-neutrino and chargino-charged lepton mass matrices, Eq. (4.5) and Eq. (4.6). At lowest order then, the only particle that mixes with the neutrino is the Zino via

$$M_{\tilde{Z}\nu} = -\frac{g}{2\cos\theta_W} v_3, \quad (5.11)$$

which gives a mixing between Zino and neutrino approximately given by

$$|U_{\tilde{Z}\nu}| \simeq \left| \frac{M_{\tilde{Z}\nu}}{M_{\tilde{Z}\tilde{Z}}} \right| = \frac{g}{2c_W} \frac{v_3}{M_1 s_W^2 + M_2 c_W^2}, \quad (5.12)$$

which is a good approximation if the Zino is approximately a mass eigenstate. As for the photino-neutrino mixing, we note that photinos do not directly couple to neutrinos. However, an effective photino-neutrino mixing is induced indirectly via the combination of photino-

Zino and Zino-neutrino mixing, as shown diagrammatically in Fig. 5.3. This mixing is approximately given by

$$M_{\tilde{\gamma}\nu} \simeq \frac{M_{\tilde{\gamma}\tilde{Z}}}{M_{\tilde{Z}\tilde{Z}}} M_{\tilde{Z}\nu} = - \left( \frac{(M_2 - M_1)s_W c_W}{M_1 s_W^2 + M_2 c_W^2} \right) \frac{g}{2c_W} v_3. \quad (5.13)$$

One finds that the corresponding mixing is

$$|U_{\tilde{\gamma}\nu}| \simeq \left| \frac{M_{\tilde{\gamma}\nu}}{M_{\tilde{\gamma}\tilde{\gamma}}} \right| = \left( \frac{(M_2 - M_1)s_W c_W}{M_1 s_W^2 + M_2 c_W^2} \right) \frac{g}{2c_W} \frac{v_3}{M_1 c_W^2 + M_2 s_W^2}. \quad (5.14)$$

Comparing with the above, we see that  $|U_{\tilde{\gamma}\nu}|$  is proportional to  $|U_{\tilde{Z}\nu}|$ ,

$$|U_{\tilde{\gamma}\nu}| \simeq \left| \frac{M_{\tilde{\gamma}\tilde{Z}}}{M_{\tilde{\gamma}\tilde{\gamma}}} \right| |U_{\tilde{Z}\nu}| = \frac{(M_2 - M_1)s_W c_W}{M_1 c_W^2 + M_2 s_W^2} |U_{\tilde{Z}\nu}|. \quad (5.15)$$

The chargino-charged lepton mixing is determined by the matrix element

$$M_{\tilde{W}\tau} = \frac{g}{\sqrt{2}} v_3. \quad (5.16)$$

This gives us for the mixing parameter

$$|U_{\tilde{W}\tau}| \simeq \left| \frac{M_{\tilde{W}\tau}}{M_{\tilde{W}\tilde{W}}} \right| = \frac{g}{\sqrt{2}} \frac{v_3}{M_2}. \quad (5.17)$$

If we compare this with the Zino-neutrino mixing, we find the relationship

$$|U_{\tilde{W}\tau}| \simeq \left| \frac{M_{\tilde{W}\tau}}{M_{\tilde{W}\tilde{W}}} \right| \left| \frac{M_{\tilde{Z}\tilde{Z}}}{M_{\tilde{Z}\nu}} \right| |U_{\tilde{Z}\nu}| = \sqrt{2} c_W \frac{M_1 s_W^2 + M_2 c_W^2}{M_2} |U_{\tilde{Z}\nu}|. \quad (5.18)$$

The mixing  $|U_{\tilde{W}\tau}|$  is therefore related to  $|U_{\tilde{Z}\nu}|$  by  $SU(2)_L$  gauge invariance,

$$|U_{\tilde{W}\tau}| \simeq \sqrt{2} c_W \left| \frac{M_{\tilde{Z}\tilde{Z}}^n}{M_{\tilde{W}}} \right| |U_{\tilde{Z}\nu}|. \quad (5.19)$$

The relative values of the mixing parameters therefore only depend on the  $2 \times 2$  sub-block of the mass matrix,

$$M_N^{2 \times 2} = \begin{pmatrix} M_1 c_W^2 + M_2 s_W^2 & (M_2 - M_1)s_W c_W \\ (M_2 - M_1)s_W c_W & M_1 s_W^2 + M_2 c_W^2 \end{pmatrix}. \quad (5.20)$$

The only unknown parameters remaining in the decay rates are the gravitino mass and the gaugino masses at low energies. We fix the ratio between the gaugino masses by assuming that the gaugino masses unify at the grand unification scale,  $M_X = 2 \times 10^{16}$  GeV, such that  $M_1(M_X) = M_2(M_X)$ . One can then obtain the ratio between the gaugino masses at low energies by renormalization group evolution, which yields a ratio of

$$M_1(M_Z) = \frac{5}{3} \tan^2 \theta_W M_2(M_Z) \simeq \frac{1}{1.89} M_2(M_Z). \quad (5.21)$$

Under the assumption of gaugino mass universality, we thus get ratios between the decay rates that only depend on the gravitino mass. Since we do not need to know the absolute values of the mixing parameters, but only the ratios between them, we can express them all in terms of the common factor  $|U_{\tilde{Z}\nu}|$ . From the above relations, we get approximately  $|U_{\tilde{\gamma}\nu}| \simeq 0.31|U_{\tilde{Z}\nu}|$  and  $|U_{\tilde{W}\tau}| \simeq 1.09|U_{\tilde{Z}\nu}|$ , or

$$|U_{\tilde{\gamma}\nu}| : |U_{\tilde{Z}\nu}| : |U_{\tilde{W}\tau}| \simeq 1 : 3.2 : 3.5. \quad (5.22)$$

Using these relations between the mixing parameters, we can calculate the branching ratios in which the mixing parameters will cancel out, leaving only the dependency on the gravitino mass  $m_{3/2}$ :

$$\text{BR}(\psi_{3/2} \rightarrow \gamma\nu)(m_{3/2}) \simeq \frac{\Gamma(\psi_{3/2} \rightarrow \gamma\nu)}{\Gamma_{\text{tot}}}, \quad (5.23)$$

$$\text{BR}(\psi_{3/2} \rightarrow W^\pm l^\mp)(m_{3/2}) \simeq \frac{\Gamma(\psi_{3/2} \rightarrow W^\pm l^\mp)}{\Gamma_{\text{tot}}}, \quad (5.24)$$

$$\text{BR}(\psi_{3/2} \rightarrow Z^0\nu)(m_{3/2}) \simeq \frac{\Gamma(\psi_{3/2} \rightarrow Z^0\nu)}{\Gamma_{\text{tot}}} \quad (5.25)$$

with the total decay rate  $\Gamma_{\text{tot}}$  given by the sum of all the kinematically accessible decay rates.

$$\Gamma_{\text{tot}} \simeq \Gamma(\psi_{3/2} \rightarrow \gamma\nu) + \Gamma(\psi_{3/2} \rightarrow W^\pm l^\mp) + \Gamma(\psi_{3/2} \rightarrow Z^0\nu). \quad (5.26)$$

The resulting branching ratios as a function of the gravitino mass are plotted in Fig. 5.4. In Tab. 5.2, the numerical values of the branching ratios for a number of different gravitino masses are listed.

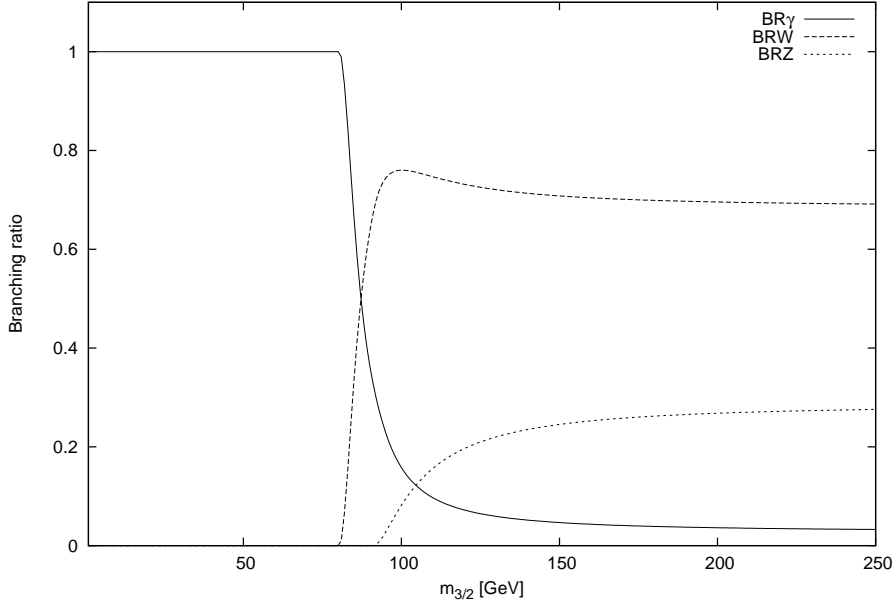


Figure 5.4: Branching ratios for the decay processes  $\psi_{3/2} \rightarrow \gamma\nu$ ,  $\psi_{3/2} \rightarrow Z^0\nu$  and  $\psi_{3/2} \rightarrow W^\pm l^\mp$  as a function of the gravitino mass.

$m_{3/2}$	$\text{BR}(\psi_{3/2} \rightarrow \gamma\nu)$	$\text{BR}(\psi_{3/2} \rightarrow Z^0\nu)$	$\text{BR}(\psi_{3/2} \rightarrow W^\pm l^\mp)$
10 GeV	1	0	0
85 GeV	0.66	0.34	0
100 GeV	0.16	0.76	0.08
150 GeV	0.05	0.71	0.24
250 GeV	0.03	0.69	0.28

Table 5.2: Branching ratios into the different  $R$ -parity violating channels for some gravitino masses.

### 5.3 Energy Spectra from Fragmentation

The first of the decay channels we computed,  $\psi_{3/2} \rightarrow \gamma\nu$ , is simply a two-body decay that produces a monochromatic photon and neutrino with an energy of  $E = m_{3/2}/2$  each. The other two decay channels,  $\psi_{3/2} \rightarrow W^\pm l^\mp$  and  $\psi_{3/2} \rightarrow Z^0\nu$ , however, produce a real gauge boson, which will subsequently fragment and produce many secondary particles in the process. The determination of the continuous differential energy spectra of the various particle species from the fragmentation of the gauge bosons over the complete energy range is a very complicated task. Nevertheless, the process is determined completely by Standard Model physics. We therefore tackled the problem using Monte Carlo methods. We used the parton shower event generator PYTHIA 6.4 [38] to simulate the gauge boson fragmentation. One should keep in mind that Monte Carlo data is not real physical data. However, it does match experimental data well, where available, and we checked the PYTHIA results for the gamma-ray spectrum against measurements from the ALEPH experiment at LEP to make sure we had set up the program correctly.

PYTHIA was created for use in collider physics simulations, so to use it in an astrophysical setting, making some modifications is mandatory. The changes mainly affect particles that are stable within a collider experiment, but unstable on astrophysical scales. The changes that were made include the following:

- Define a new particle  $\psi_{3/2}$  with mass  $m_{3/2}$  and make it decay exclusively via  $\psi_{3/2} \rightarrow W^\pm l^\mp$  OR  $\psi_{3/2} \rightarrow Z^0\nu$
- Set the leptons in the two-body gravitino decay to always have  $\tau$  flavor
- Disable bremsstrahlung off the incoming electron and positron legs
- Allow neutron decay and define the appropriate decay channel  $n \rightarrow pe^- \bar{\nu}_e$
- Make kaons, pions and muons unstable
- Force all unstable particles to decay eventually

Some of these points are crucial, since for example a major part of the antiprotons will come from the decay of neutrons, which are of course completely stable in a collider setting. The fragmentation itself was simulated by initializing the event generator as an  $e^+e^-$  collider process with a center-of-mass energy of  $E_{\text{cms}} = 2m_{3/2}$ . To simulate the decay of gravitinos, we defined a new particle with mass  $m_{3/2}$  decaying with a branching ratio of 100% into either

	$W^\pm l^\mp$	$Z^0 \nu$
$\gamma$	16.1	17.0
$e^+$	8.1	8.2
$\bar{p}$	0.8	0.8

Table 5.3: Average multiplicities of particles created in gauge boson fragmentation

$Z^0 \nu$  or into  $W^\pm l^\mp$ , depending on whether neutral or charged gauge boson fragmentation was simulated. Since we expect the third-generation coupling to be the largest, we set the leptons created in the two-body decay to have 100%  $\tau$  flavor. Schematically, the two different processes we simulated had the following form:

$$\begin{aligned} e^+ e^- &\rightarrow \psi_{3/2} \psi_{3/2} \rightarrow Z^0 \nu Z^0 \nu, \\ e^+ e^- &\rightarrow \psi_{3/2} \psi_{3/2} \rightarrow W^\pm l^\mp W^\pm l^\mp. \end{aligned}$$

Since the center-of-mass energy is set to  $2m_{3/2}$ , the two gravitinos per event are created at rest, giving the gauge bosons a momentum of

$$|\vec{p}_{W,Z}| \simeq \frac{m_{3/2}^2 - M_{W,Z}^2}{2m_{3/2}}, \quad (5.27)$$

where the masses of the leptons are neglected.

For determining the spectra of particles from the fragmentation of the gauge bosons, we simulated a large number of events to keep statistical fluctuations to a minimum. The energies of the stable final state particles of interest were then extracted from the PYTHIA output. The collected statistics were then binned in the logarithmic variable  $\xi = \ln(E/\text{GeV})$ , giving us the differential spectrum  $dN/d\xi$ . In Figures 5.5, 5.6 and 5.7, the resulting energy spectra are shown for photons, positrons and antiprotons, respectively, for a gravitino mass of 150 GeV. The bins were then interpolated and converted to the differential energy spectrum using the relation

$$\frac{dN}{dE} = \frac{1}{E} \frac{dN}{d\xi}. \quad (5.28)$$

Most of the photons and positrons come from pion decay, whereas the majority of antiprotons is created in antineutron decays.

With the results from the Monte Carlo simulation, we now know the complete source term for particles injected by gravitino dark matter decay. Due to the fact that the gravitino interactions are completely fixed by symmetries, we get a very predictive scenario with essentially only two free parameters, namely the gravitino mass and lifetime. The gravitino mass will determine the spectral shape of the secondary spectra and the gravitino lifetime their normalization. Once these two parameters are fixed, no freedom remains in the model from the particle physics point of view. To relate the source term to measurements made on or near Earth, however, we need to propagate the particles through the Galaxy or even over intergalactic distances in the case of gamma rays. This will introduce the main uncertainties in the predictions. We begin with gamma rays in the following chapter, after which we turn

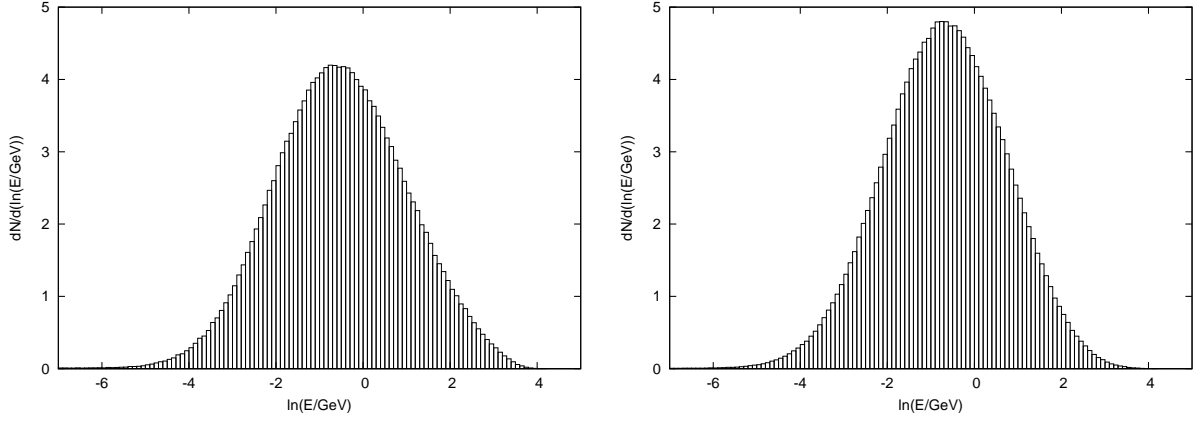


Figure 5.5: The fragmentation spectra of photons as obtained from PYTHIA for  $m_{3/2} = 150$  GeV. The spectrum from  $W^\pm$  fragmentation is on the left, the spectrum from  $Z^0$  fragmentation on the right.

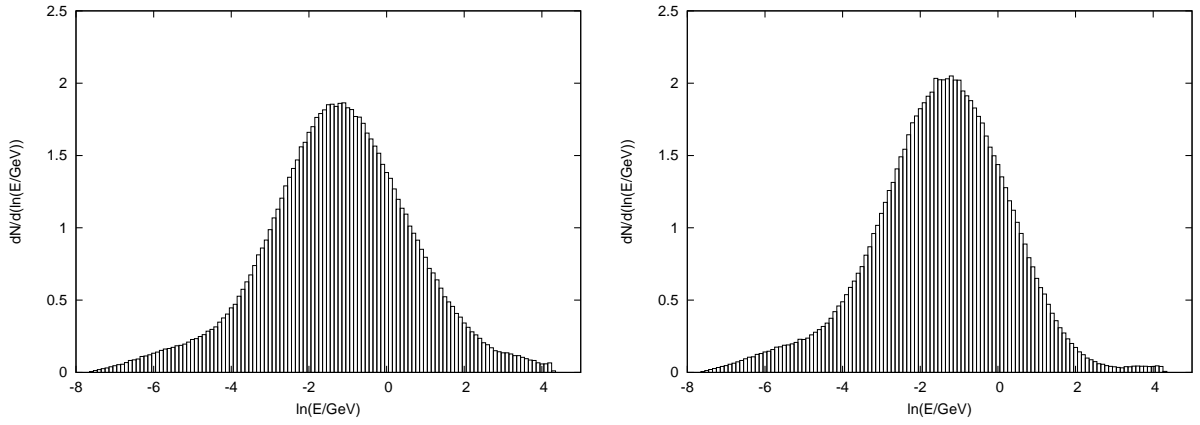


Figure 5.6: The fragmentation spectra of positrons as obtained from PYTHIA for  $m_{3/2} = 150$  GeV. The spectrum from  $W^\pm$  fragmentation is on the left, the spectrum from  $Z^0$  fragmentation on the right.

to the antimatter signatures.

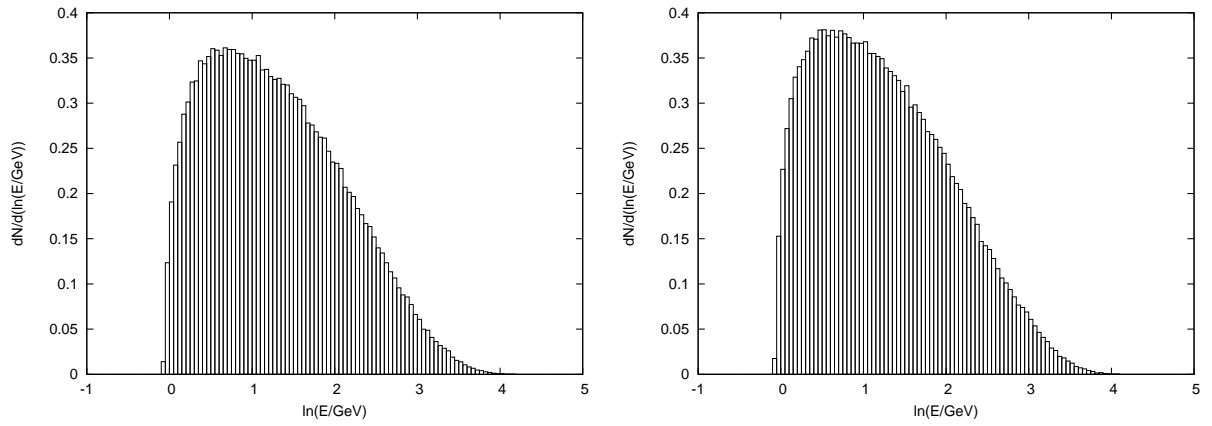


Figure 5.7: The fragmentation spectra of antiprotons as obtained from PYTHIA for  $m_{3/2} = 150$  GeV. The spectrum from  $W^\pm$  fragmentation is on the left, the spectrum from  $Z^0$  fragmentation on the right.

## Chapter 6

# Gamma Rays from Gravitino Dark Matter Decay

We begin our analysis of the indirect signatures of gravitino decay with the examination of the gamma-ray spectrum. Gamma rays are a natural probe, since any dark matter particle that is not completely sterile will at least indirectly couple to photons. Furthermore, photons propagate freely over cosmological distances, therefore preserving spectral information and pointing toward their source. Of the possible indirect dark matter signatures, the gamma-ray spectrum is certainly the cleanest one. If no signal in the gamma-ray spectrum can be distinguished, the extragalactic gamma-ray spectrum at least puts a stringent constraint on the dark matter lifetime.

### 6.1 The Diffuse Extragalactic Gamma-Ray Spectrum

Cosmic gamma rays can only be directly measured from space, since their high energy triggers air showers as they enter the Earth's atmosphere. To this day, there has been only one measurement of the extragalactic gamma-ray spectrum. This measurement was performed with the EGRET instrument aboard NASA's Compton Gamma Ray Observatory, which measured gamma rays between 30 MeV and 10 GeV.

The diffuse extragalactic gamma-ray background consists of all unresolved sources of high-energy gamma rays in the Universe. It is thought that the dominant contribution to the diffuse gamma-ray flux comes from active galactic nuclei (AGN). Other sources may include galaxy clusters, energetic particles from large scale structure formation shock waves and distant gamma-ray burst events. Extracting the diffuse extragalactic spectrum is a tricky business, as the extragalactic spectrum is basically the difference between the total diffuse spectrum measured and the Galactic foreground gamma-ray emission. Therefore, one needs to precisely know the Galactic foreground in order to reliably determine the extragalactic spectrum. This also means that any determination of the extragalactic diffuse gamma-ray background will be model-dependent.

The first analysis by Sreekumar et al. for the EGRET collaboration gave a power law

behavior with a spectral index compatible with an origin in gamma-ray blazars [39],

$$E^2 \frac{dJ}{dE} = 1.37 \times 10^{-6} \left( \frac{E}{\text{GeV}} \right)^{-0.1} (\text{cm}^2 \text{ str s})^{-1} \text{ GeV} \quad (6.1)$$

between 50 MeV – 10 GeV. However, a more recent re-analysis by Moskalenko, Strong and Reimer, made in the framework of the GALPROP numerical code and optimized in order to better reproduce the Galactic foreground emission, gave a steeper spectrum and revealed a clear, multi-GeV deviation from a power law behavior at energies above 1 GeV [40]. This spectrum is plotted in Fig. 6.1. The nature of the GeV excess is presently unclear. It may have an origin in blazars, but other, more exotic explanations like a contribution from the annihilation of heavy neutralino dark matter have been proposed [41]. It has also been claimed that this effect may be purely instrumental, resulting from a miscalibration of the detector [42].

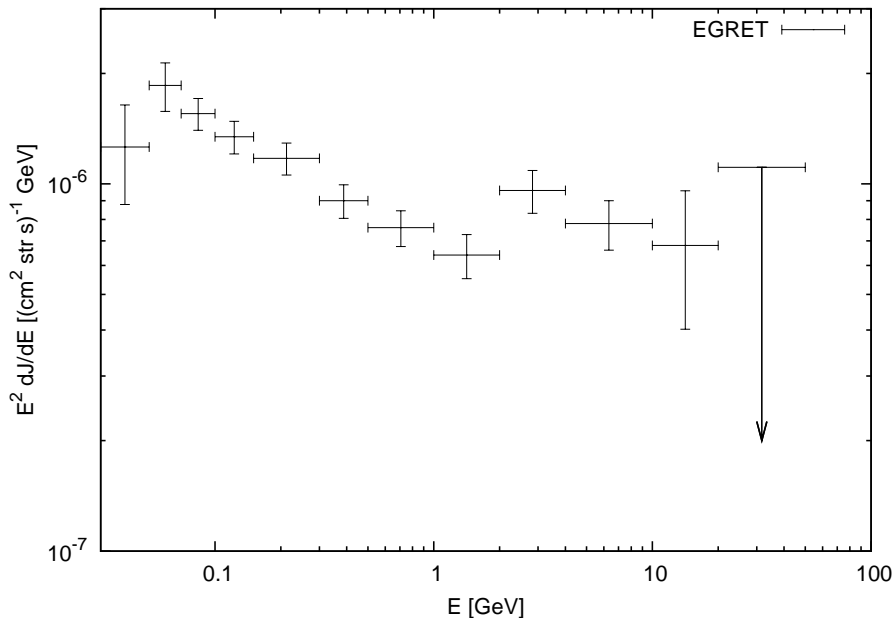


Figure 6.1: The extragalactic gamma-ray spectrum as extracted by Moskalenko, Strong and Reimer [40]. The clear deviation from a power law above 1 GeV is visible.

Interestingly, the position of the bump is in a natural energy range for photons coming from the decay of GeV scale dark matter, so we consider the intriguing possibility that the EGRET excess may have an origin in gravitino dark matter decay.

## 6.2 Gamma Rays from Gravitino Dark Matter

We now discuss the potential gamma-ray signatures from gravitino decay, or more generally from any kind of decaying dark matter. There are two contributions to the gamma-ray spectrum from decaying dark matter: one from the decays of dark matter particles in our own Milky Way halo and the other one from the decay of dark matter in the halos of other galaxies

at cosmological distances.

The differential gamma-ray flux is defined as the number of photons per unit energy, time, solid angle and detector surface,

$$\frac{dJ}{dE} = \frac{dN_\gamma^{\text{rec}}}{dE dt d\Omega dS}. \quad (6.2)$$

We first discuss the case of a light gravitino that can not decay into gauge bosons. One then gets an essentially monochromatic spectrum from the two-body decay  $\psi_{3/2} \rightarrow \gamma\nu$ . Assuming a flat Robertson-Walker universe,  $\Omega_M + \Omega_\Lambda = 1$ , we get for  $\tau_{3/2} \gg H_0^{-1}$  and using the relationship between redshift and comoving distance,

$$\frac{d\chi}{dz} = \frac{(1+z)^{-3/2}}{a_0 H_0 \sqrt{\Omega_M(1 + \Omega_\Lambda/\Omega_M(1+z)^{-3})}}, \quad (6.3)$$

one finds that in this case, the extragalactic contribution to the gamma-ray spectrum is given by

$$\left[ E^2 \frac{dJ}{dE} \right]_{\text{extra}} = C_\gamma \left( 1 + \frac{\Omega_\Lambda}{\Omega_M} \left( \frac{2E}{m_{3/2}} \right)^3 \right)^{-1/2} \left( \frac{2E}{m_{3/2}} \right)^{5/2} \theta \left( 1 - \frac{2E}{m_{3/2}} \right), \quad (6.4)$$

which essentially corresponds to a redshifted line spectrum. In this expression, we have defined the constant

$$C_\gamma = \frac{\Omega_{3/2} \rho_c}{8\pi \tau_{3/2} H_0 \Omega_M^{1/2}} \simeq 10^{-7} \left( \frac{\tau_{3/2}}{10^{28} \text{ s}} \right) \text{ GeV (cm}^2 \text{ s str)}^{-1}, \quad (6.5)$$

which roughly determines the overall magnitude of the signal. Comparing to the EGRET data, we find that if the gravitino lifetime  $\tau_{3/2}$  is less than  $\sim 10^{28}$  s, we can expect a sizable contribution to the gamma-ray flux that may be distinguishable against the background.

The component of the signal from halo decays of dark matter in the case of a light gravitino is simply given by

$$\left[ E^2 \frac{dJ}{dE} \right]_{\text{halo}} = D_\gamma(b, l) \delta \left( 1 - \frac{2E}{m_{3/2}} \right), \quad (6.6)$$

where the constant  $D_\gamma$  is defined as

$$D_\gamma(b, l) = \frac{1}{8\pi \tau_{3/2}} \int_{\text{los}} \rho_{\text{DM}}(\vec{l}) d\vec{l}, \quad (6.7)$$

where the integration extends over the line of sight (los). The halo component of the signal has an angular dependence which stems from the fact that we are not observing the flux from the center of the Galaxy. The magnitude of the halo contribution therefore depends on the amount of dark matter in the Milky Way halo in each direction of the sky.

The final component of the gamma-ray flux is the background, which we assume is still given by a power law spectrum, probably originating in faint unresolved active galactic nuclei, whose slope and normalization are left free. The total gamma-ray spectrum is therefore finally

given by

$$\left[ E^2 \frac{dJ}{dE} \right]_{\text{total}} \simeq \left[ E^2 \frac{dJ}{dE} \right]_{\text{halo}} + \left[ E^2 \frac{dJ}{dE} \right]_{\text{extra}} + \left[ E^2 \frac{dJ}{dE} \right]_{\text{back}}. \quad (6.8)$$

For comparison with the analysis by Moskalenko, Strong and Reimer [40], which assumes an isotropic signal, we must deal with the angular dependence of the signal. Since we are interested in the diffuse flux, we simply average  $D_\gamma$  over the whole sky, excluding the region of the Galactic disk between  $+10^\circ$  and  $-10^\circ$  Galactic latitude. The high-luminosity Galactic disk must be excluded if we want to compare with the diffuse flux. We define the averaged constant  $\bar{D}_\gamma$  as

$$\bar{D}_\gamma = \frac{1}{8\pi\tau_{3/2}} \left[ \int_0^{2\pi} dl \int_{10\pi/180}^{\pi/2} db \cos b \int_0^\infty dr \rho_{\text{DM}}(r, l, b) \right] \times \left[ \int_0^{2\pi} dl \int_{10\pi/180}^{\pi/2} db \cos b \right]^{-1}. \quad (6.9)$$

For the numerical results in this chapter, we adopt an NFW halo profile, but due to the averaging procedure, it really makes no difference which halo profile we choose. Interestingly, the intensity of the halo and extragalactic contribution is of the same order, with the ratio between the coefficients being given purely by cosmological parameters and the averaged dark matter halo density integrated along the line of sight,

$$\frac{\bar{D}_\gamma}{C_\gamma} = \frac{H_0 \Omega_M^{1/2}}{\Omega_{3/2} \rho_c} \left\langle \int \rho_{\text{DM}}(\vec{l}) d\vec{l} \right\rangle \simeq 0.6. \quad (6.10)$$

The coefficient  $C_\gamma$  is thus slightly larger. Nevertheless, the halo contribution is dominant because the redshift of the extragalactic contribution flattens its spectrum.

The resulting spectrum for a gravitino of  $m_{3/2} = 10$  GeV,  $\tau_{3/2} = 10^{27}$  s is shown in Fig. 6.2. The dominant contribution comes from the monochromatic halo line which has been broadened by a convolution with a Gaussian of 15% width to take the finite energy resolution of the detector into account. The other contribution corresponds to a redshifted line spectrum. While it is interesting that we can get a sizable contribution to the gamma-ray flux in the right energy range, the qualitative agreement of the spectrum with the EGRET data is only moderately convincing, as the excess seems to be much broader than a line spectrum.

A more interesting case arises when the gravitino is heavier than the electroweak gauge bosons,  $m_{3/2} > M_{W,Z}$ . We can then expect a continuous contribution to the spectrum coming from the fragmentation of the gauge bosons in addition to the monochromatic line. In this case, the differential energy spectrum of photons from gravitino decay is given by

$$\begin{aligned} \frac{dN_\gamma}{dE} &\simeq \text{BR}(\psi_{3/2} \rightarrow \gamma\nu) \delta\left(E - \frac{m_{3/2}}{2}\right) + \text{BR}(\psi_{3/2} \rightarrow W^\pm l^\mp) \frac{dN_\gamma^W}{dE} \\ &\quad + \text{BR}(\psi_{3/2} \rightarrow Z^0\nu) \frac{dN_\gamma^Z}{dE}. \end{aligned} \quad (6.11)$$

where  $dN_\gamma^W/dE$  and  $dN_\gamma^Z/dE$  denote the energy spectra from fragmentation as obtained in Chapter 5. To determine the flux corresponding to the continuous spectrum, we now have to use more general expressions for the halo and extragalactic component of the signal. If

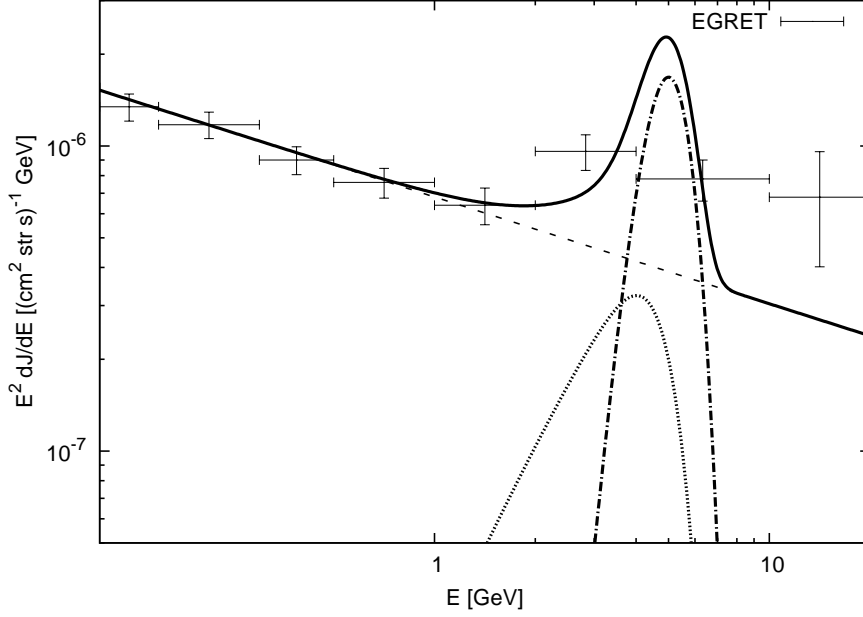


Figure 6.2: Gamma-ray spectrum for a relatively light gravitino with  $m_{3/2} = 10$  GeV,  $\tau_{3/2} = 10^{27}$  s. The background is chosen as  $E^2 dJ/dE = 6.8 \times 10^{-7} (E/\text{GeV})^{-0.35} (\text{cm}^2 \text{ str s})^{-1} \text{ GeV}$ .

the energy spectrum of the photons coming from the gravitino decay is not a delta line but a general distribution, the previous expression for the extragalactic component generalizes to

$$\left[ E^2 \frac{dJ}{dE} \right]_{\text{extra}} = \frac{2E^2}{m_{3/2}} C_\gamma \int_1^\infty d(1+z) \frac{dN_\gamma}{dE^{\text{em}}} [(1+z)E] (1+z)^{-3/2} \left( 1 + \frac{\Omega_\Lambda}{\Omega_M} (1+z)^{-3} \right)^{-1/2}, \quad (6.12)$$

where the energy spectrum is integrated over the redshift  $z$ .

The halo component of the signal is now given by the simple expression

$$\left[ E^2 \frac{dJ}{dE} \right]_{\text{halo}} = \frac{2E^2}{m_{3/2}} \bar{D}_\gamma \frac{dN_\gamma}{dE}. \quad (6.13)$$

See Appendix B for a derivation of the expressions for the gamma-ray fluxes.

In addition to the continuous spectrum from gauge boson fragmentation, one still gets the line from the two-body decay  $\psi_{3/2} \rightarrow \gamma\nu$  at half the gravitino mass. In Fig. 6.4, all the different contributions to the signal are shown for a gravitino mass of 150 GeV and a lifetime of  $10^{26}$  s. The continuous components from gauge boson fragmentation are marked in the figure with the corresponding decay channel, where the lower curves correspond to the redshifted extragalactic contribution in each case. We can already see that the continuous component of the signal may well improve the fit if added to a power law background.

In view of the systematic uncertainties, making a quantitative simultaneous fit of mass and lifetime to the EGRET data does not appear reasonable at this point. Instead, we content our-

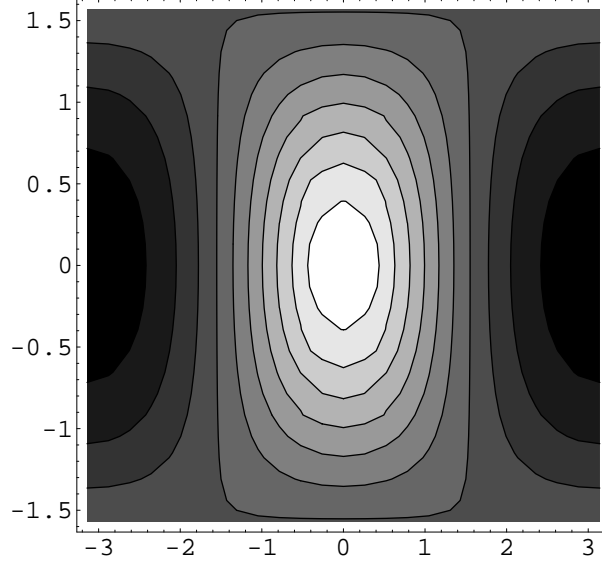


Figure 6.3: Anisotropy of the halo signal for the isothermal halo profile. Between the intensity in the direction of the center of the galaxy at  $l = 0$ ,  $b = 0$  and the anticenter at  $l = \pi$ ,  $b = 0$  there is a factor 1.7. Combined with the other components of the gamma-ray spectrum, the anisotropy is compatible with EGRET measurements.

$l$ [°]	$b$ [°]	$I \times 10^6$ (EGRET) [ $\text{cm}^{-2} \text{s}^{-1} \text{sr}^{-1}$ ]	$I \times 10^6$ (Model) [ $\text{cm}^{-2} \text{s}^{-1} \text{sr}^{-1}$ ]	Description
0 – 360	$\gtrsim \pm 10$	$11.10 \pm 0.12$	11.31	N+S hemispheres
0 – 360	$< -10$	$11.70 \pm 0.15$	11.31	N hemisphere
0 – 360	$> +10$	$9.28 \pm 0.21$	11.31	S hemisphere
270 – 90	$\gtrsim \pm 10$	$11.90 \pm 0.17$	11.64	Inner Galaxy N+S
90 – 270	$\gtrsim \pm 10$	$9.75 \pm 0.17$	10.97	Outer Galaxy N+S
0 – 180	$\gtrsim \pm 10$	$10.80 \pm 0.17$	11.31	Pos. longitudes N+S
180 – 360	$\gtrsim \pm 10$	$11.60 \pm 0.16$	11.31	Neg. longitudes N+S
270 – 90	$> +10$	$13.00 \pm 0.22$	11.64	Inner Galaxy N
270 – 90	$< -10$	$9.14 \pm 0.32$	11.64	Inner Galaxy S
90 – 270	$> +10$	$10.60 \pm 0.22$	10.97	Outer Galaxy N
90 – 270	$< -10$	$8.18 \pm 0.34$	10.97	Outer Galaxy S

Table 6.1: Comparison of the anisotropy in the diffuse extragalactic gamma-ray spectrum between the present model and the EGRET observations.  $I$  denotes the integrated flux  $E^2 dJ/dE$  between 0.1 and 10 GeV, averaged over the corresponding area of the sky. The numbers for the EGRET data are taken from [40].

selves with a qualitative manual fit to find a reasonable choice for the parameters  $m_{3/2}$ ,  $\tau_{3/2}$ . The normalization of the power law background is treated as a free parameter. The gravitino mass cannot be constrained very well on the basis of the EGRET excess due to its multi-GeV width and the relatively large error bars, but we find that a mass of around 150 GeV works

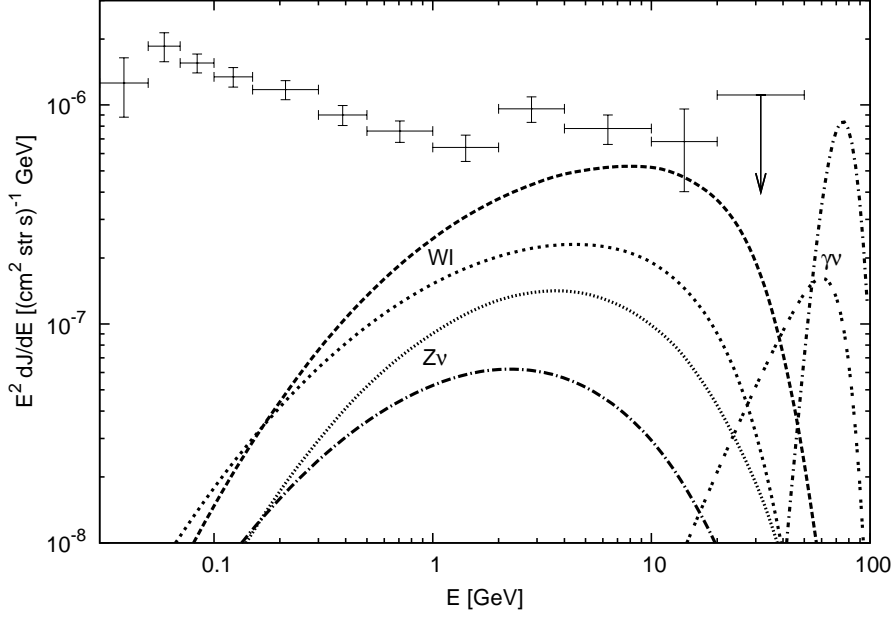


Figure 6.4: Components of the gamma-ray signal from gravitino decay for  $m_{3/2} = 150$  GeV and  $\tau_{3/2} = 10^{26}$  s. There is a contribution from gauge boson fragmentation for the  $W$  and  $Z$  channel, where the lower curves correspond to the redshifted extragalactic contribution. The monochromatic line familiar from the case of a lighter gravitino is also present with relatively high intensity.

best. The lifetime, on the other hand, can be constrained relatively well to around  $10^{26}$  s. The resulting spectrum is shown in Fig. 6.5 for  $m_{3/2} = 150$  GeV and  $\tau_{3/2} = 1.3 \times 10^{26}$  s. We find these parameters to agree qualitatively well with the EGRET excess. A mass of 150 GeV is a bit on the heavy side for the lightest supersymmetric particle, but is by no means unrealistic.

The spectral shape of the signal is quite distinct due to the combination of a continuous spectrum with a monochromatic line. The relatively intense spectral line is characteristic of the present scenario. In the case of neutralino dark matter, one would also expect a monochromatic line from the annihilation  $\chi_1^0 \chi_1^0 \rightarrow \gamma\gamma$ , but its intensity is strongly suppressed due to the fact that neutralinos only couple to photons at the quantum level [43]. Nevertheless, strong monochromatic lines could also be expected in other scenarios, e.g. in the case of inert Higgs dark matter [44]. Generally, intense monochromatic lines are not expected from conventional astrophysical processes, and would, if observed, constitute a sort of smoking-gun signature for an exotic process.

So far, we have neglected one important issue, namely the anisotropy of the gamma-ray signal from gravitino decay. As we have seen, the halo component of the signal possesses an angular dependence on the line of sight due to our off-center position in the Galaxy. This anisotropy must not be too large, since the extragalactic gamma-ray spectrum is presumably at least roughly isotropic. Therefore, we need to check if our signal is compatible with the limits on anisotropy from EGRET observations. In fact, these observations suffer from low statistics, which necessitated averaging the diffuse gamma-ray flux over quarter spheres of the

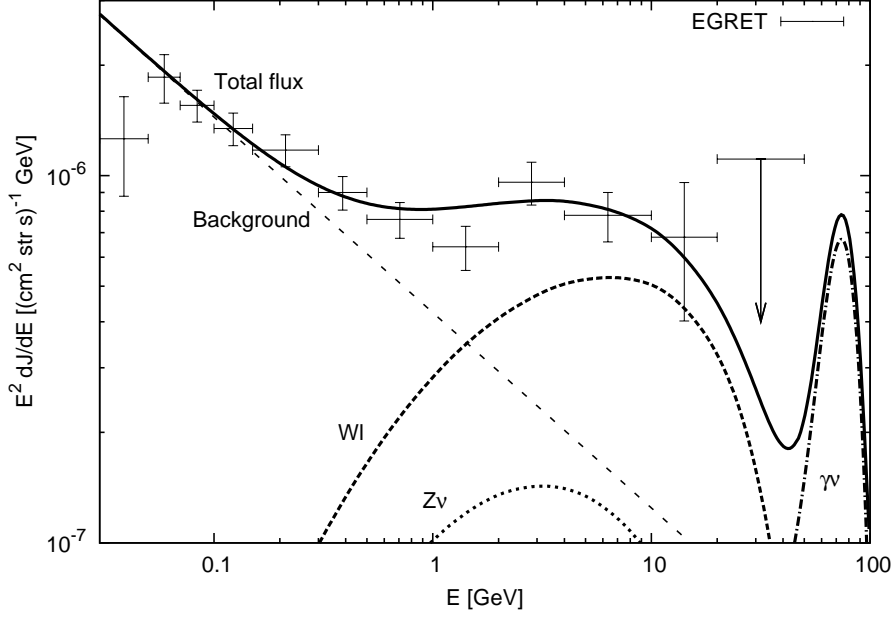


Figure 6.5: The gamma-ray spectrum including the contribution from the decay of gravitinos with  $m_{3/2} = 150$  GeV and  $\tau_{3/2} = 1.3 \times 10^{26}$  s. The background is chosen as  $E^2 dJ/dE = 4.3 \times 10^{-7} (E/\text{GeV})^{-0.5} (\text{cm}^2 \text{ str s})^{-1} \text{ GeV}$ .

whole sky. The resulting integrated fluxes between 0.1 and 10 GeV are shown in Tab. 6.2 for different quarter spheres and hemispheres, together with the same quantities as predicted by the model for  $m_{3/2} = 150$  GeV,  $\tau_{3/2} = 1.3 \times 10^{26}$  s. We find that the anisotropy of the gamma-ray signal is easily compatible with the experimental constraints. This is because the angular dependence of the halo contribution is softened by the isotropic extragalactic contribution and the isotropic power law background, so that the averaged flux over one quarter sphere of the sky differs by only 6% between outer and inner Galaxy. Whether an anisotropy in the diffuse extragalactic gamma-ray flux is actually present will be judged by future experiments with improved angular resolution.

### 6.3 Experimental Prospects

The extragalactic gamma-ray spectrum will soon be re-examined in detail by the Large Area Telescope aboard the GLAST satellite, which was successfully launched in mid-June 2008. GLAST will have a vastly superior energy and angular resolution compared to EGRET. It will be able to measure gamma-rays in the range 20 MeV – 300 GeV with an energy resolution of less than 10%, which should enable it to settle the current open questions conclusively. If the monochromatic line from gravitino decay is actually present, it will be in the energy range accessible to GLAST, making its confirmation or refutation inevitable. If, on the other hand, the line or the GeV excess are not confirmed, the present scenario will be ruled out or at least reduced to a subdominant contribution. It remains to be seen if GLAST will confirm or refute the existence of the GeV gamma-ray excess. The line may also be observable by Cerenkov telescopes in nearby galaxies such as M31 [32].

## Chapter 7

# Propagation of Charged Particles in the Galaxy

Before we can begin a discussion of the antimatter signatures of gravitino dark matter, we must address the question of how charged particles propagate in our Galaxy. The propagation of charged particles is much less straightforward (literally) than that of gamma rays due to effects of scatterings and energy losses. Any extragalactic contributions to the cosmic-ray fluxes are negligible, so we only need to regard creation and propagation of charged particles within the Milky Way halo. This discussion applies to both positrons and antiprotons, whose propagation we describe using the same model. We will address the general points here, particularizing them in the following chapters.

### 7.1 Lessons from Observations of Cosmic Rays

Cosmic rays are particles that are accelerated to high energies by supernova shockwaves. From measuring the ratio between primary and secondary cosmic rays, especially the Boron-to-Carbon ratio, one can infer how much matter cosmic rays traverse before reaching us. Simultaneously, measurements of isotopic ratios can tell us how much time passed between injection of a primary cosmic ray and its detection. By combining these pieces of information, one can infer that cosmic rays spend most of the time during their journey in a region of space that is much less dense than the Galactic disk, where they are believed to travel on the magnetic field lines generated by the matter in the Galaxy. We call this larger region, which contains the Milky Way disk, the diffusion halo. For reasons of symmetry, we can expect the diffusion halo to have approximately cylindrical shape (except at the boundaries).

### 7.2 The Diffusion Model

We model the propagation using a two-layer diffusion model with cylindrical symmetry [45]. We will make a number of simplifying assumptions about the nature of the problem that allow us to solve the resulting diffusion-loss equation in a semi-analytical way. The Galactic disk is taken to be a thin disk with half-height  $h = 100$  pc. The vertical size of the diffusion zone itself is unknown, but observations favor a half-height  $L$  between 1 and 15 kpc. The radial extent is chosen as  $R = 20$  kpc, where the precise value is not important, as it is much larger

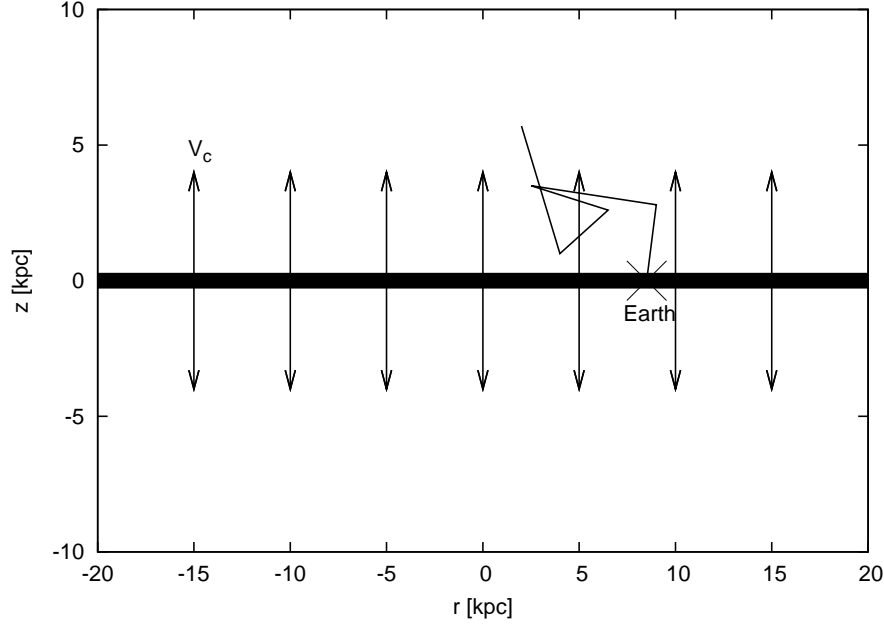


Figure 7.1: Schematic representation of the cylindrical diffusion zone. The solar system is located at  $r = 8.5$  kpc,  $z = 0$  kpc. The thick black line represents the gaseous disk of the Milky Way, where the charged particles interact with the interstellar medium, either losing energy, experiencing reacceleration, creating secondary particles or being annihilated. Within the diffusive volume, with dimensions here chosen as  $R = 20$  kpc,  $L = 10$  kpc, charged particles move in a random walk under the influence of magnetic inhomogeneities. The convective wind sweeps charged particles away from the Galactic disk. On the boundaries of the diffusive volume, particles escape from the Galaxy.

than the distance cosmic rays can travel in any case. The diffusion-loss equation describing the propagation of charged particles in the halo is

$$\begin{aligned} \frac{\partial}{\partial t} f(T, \vec{r}, t) = & \nabla[K(T, \vec{r}, t)\nabla f(T, \vec{r}, t)] + \frac{\partial}{\partial T}[b(T, \vec{r}, t)f(T, \vec{r}, t)] \\ & - \nabla[\vec{V}_c(\vec{r})f(T, \vec{r}, t)] - 2h\delta(z)\Gamma^{\text{ann}} f(T, \vec{r}, t) + Q(T, \vec{r}), \end{aligned} \quad (7.1)$$

where  $T$  denotes the kinetic energy of the particles. In the following, we will assume that steady-state holds,  $\partial_t f(T, \vec{r}, t) = 0$ . The first term on the right-hand side accounts for the diffusion of charged particles due to their scattering on magnetic inhomogeneities, resulting in a random walk-like motion through the diffusion zone. If we only regard this term on the right-hand side and take  $K$  to be constant, the diffusion equation reduces to the familiar heat equation. The second term describes energy losses due to inverse Compton scattering on the cosmic microwave background and on diffuse starlight, as well as synchrotron radiation and ionization losses. The third term represents the drift of charged particles away from the Galactic disk due to the wind of charged plasma emitted by the stars. The fourth term takes annihilating interactions in the disk into account. Finally, the last element is the source term that we derived in Chapter 5. The diffusion constant is assumed to be spatially constant

throughout the diffusion zone and to have the form

$$K(T) = K_0 \beta(T) \mathcal{R}(T)^\delta, \tag{7.2}$$

where  $\beta$  is the velocity of the particle in units of  $c$ . The rigidity  $\mathcal{R}$  is defined as the momentum in GeV per unit charge,  $\mathcal{R} \equiv p[\text{GeV}]/Z$ . The normalization  $K_0$  of the diffusion constant and the spectral index  $\delta$  have to be determined from measurements of cosmic rays.

We represent the solution for the number density  $f_X$  of the diffusion-loss equation as a convolution of the injection spectrum with a Green function,

$$f_X(T) = \frac{1}{m_{3/2} \tau_{3/2}} \int_0^{T_{\max}} dT' G_X(T, T') \frac{dN_X}{dT'}, \tag{7.3}$$

where  $X = e^+, \bar{p}$ . The maximum energy in the kinetic energy integration is given by  $T_{\max} = m_{3/2} - m_X$ . The Green function  $G_X$  encodes all the details of the propagation and the geometry of the dark matter distribution. It is independent of the nature of the dark matter particle in question. The dark matter properties enter in the mass, lifetime and differential energy spectrum. For the antimatter signatures, only the case of a heavier gravitino,  $m_{3/2} > m_{W,Z}$  will be of interest since the decay  $\psi_{3/2} \rightarrow \gamma\nu$  does not produce antimatter. The energy spectrum is thus given by

$$\frac{dN_X}{dE} \simeq \text{BR}(\psi_{3/2} \rightarrow Wl) \frac{dN_X^{Wl}}{dE} + \text{BR}(\psi_{3/2} \rightarrow Z^0\nu) \frac{dN_X^{Z\nu}}{dE}, \tag{7.4}$$

where we again use the energy spectra obtained in Chapter 5.

Under certain assumptions, the transport equation can be solved semi-analytically. We will regard the propagation of positrons and antiprotons as different limiting cases of the full diffusion equation. The solutions are derived in Appendix C. Due to linearity, the transport equation can be solved separately for background and signal, and the results can then be added to obtain the resulting fluxes. Background cosmic rays originate exclusively from the disk, while primary cosmic rays from dark matter annihilation or decay can come from anywhere within the diffusive halo.

### 7.3 Determination of the Propagation Model Parameters

The propagation model has a number of parameters that must be determined from experiment, namely the half-height  $L$  of the diffusion zone, the magnitude of the convective wind  $V_C$ , as well as the normalization of the diffusion constant  $K_0$  and the spectral index  $\delta$ . The values of the propagation parameters are determined by fitting the predictions of a model to the measured ratio between two cosmic-ray fluxes, most importantly the Boron-to-Carbon ratio [46]. However, there is a degeneracy in the diffusion parameters that is difficult to resolve by measuring cosmic-ray ratios. The degeneracy stems from the fact that dark matter decay products can be created in the entire halo and not just in the Galactic disk. The corresponding flux will therefore be sensitive to the half-height  $L$  of the diffusion zone. However, a larger flux can be compensated by a simultaneous increase in the diffusion coefficient  $K_0$ , allowing for longer propagation in the halo. The parameters shown in Tab. 7.1 and 7.2 yield roughly

Model	$\delta$	$K_0$ [kpc <sup>2</sup> /Myr]	$L$ [kpc]
M2	0.55	0.00595	1
MED	0.70	0.0112	4
M1	0.46	0.0765	15

Table 7.1: Positron propagation parameters compatible with B/C analysis. The M2, MED and M1 parameter sets yield the minimum flux, medium and maximum positron flux, respectively [47].

Model	$\delta$	$K_0$ [kpc <sup>2</sup> /Myr]	$L$ [kpc]	$V_C$ [km/s]
MAX	0.46	0.0765	15	5
MED	0.70	0.0112	4	12
MIN	0.85	0.0016	1	13.5

Table 7.2: Antiproton propagation parameters compatible with B/C analysis. As the names indicate, the different sets of parameters correspond to the maximum, medium and minimum antiproton flux [47].

the same  $\chi^2$  for the B/C ratio, while the corresponding primary antiproton fluxes from dark matter can vary over two orders of magnitude. We note that the MED diffusion model appears in both tables, and that we can also use the MIN set of parameters from Tab. 7.2 as parameters for the positron propagation, giving us four different models for the positrons in total. The degeneracy in the determination of the propagation parameters can in principle be broken by measurements of isotopic ratios of radioactive elements, such as the  $^{10}\text{Be}/^9\text{Be}$ ,  $^{36}\text{Cl}/^{35}\text{Cl}$  and  $^{27}\text{Al}/^{26}\text{Al}$  ratio. Results from such measurements are not accurate enough to break the degeneracy, however. Calculations of the antiproton spectrum will be affected much more by the indeterminacy in the propagation parameters than the corresponding calculations for positrons, since antiprotons can travel far greater distances than positrons and are therefore more sensitive to the size of the diffusion zone. We will discuss this issue further in Chapter 9 in connection with the results for the antiproton spectra presented there.

## 7.4 Solar Modulation

A further complication in the determination of the charged particle spectra at the Earth is introduced by an effect known as solar modulation. The solar wind, a stream of plasma consisting mainly of electrons and protons ejected from the Sun's upper atmosphere, sweeps low-energy particles away from the heliosphere, thereby flattening the spectrum and redistributing particles toward lower energies. The strength of solar modulation is not constant over time, but varies with solar activity. In the simple force field approximation [48, 49], the top-of-atmosphere flux  $\Phi_{\text{TOA}}$  is related to the interstellar flux  $\Phi_{\text{IS}}$  by the relation [50]

$$\Phi_{\text{TOA}}(T_{\text{TOA}}) = \frac{p^2(T_{\text{TOA}})}{p^2(T_{\text{IS}})} \Phi_{\text{IS}}(T_{\text{IS}}), \quad (7.5)$$

where  $T_{\text{IS}} = T_{\text{TOA}} + \phi_F$ , and  $p$  is the momentum of the cosmic-ray particle. We have introduced the so-called Fisk potential  $\phi_F$  which ranges from 500 MV at the solar minimum to 1300 MV at maximum solar activity, where these values are determined purely on the basis of observations.

## Chapter 8

# Positrons from Gravitino Dark Matter Decay

In addition to the information gained from regarding the gamma-ray flux, important clues can also be obtained by looking at other cosmic-ray particles. Especially rare species with low background fluxes are of interest. This includes primarily cosmic-ray antimatter, i.e. positrons and antiprotons, as well as light nuclei. Positrons are discussed in this chapter, while antiprotons are dealt with in the next one.

### 8.1 The Experimental Status

Cosmic-ray positrons of standard astrophysical origin are created by spallations of positrons and Helium nuclei on the interstellar medium. Most experiments actually do not report the absolute positron flux, but the positron fraction, which is defined as the ratio between the positron flux and the sum of positron and electron fluxes,

$$\text{PF}(T) = \frac{\Phi_{e^+}(T)}{\Phi_{e^-}(T) + \Phi_{e^+}(T)}. \quad (8.1)$$

This is done for practical reasons, as many sources of systematic error, such as detector acceptance or trigger efficiency, cancel out when regarding the ratio between the fluxes. Furthermore, the effects of solar modulation cancel out when regarding the positron fraction – at least under the assumption that solar modulation is charge-sign independent, which is approximately true. The positron fraction has been measured by a number of balloon and space-based experiments. The results for the positron fraction from the experiments HEAT [51], CAPRICE [52], MASS [53] and AMS-01 [54] are shown in figure 8.1, together with the theoretical expectation obtained from the GALPROP numerical code [55]. One can see that there presently is significant tension in the experimental data on the positron fraction. It is worth pointing out, however, that all experiments seem to point toward an excess of positrons over the theoretical expectation at energies above  $\sim 7$  GeV. Rather suspiciously, this is also just the energy range where one could expect a contribution from gravitino dark matter decay.

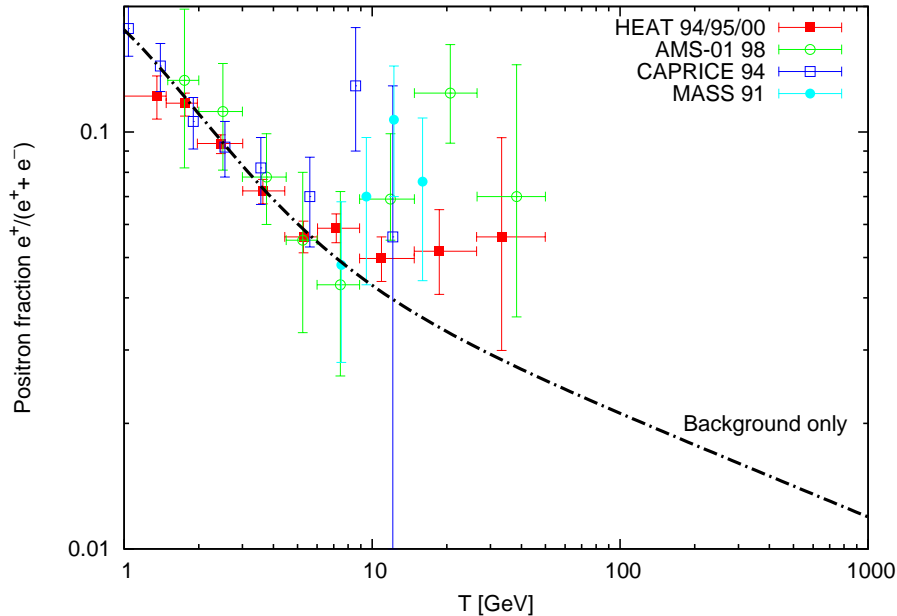


Figure 8.1: Results of measurements of the positron fraction from the experiments HEAT [51], CAPRICE [52], MASS [53] and AMS-01 [54] together with the theoretical prediction from [55]. All experiments report an excess over the theoretical prediction at higher energies to varying degrees.

## 8.2 Solution of the Transport Equation

The propagation of positrons in the Galaxy is considerably more complicated than that of photons. After positrons are injected, they move under the influence of the tangled Galactic magnetic fields, diffusing and losing energy through synchrotron radiation and inverse Compton scattering off the cosmic microwave background and off diffuse starlight. On their path through the Galaxy, positrons get scattered many times. As a result, measurements of cosmic-ray positrons can provide no directional information about the origin of the positrons and little spectral information.

For the positrons, the pair annihilation term in the propagation equation is negligible. The influence of the Galactic wind on the positron spectrum also plays no role. The diffusion equation for the positrons is therefore

$$0 = \nabla[K(T, \vec{r})\nabla f_{e^+}(T, \vec{r})] + \frac{\partial}{\partial T}[b(T, \vec{r})f_{e^+}(T, \vec{r})] + Q(T, \vec{r}), \quad (8.2)$$

where the rate of energy loss is assumed to be a spatially constant function parametrized as

$$b(T) = \frac{T^2}{T_0\tau_E}, \quad (8.3)$$

with  $T_0 \equiv 1$  GeV and  $\tau_E = 10^{16}$  s.

Model	$a$	$b$
M2	-0.9716	-10.012
MED	-1.0203	-1.4493
M1	-0.9809	-1.1456

Table 8.1: Parameters for an analytical approximation to the propagation Green's function, using the NFW halo profile

The geometry of the problem suggests the use of Bessel functions. Indeed, in the solution for the number density  $f_{e^+}$  of positrons, written as a convolution with a propagation Green function,

$$f_{e^+}(T) = \frac{1}{m_{3/2}\tau_{3/2}} \int_0^{m_{3/2}} dT' G_{e^+}(T, T') \frac{dN_{e^+}}{dT}, \quad (8.4)$$

the Green function itself can be expressed as an expansion in Bessel and sine functions. The explicit form is given by [45]

$$G_{e^+}(T, T') = \sum_{m,n=1}^{\infty} B_{mn}(T, T') J_0\left(\zeta_n \frac{r_{\odot}}{R}\right) \sin\left(\frac{m\pi}{2}\right), \quad (8.5)$$

where the expansion coefficients are given by

$$B_{mn}(T, T') = \frac{\tau_E T_0}{T^2} C_{mn} \exp\left\{\left(\frac{\zeta_n^2}{R^2} + \frac{m^2 \pi^2}{4L^2}\right) \frac{K_0 \tau_E}{\delta - 1} \left[\left(\frac{T}{T_0}\right)^{\delta-1} - \left(\frac{T'}{T_0}\right)^{\delta-1}\right]\right\}, \quad (8.6)$$

with the geometry of the problem being encoded in the coefficients

$$C_{mn} = \frac{2}{J_1^2(\zeta_n) R^2 L} \int_0^R dr' r' \int_{-L}^L dz' \rho_{\text{DM}}(\vec{r}') J_0\left(\zeta_n \frac{r'}{R}\right) \sin\left[\frac{m\pi}{2L}(L - z')\right]. \quad (8.7)$$

See Appendix C for a detailed derivation of the solution.

The interstellar primary positron flux from gravitino decay is now given by

$$\Phi_{e^+}^{\text{prim}}(T) = \frac{c}{4\pi} \frac{1}{m_{3/2}\tau_{3/2}} \int_0^{m_{3/2}} dT' G_{e^+}(T, T') \frac{dN_{e^+}(T')}{dT'}. \quad (8.8)$$

We also give an analytical approximation to the propagation Green function which can be useful for practical purposes, as the approximate expression is easier to handle than the full equations. Also, the computation of the expansion coefficients and the numerical integrations represent a somewhat heavy chore for a standard desktop computer. The function we choose to fit the Green function is

$$G_{e^+}^a(T, T') = \frac{10^{16}}{T^2} e^{a+b(T^{\delta-1}-T'^{\delta-1})} \theta(T' - T) \text{ cm}^{-3} \text{ s}. \quad (8.9)$$

The numerical values for the coefficients for different sets of diffusion parameters are given in table 8.1. The analytical approximation works better than 15 – 20% over the whole energy

range. This Green function can be used to calculate the positron fluxes from any kind of decaying dark matter. One should note that the values of the coefficients depend on the local dark matter density, here chosen as  $\rho_{\odot} = 0.3 \text{ GeV cm}^{-3}$ . For a different choice of local halo density or different units, they have to be scaled appropriately.

### 8.3 Positrons from Gravitino Decay

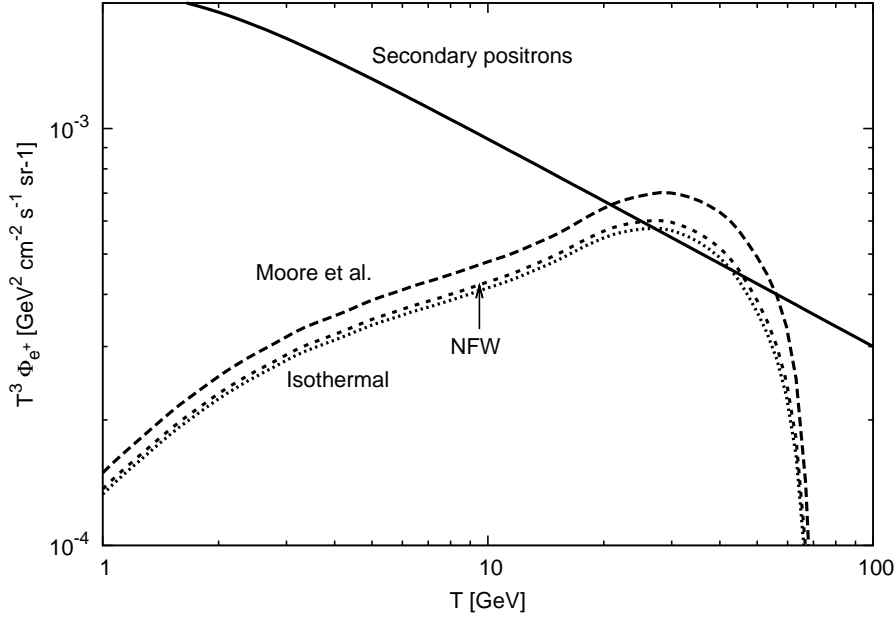


Figure 8.2: Interstellar primary positron flux for different halo profiles and  $m_{3/2} = 150 \text{ GeV}$ ,  $\tau_{3/2} = 1.3 \times 10^{26} \text{ s}$ . The flux of secondary positrons is also shown for comparison.

For the background fluxes of primary and secondary electrons, as well as secondary positrons, we use the parametrizations obtained by Baltz and Edsjö [55] from the GALPROP code [56].

$$\Phi_{e^-}^{\text{prim}}(T) = \frac{0.16(T/T_0)^{-1.1}}{1 + 11(T/T_0)^{0.9} + 3.2(T/T_0)^{2.15}} \text{ (GeV}^{-1}\text{cm}^{-2}\text{s}^{-1}\text{sr}^{-1}\text{)}, \quad (8.10)$$

$$\Phi_{e^-}^{\text{sec}}(T) = \frac{0.70(T/T_0)^{0.7}}{1 + 110(T/T_0)^{1.5} + 600(T/T_0)^{2.9} + 580(T/T_0)^{4.2}} \quad (8.11)$$

$$\times \text{ (GeV}^{-1}\text{cm}^{-2}\text{s}^{-1}\text{sr}^{-1}\text{)}, \quad (8.12)$$

$$\Phi_{e^+}^{\text{sec}}(T) = \frac{4.5(T/T_0)^{0.7}}{1 + 650(T/T_0)^{2.3} + 1500(T/T_0)^{4.2}} \text{ (GeV}^{-1}\text{cm}^{-2}\text{s}^{-1}\text{sr}^{-1}\text{)}. \quad (8.13)$$

The positron fraction including primaries is then

$$\text{PF}(T) = \frac{\Phi_{e^+}^{\text{prim}}(T) + \Phi_{e^+}^{\text{sec}}(T)}{\Phi_{e^+}^{\text{prim}}(T) + \Phi_{e^+}^{\text{sec}}(T) + k \Phi_{e^-}^{\text{prim}}(T) + \Phi_{e^-}^{\text{sec}}(T)}, \quad (8.14)$$

where we treat  $k$  as a free parameter, since the normalization of the primary electron flux is unknown and chosen to match observations [55]. When there is no contribution from primary sources to the positron flux, the low-energy part of the spectrum is best fitted for  $k = 0.88$  [57].

In Fig. 8.2, we show the numerical results for the interstellar positron flux that we get for the same set of parameters we used to fit the EGRET excess,  $m_{3/2} = 150$  GeV and  $\tau_{3/2} = 1.3 \times 10^{26}$  s. The flux is plotted for the M2 propagation model using the three different halo profiles discussed in Chapter 5. As one can see, the difference is rather small, and the choice of halo profile largely irrelevant, which is in sharp contrast to the case of annihilating dark matter. There, the dependence of the fluxes on  $\rho_{\text{DM}}^2$  makes the results strongly dependent on the halo profile of choice. The secondary positron flux is also shown for comparison. Interestingly, the primary and secondary flux are of comparable magnitude, with the primary flux actually dominating over the secondary flux above  $\sim 20$  GeV. For a lifetime of  $\sim 10^{26}$  s we therefore get a sizable contribution from gravitino decay.

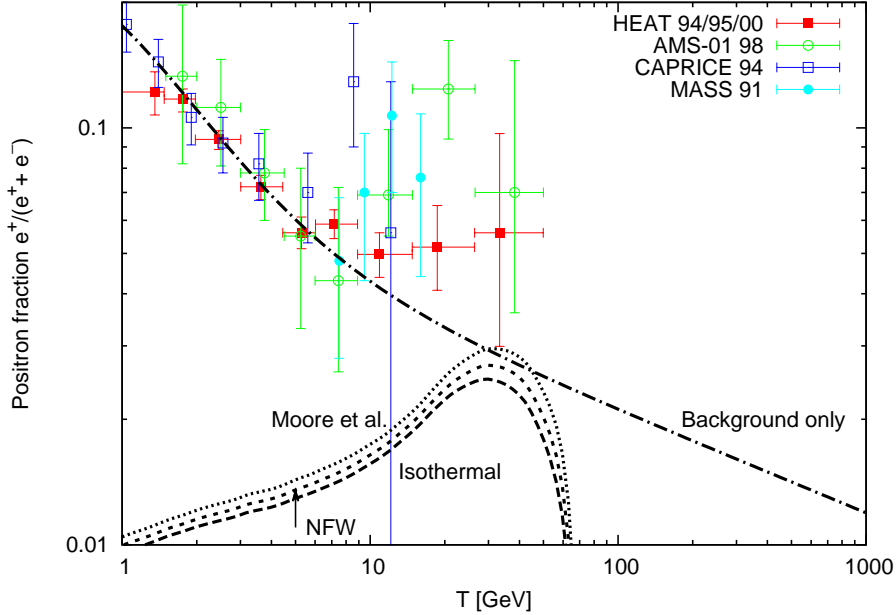


Figure 8.3: Primary contribution to the positron fraction from gravitino decay in the M2 model for different halo profiles and  $m_{3/2} = 150$  GeV,  $\tau_{3/2} = 1.3 \times 10^{26}$  s.

In Fig. 8.3, we show the primary contribution to the positron fraction corresponding to the primary interstellar flux from Fig. 8.2. Excitingly, we find a prominent bump in the energy region where HEAT and other experiments report an excess over the theoretically expected flux. We also want to compare this with the results for other propagation parameters, which are shown in Fig. 8.4. There we see that the particular choice of propagation model mainly affects the results at low energies, while near the interesting region, around 20 – 30 GeV, the result is relatively independent of the chosen parameter set.

Encouraged by this observation, we attempt to also interpret the HEAT excess in terms

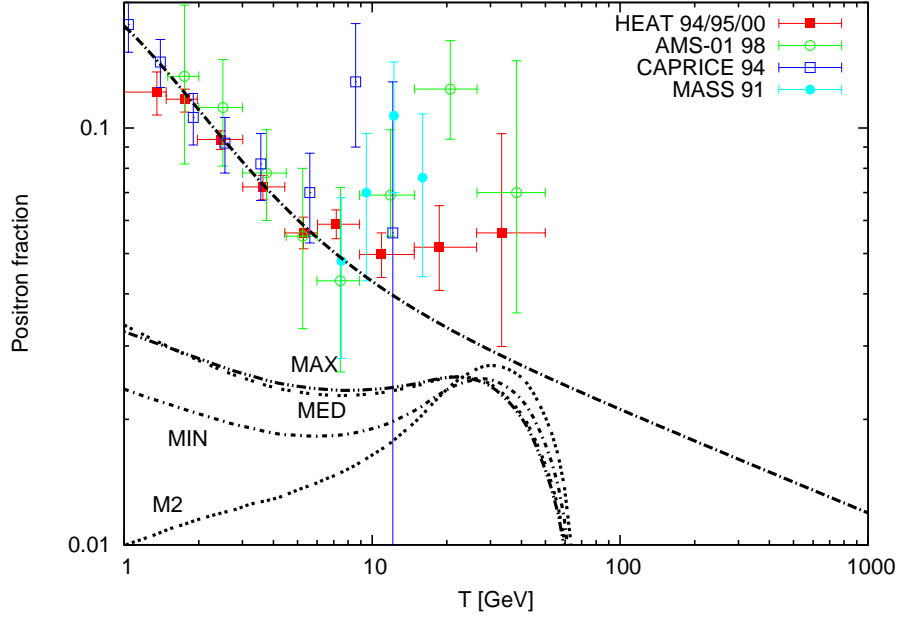


Figure 8.4: Positron fraction signal from gravitino decay,  $m_{3/2} = 150$  GeV,  $\tau_{3/2} = 1.3 \times 10^{26}$  s for the different propagation models.

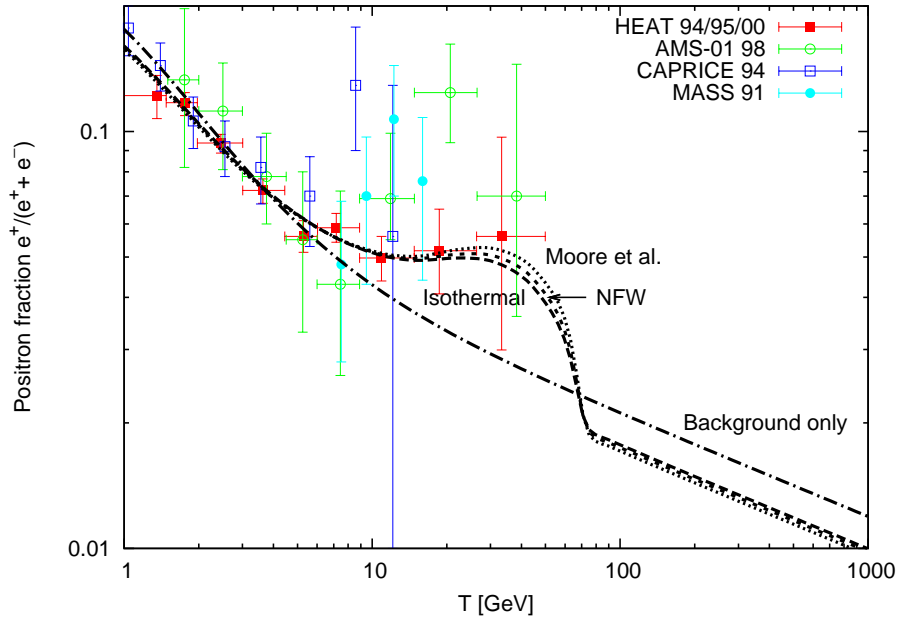


Figure 8.5: Positron fraction including signal and background for different halo profiles and  $m_{3/2} = 150$  GeV,  $\tau_{3/2} = 1.3 \times 10^{26}$  s. The background normalization is kept free.

of gravitino dark matter decay. Keeping the normalization  $k$  of the primary electron flux free, we attempt to make a fit in  $k$  to the combined HEAT data for  $m_{3/2} = 150$  GeV and  $\tau_{3/2} = 1.3 \times 10^{26}$  s. The resulting positron fraction in the M2 set of propagation parameters

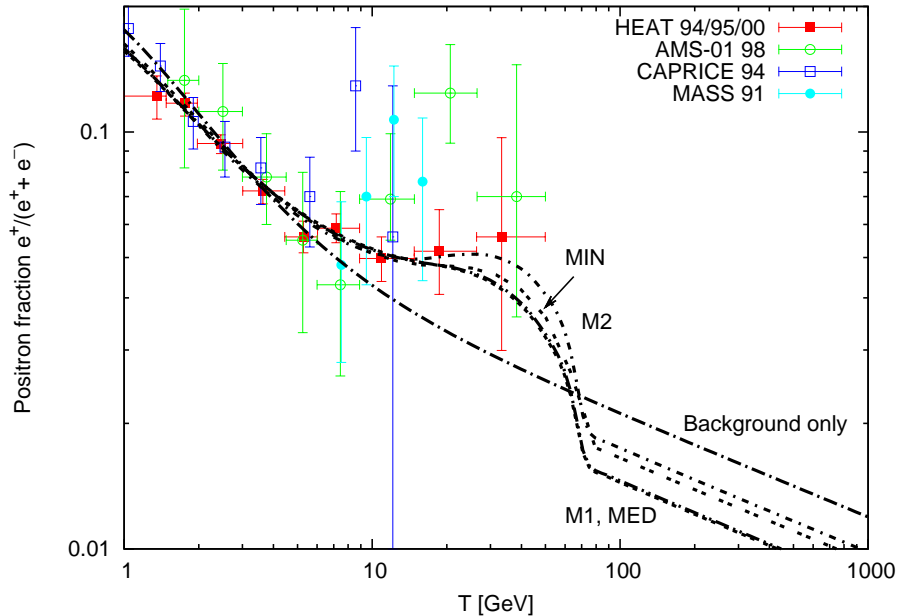


Figure 8.6: Positron fraction for the different propagation models using the NFW profile.

is plotted in Fig. 8.5. We find that the result agrees very well with the combined HEAT data. The difference between the different halo profiles is partially absorbed by the background normalization. To quantify the influence of the diffusion model parameters on the result, we compare the results for the four different parameter sets in Fig. 8.6. We see that the presence of the bump is quite a robust feature and not very sensitive to the various astrophysical uncertainties. Interestingly, the model with the smallest contribution to the positron fraction actually yields the most prominent bump, which is a result of leaving the primary electron normalization free.

We therefore come to the conclusion that for the same choice of gravitino parameters we obtained by making a qualitative fit to the EGRET excess, we can simultaneously explain the HEAT excess in the positron fraction. The best fit is achieved for  $k = 1.07, 1.28$  and  $1.29$  for the M2, MED and M1 model, respectively. The decay of gravitino dark matter might therefore account for both these anomalies at the same time. This is a very intriguing coincidence. Actually, we have found that a significant contribution to the positron fraction is necessary for gravitino lifetimes  $\tau_{3/2} \sim 10^{26}$  s. The reverse statement also applies: if we had begun with interpreting the excess in the positron fraction in terms of gravitino decay, we would have found that this necessarily produces a significant excess in the diffuse extragalactic gamma-ray spectrum just like the one observed by EGRET.

It is also worth mentioning that this result of being able to simultaneously explain the EGRET and HEAT excesses is not specific to gravitino dark matter. Similar signatures can also be expected for other kinds of decaying dark matter with a lifetime of  $\sim 10^{26}$  s which couple to  $W^\pm$  and/or  $Z^0$  bosons, provided that the gauge bosons are injected with momenta  $\sim 50$  GeV.

Nevertheless, in view of the considerable experimental and theoretical uncertainties, the result should be taken with a grain of salt. For a detailed discussion of the theoretical uncertainties regarding primary positron contributions, see [47].

## 8.4 Experimental Prospects

The satellite experiment PAMELA [58], which is dedicated to the detection of cosmic rays including antimatter, has been in orbit and taking data for two years, and first results are expected to be released in the near future. This experiment is expected to bring a breakthrough in the determination of the positron fraction. If PAMELA found a result resembling the curves shown in Fig. 8.6, it would be a very compelling case for an exotic signal on top of the astrophysical background. On the other hand, if PAMELA finds no evidence for a primary component of the positron fraction, the interpretation of the EGRET excess in terms of gravitino decay will also be ruled out. The AMS-02 experiment [59] is planned to be deployed on the International Space Station at some point in the future. It will even surpass the PAMELA accuracy by far, but at present it is unclear when (and if) AMS-02 will be launched.

## Chapter 9

# Antiprotons from Gravitino Dark Matter Decay

Cosmic-ray antiprotons are even rarer than positrons. Their spectrum should therefore be very sensitive to exotic sources. However, the antiproton spectrum has been measured to a relatively high accuracy by different space-based experiments and is described quantitatively well by current models without primary antiproton sources. A signal of primaries from gravitino decay should therefore not contribute significantly to the overall flux. The cosmic-ray antiproton flux therefore provides an important consistency check. We will examine the situation in detail in this chapter.

### 9.1 The Experimental Status

The cosmic-ray antiproton spectrum has been measured by a number of experiments during the past decade, most of them operating during the period of solar minimum activity. The results from various experiments are shown in Fig. 9.1. The data are taken from BESS [60, 61], IMAX [62] and CAPRICE [63, 64].

Secondary antiprotons are created by spallations of cosmic-ray nuclei on the interstellar medium and will compose the background to our signal. By far the most abundant species of cosmic rays are protons and Helium nuclei, whose abundance has been measured to high accuracy. The dominant astrophysical process contributing to antiproton production comes from proton-proton reactions. However, in current theoretical models, proton-Helium, Helium-proton, and Helium-Helium processes have also been taken into account. These models of secondary antiproton production are found to reproduce the results of measurements quite well, so the allowed margin for a potential contribution from exotic primary sources is quite small.

### 9.2 Solution of the Transport Equation

For antiprotons, energy losses can be neglected due to their relatively high mass. They can thus travel far greater distances than positrons, being essentially able to traverse the whole Milky Way. All the other terms in the diffusion equation do figure for the antiprotons,

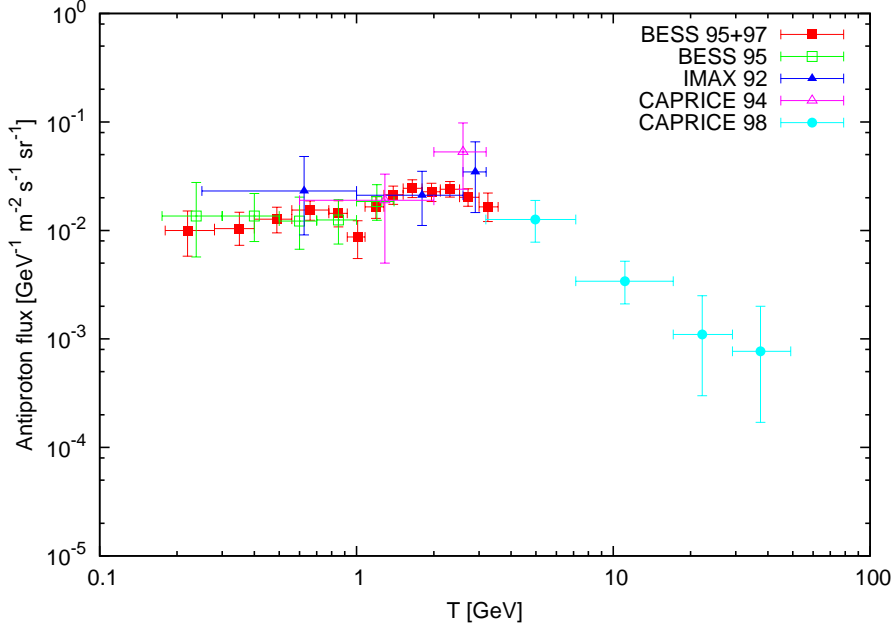


Figure 9.1: Results of measurements of the top-of-atmosphere antiproton spectrum from BESS [60, 61], IMAX [62] and CAPRICE [63, 64].

however. The diffusion equation for the antiprotons is therefore given by

$$0 = \nabla(K(T, \vec{r})\nabla f_{\bar{p}}(T)) - \nabla(\vec{V}_c(\vec{r})f_{\bar{p}}(T)) - 2h\delta(z)\Gamma_{\bar{p}p}^{\text{ann}}(T)f_{\bar{p}}(T) + Q(T, \vec{r}). \quad (9.1)$$

In our solution, we neglect tertiary antiproton contributions. Tertiary antiprotons originate from non-annihilation inelastic scatterings on the interstellar medium. They are no new contribution, but correspond to non-annihilating inelastic scatterings.

We assume the Galactic wind to be spatially constant and to have axial direction away from the disk,

$$\vec{V}_c(z) = (2\theta(z) - 1)V_C\vec{e}_z. \quad (9.2)$$

The proton-antiproton annihilation rate is determined by the interstellar Hydrogen and Helium abundances and their respective annihilation cross sections,

$$\Gamma_{\bar{p}p}^{\text{ann}}(T) = (n_{\text{H}} + 4^{2/3}n_{\text{He}})\sigma_{\bar{p}p}^{\text{ann}}(T)v_{\bar{p}}(T). \quad (9.3)$$

The interstellar number densities of Hydrogen and Helium are taken to be  $n_{\text{H}} = 1 \text{ cm}^{-3}$  and  $n_{\text{He}} = 0.07 \text{ cm}^{-3}$ , respectively. We assume that the Hydrogen-antiproton scattering cross section is related to the Helium-antiproton cross section  $\sigma_{\bar{p}p}^{\text{ann}}$  by the simple geometrical factor  $4^{2/3}$ . For the proton-antiproton annihilation cross section we use the parametrization given by Tan and Ng [65]:

$$\sigma_{\bar{p}p}^{\text{ann}}(T) = \begin{cases} 661(1 + 0.0115(T/T_0)^{-0.774} - 0.948(T/T_0)^{0.0151}) \text{ mb}, & T < 15.5 \text{ GeV}, \\ 36(T/T_0)^{-0.5} \text{ mb}, & T \geq 15.5 \text{ GeV}. \end{cases} \quad (9.4)$$

The solution for the antiproton number density is written as

$$f_{\bar{p}}(T) = \int_0^{m_{3/2} - m_p} dT' G_{\bar{p}}(T, T') \frac{dN_{\bar{p}}}{dT'}, \quad (9.5)$$

and the resulting interstellar flux is

$$\Phi_{\bar{p}}^{\text{prim}}(T) = \beta(T) \frac{c}{4\pi} f_{\bar{p}}(T), \quad (9.6)$$

with the antiproton velocity  $\beta(T) = \sqrt{T^2 + 2Tm_p}/(T + m_p)$ . Solving the propagation equation, we find that the Green function for antiprotons is given by [45]

$$G_{\bar{p}}(T, T') = \sum_{i=1}^{\infty} \exp\left(-\frac{V_C L}{2K(T)}\right) \frac{y_i(T)}{A_i(T) \sinh(S_i(T)L/2)} J_0\left(\zeta_i \frac{r_{\odot}}{R}\right) \delta(T - T'), \quad (9.7)$$

with the energy dependent factors

$$A_i(T) = 2h\Gamma_{\bar{p}p}^{\text{ann}}(T) + V_C + K(T)S_i(T) \coth\left(\frac{S_i(T)L}{2}\right) \quad (9.8)$$

and

$$S_i(T) = \sqrt{\frac{V_C^2}{K(T)^2} + 4\frac{\zeta_i^2}{R^2}}, \quad (9.9)$$

as well as

$$y_i(T) = \frac{4}{J_1^2(\zeta_i)R^2} \int_0^R dr' r' J_0\left(\zeta_i \frac{r'}{R}\right) \int_0^L dz' \exp\left(\frac{V_C}{2K(T)}(L - z')\right) \times \\ \times \sinh\left(\frac{S_i(T)}{2}(L - z')\right) \rho_{\text{DM}}(\vec{r}'). \quad (9.10)$$

A detailed derivation of this solution can be found in Appendix C.

Again, we give an analytical approximation to the Green function which might be useful for practical purposes. We choose as an approximating function

$$G_{\bar{p}}(T, T') = 10^{14} e^{x+y \ln T + z \ln^2 T} \delta(T' - T). \quad (9.11)$$

The coefficients  $x$ ,  $y$  and  $z$  are given in Table 9.1 for the MIN, MED and MAX set of propagation parameters and the NFW halo profile. The approximation works better than 5 – 10% accuracy over the whole energy range. Again, for the numerical results in this chapter, we have used the full expressions and not the analytical approximation.

We also need to take solar modulation into account to obtain the actual top-of-atmosphere spectrum as measured by experiments. According to Eq. (7.5), in the force field approximation, the top-of-atmosphere flux  $\Phi_{\text{TOA}}$  after solar modulation is related to the interstellar flux  $\Phi_{\text{IS}}$  by [50]

$$\Phi_{\text{TOA}}(T_{\text{TOA}}) = \frac{2m_p T_{\text{TOA}} + T_{\text{TOA}}^2}{2m_p T_{\text{IS}} + T_{\text{IS}}^2} \Phi_{\text{IS}}(T_{\text{IS}}). \quad (9.12)$$

Model	$x$	$y$	$z$
MIN	-0.0537	0.7052	-0.1840
MED	1.8002	0.4099	-0.1343
MAX	3.3602	-0.1438	-0.0403

Table 9.1: Coefficients for the numerical approximation to the antiproton Green function, using a NFW profile.

where  $T_{\text{IS}} = T_{\text{TOA}} + \phi_F$  with the Fisk potential  $\phi_F$ . For the numerical computations we assume a value of  $\phi_F = 500$  MV, which corresponds to minimal solar activity, as most experiments measuring the antiproton flux were undertaken around the minimum of the eleven-year solar cycle. The effect of solar modulation is depicted in Fig. 9.3, where the interstellar and top-of-atmosphere fluxes are shown together for a solar modulation potential of  $\phi_F = 500$  MV.

### 9.3 Antiprotons from Gravitino Decay

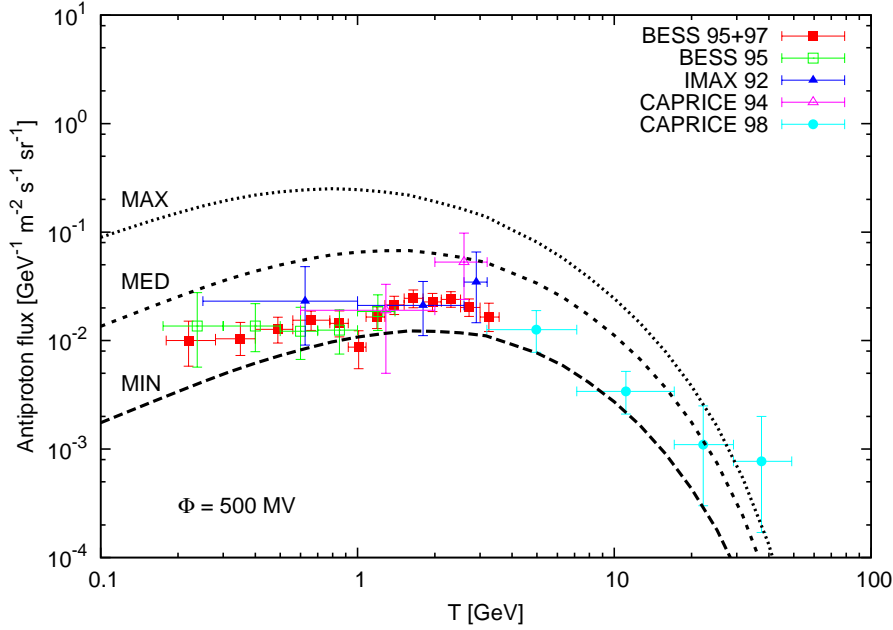


Figure 9.2: Primary top-of-atmosphere antiproton fluxes for different choices of propagation parameters using the NFW profile and  $m_{3/2} = 150$  GeV,  $\tau_{3/2} = 1.3 \times 10^{26}$  s.

The resulting primary fluxes after solar modulation are plotted in Fig. 9.2 for the NFW halo profile and the familiar set of parameters  $m_{3/2} = 150$  GeV,  $\tau_{3/2} = 1.3 \times 10^{26}$  s. The results illustrate the aforementioned problem with the determination of the diffusion parameters, as the fluxes vary over two orders of magnitude depending on which propagation parameters are chosen. Also, we find that the flux of primary antiprotons is clearly too large for a wide range of propagation parameters. For the MAX and MED models, we get a flux that lies

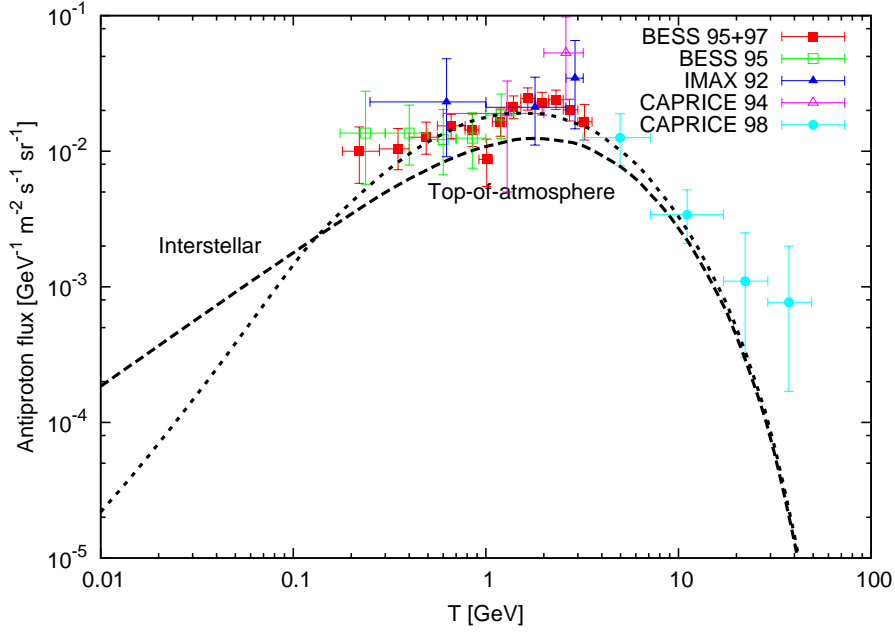


Figure 9.3: The effect of solar modulation on the antiproton spectrum. The primary top-of-atmosphere and interstellar antiproton fluxes are shown for the NFW profile in the MIN model and  $m_{3/2} = 150$  GeV,  $\tau_{3/2} = 1.3 \times 10^{26}$  s. The solar modulation parameter has been chosen as  $\phi_F = 500$  MV. The spectrum is mainly affected at low energies.

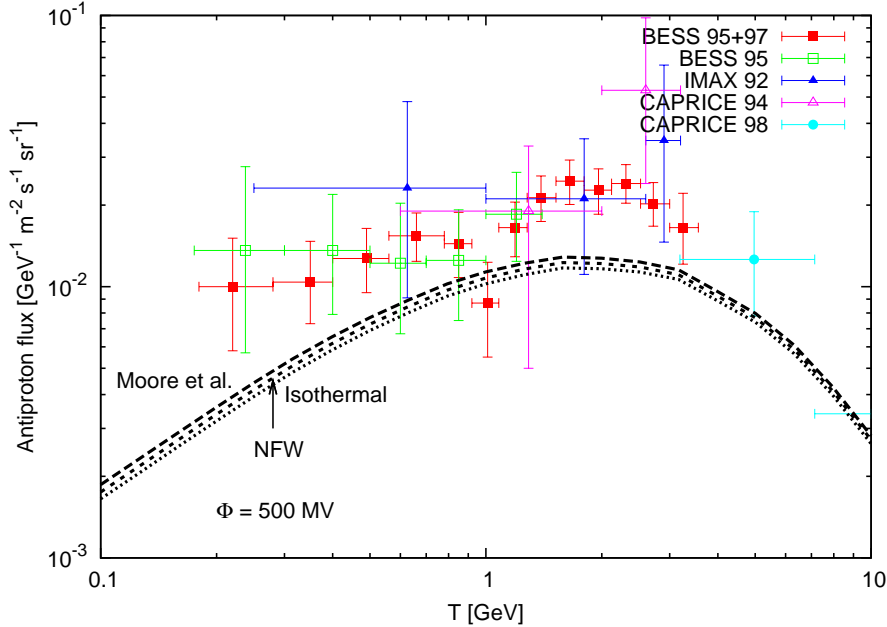


Figure 9.4: Primary top-of-atmosphere antiproton fluxes for different halo profiles in the MIN propagation model for  $m_{3/2} = 150$  GeV,  $\tau_{3/2} = 1.3 \times 10^{26}$  s.

above the experimentally measured one without even taking the conventional astrophysical background into account. For these sets of propagation parameters, the scenario is most likely not phenomenologically viable. However, for the MIN model we find a flux that lies below measurements and that might therefore be compatible with observations.

We now want to analyze the primary antiproton flux in the MIN propagation model in more detail. In Fig. 9.4 we compare the top-of-atmosphere flux for different halo profiles. As in the case of the positrons, we find a very small dependence on the choice of halo profile. To calculate the total flux, we adopt the background antiproton flux from [66]. We choose this background for consistency, since it was obtained using the same semi-analytical diffusion model and the same set of propagation parameters. In Fig. 9.5 we show the background, signal and total antiproton fluxes for our favorite parameters and the MIN propagation model. We see that the total flux exceeds the measured flux by a factor  $\sim 2$ . Therefore, even the minimal flux is too large for the set of gravitino parameters that we found to interpret the EGRET and HEAT excesses.

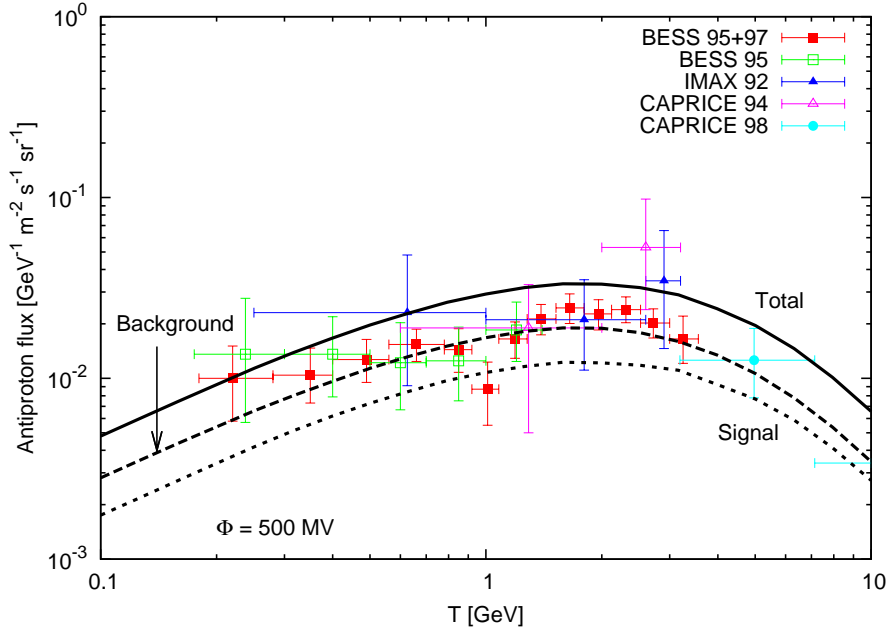


Figure 9.5: Primary signal and background top-of-atmosphere antiproton fluxes in the MIN propagation model for  $m_{3/2} = 150$  GeV,  $\tau_{3/2} = 1.3 \times 10^{26}$  s. The background flux was taken from [66]. The resulting total flux lies approximately a factor of 2 above measurements.

Nevertheless, with the primary flux varying over two orders of magnitude depending on the choice of propagation parameters, it seems premature to rule out the present scenario on the basis of this rather small excess. It certainly appears conceivable that there are other sets of propagation parameters (with a slightly worse fit to the Boron-to-Carbon ratio) or more refined propagation models in which the antiproton flux is compatible with observations. Indeed, it has been found that within the GALPROP framework, a wide range of models (diffusive reacceleration) actually underproduces antiprotons, which has been connected to a possible contribution from primary sources [67].

In addition to the uncertainties from the degeneracies in the determination of the propagation parameters, there are also uncertainties in the nuclear cross sections, since there are few experimental results on antiproton production in nuclear collisions. Other uncertainties stem from the description of the interstellar medium and the effect of solar modulation. For a more detailed discussion, see [66]. We should also remember that we carried out the calculations in a simplified diffusion model where the effects of reacceleration, as well as energy losses and tertiary contributions were neglected. Some further questionable simplifications made include assuming a spatially constant convective wind throughout the diffusion zone, as well as a spatially constant diffusion constant. The featureless antiproton spectrum also makes it extremely difficult to disentangle a possible exotic signal from the background based on the spectral shape alone.

To summarize, the cosmic-ray antiproton flux in principle represents an even more stringent constraint on possible indirect dark matter signatures than the extragalactic gamma-ray flux. This is to some degree obliterated by the large systematic uncertainties in the astrophysics of antiproton propagation. Nevertheless, the antiproton bound must be taken seriously and puts the present model in jeopardy. The future experimental situation is analogous to the positron case, as both PAMELA and AMS-02 are expected to provide high-precision measurements. In contrast to the positron case, however, past measurements of the antiproton flux agree quite well. Therefore, the increased precision is not expected to bring any surprises regarding the antiproton spectrum. We conclude that the results on the phenomenological viability of the present scenario are inconclusive. Despite the uncertainties, in the MAX and MED model our interpretation of the EGRET and HEAT excesses in terms of gravitino decay is probably excluded, whereas the case for the MIN model is not closed just yet and certainly deserves to be investigated in more detail in view of the interesting signatures obtained in the gamma-ray and positron spectra.

## Chapter 10

# Conclusions and Outlook

The scenario of gravitino dark matter with broken  $R$ -parity is very appealing theoretically, as it naturally leads to a consistent thermal history of the Universe including both thermal leptogenesis and standard primordial nucleosynthesis. We have investigated the possible indirect signatures from the decay of gravitino dark matter, at first merely as a consistency check of the scenario. Interestingly, we have found that the decay of gravitino dark matter, or possibly some other kind of late-decaying dark matter, may naturally and simultaneously account for two anomalies in the cosmic-ray spectrum. One should keep in mind that the present scenario was not devised to explain the cosmic-ray anomalies, but to reconcile the clash between leptogenesis, nucleosynthesis and supersymmetry. However, we also found that the accompanying antiproton flux is dangerously large, potentially ruling out an interpretation of the gamma-ray and positron excesses in terms of decaying dark matter.

The resulting signatures for gamma rays, positrons and antiprotons are summarized in Fig. 10.1 for the MIN diffusion model. Nevertheless, significant systematic uncertainties in the astrophysics of cosmic-ray propagation remain. In view of the interesting signatures in gamma rays and positrons, it could be an interesting project to refine the analysis of the indirect signatures of gravitino dark matter decay in the framework of a more realistic, albeit purely numerical model, to settle the question of the phenomenological viability of the model regarding the antiproton flux.

On the experimental side, exciting new results can be expected in the near future. GLAST has successfully been launched into orbit and is commencing operation at the time of this writing. Furthermore, PAMELA is expected to release new, much improved data on the positron fraction and the antiproton flux in the near future. In addition, the AMS-02 experiment is ready for deployment on the International Space Station, but no flight schedule is fixed yet.

It is an exciting time for dark matter research. Over 75 years have passed since Fritz Zwicky first proposed the existence of dark matter based on observations of the dynamics of galaxy clusters. Many independent observations have confirmed the assumption over the years, but only at the present time, direct and indirect detection experiments are beginning to reach sensitivities that allow us to probe significant regions of the parameter space. Together with the impending commissioning of the LHC, which may enable us to produce dark matter in the laboratory and shed light on the existence of low-energy supersymmetry, we may, within

the next decade or so, actually be able to determine what the dark matter is and move to a quantitative determination of its properties.

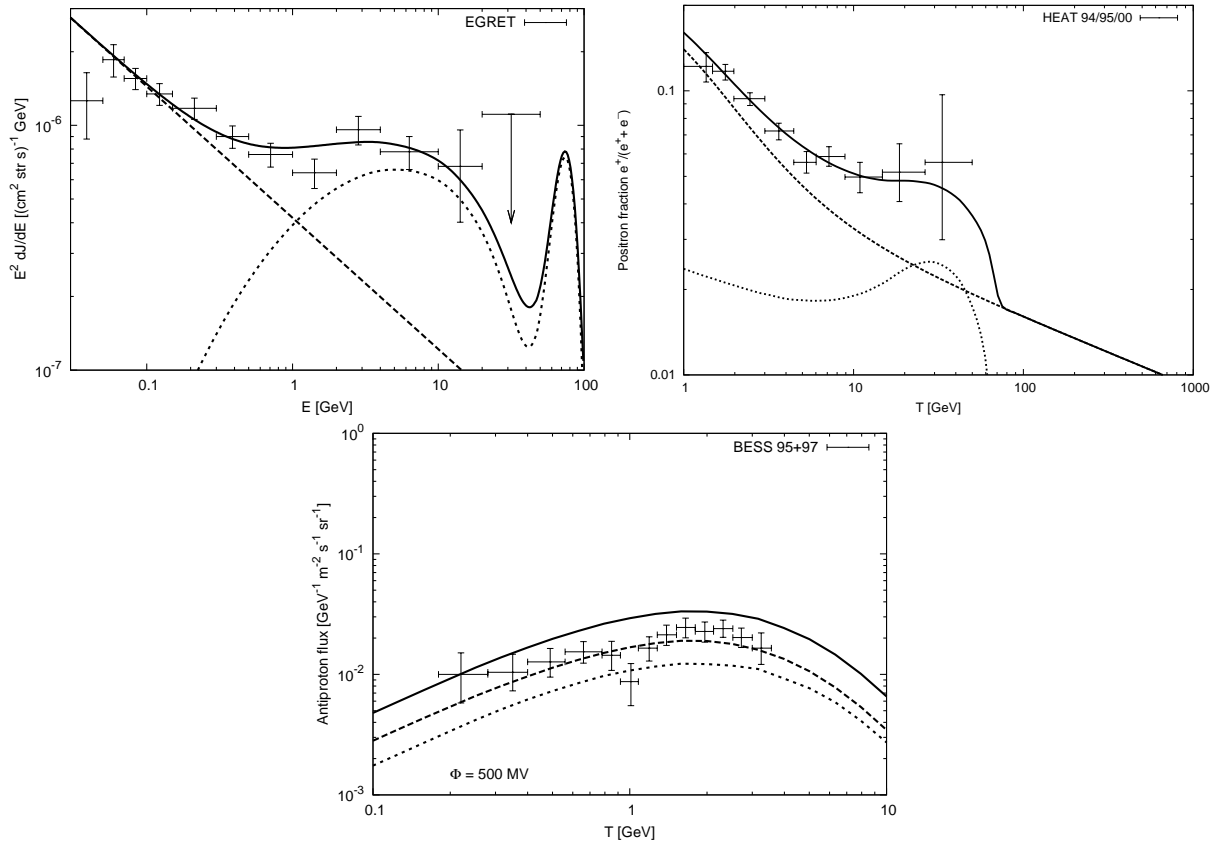


Figure 10.1: Summary of the indirect signatures of gravitino decay in the MIN propagation model for  $m_{3/2} = 150$  GeV,  $\tau_{3/2} = 1.3 \times 10^{26}$  s compared to the EGRET, HEAT and BESS data. The contribution from dark matter decay clearly improves the fit for gamma rays and positrons, but slightly overproduces antiprotons.

## Appendix A

# Calculation of Gravitino Decay Rates

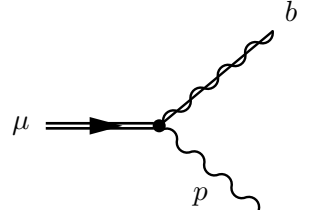
The gravitino decay rates can be calculated from the gravitino-gaugino-gauge boson interaction part of the supergravity Lagrangian,

$$\mathcal{L} = -\frac{i}{8M_{\text{P}}} \bar{\psi}_\mu [\gamma^\mu, \gamma^\rho] \gamma^\mu \lambda^a F_{\mu\rho}^a + \text{h.c.}, \quad (\text{A.1})$$

where the  $\gamma^\mu$  are the Dirac matrices, and  $F_{\mu\nu}^a$  is the field strength,

$$F_{\mu\nu}^a = \partial_\mu A_\nu^a - \partial_\nu A_\mu^a - gf^{abc} A_\mu^b A_\nu^c. \quad (\text{A.2})$$

The corresponding vertex factor is given by



$$= -\frac{i}{4M_{\text{P}}} \gamma^\mu [\not{p}, \gamma^\rho] \delta_{ab} \quad (\text{A.3})$$

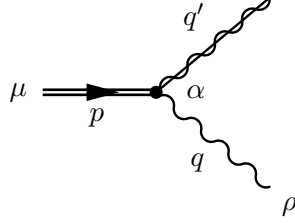
We will just illustrate the calculation for  $\psi_{3/2} \rightarrow \gamma\nu$  here, since the other results have exactly the same structure. To simplify the calculation, one can replace

$$-\frac{i}{4M_{\text{P}}} \gamma^\mu [\not{p}, \gamma^\rho] = \frac{i}{M_{\text{P}}} (\eta^{\alpha\mu} \gamma^\rho - \eta^{\mu\rho} \gamma^\alpha) p_\alpha \quad (\text{A.4})$$

For calculating spin-averaged squared matrix elements, we also need the spin sum rule for gravitino spinors. One finds that all terms allowed by Lorentz invariance figure in the polar-

ization tensor. For a gravitino with four-momentum  $p$ , we have [10]

$$\begin{aligned}\Pi_{\mu\nu}(p) &\equiv \sum_s \psi_\mu^s(p) \bar{\psi}_\nu^s(p) \\ &= -(\not{p} + m_{3/2}) \left[ \eta_{\mu\nu} - \frac{p_\mu p_\nu}{m_{3/2}^2} - \frac{1}{3} \left( \eta_{\mu\rho} - \frac{p_\mu p_\rho}{m_{3/2}^2} \right) \left( \eta_{\nu\sigma} - \frac{p_\nu p_\sigma}{m_{3/2}^2} \right) \gamma^\rho \gamma^\sigma \right].\end{aligned}\quad (\text{A.5})$$



Assigning indices and four-momenta as shown above, the matrix element for the decay  $\psi_{3/2} \rightarrow \gamma \tilde{\nu}$  is given by

$$i\mathcal{M} = \frac{i}{M_{\text{P}}} q_\alpha \epsilon_\rho^*(q) \bar{u}(q') (\eta^{\alpha\mu} \gamma^\rho - \eta^{\mu\rho} \gamma^\alpha) \bar{\psi}_\mu(p). \quad (\text{A.6})$$

We then get the corresponding squared matrix element for  $\psi_{3/2} \rightarrow \gamma \nu$  by averaging over the four incoming gravitino spin orientations and summing over outgoing lepton spins, as well as multiplying by the squared photino-neutrino mixing parameter  $|U_{\tilde{\gamma}\nu}|$ ,

$$\begin{aligned}\overline{\mathcal{M}^2} &= \frac{1}{4} \frac{|U_{\tilde{\gamma}\nu}|^2}{M_{\text{P}}^2} q_\alpha q_\beta \left( -\eta_{\rho\sigma} + \frac{q_\rho q_\sigma}{q^2} \right) \times \\ &\times \text{tr} \left[ \not{q}' (\eta^{\alpha\mu} \gamma^\rho - \eta^{\mu\rho} \gamma^\alpha) \Pi_{\mu\nu}(p) (\eta^{\beta\nu} \gamma^\sigma - \eta^{\nu\sigma} \gamma^\beta) \right].\end{aligned}\quad (\text{A.7})$$

The traces were evaluated using the Mathematica package FeynCalc [68]. The resulting expression in terms of four-vectors is

$$\overline{\mathcal{M}^2} = \frac{|U_{\tilde{\gamma}\nu}|^2}{3M_{\text{P}}^2 m_{3/2}^4} \left[ 4m_{3/2}^4 p \cdot q q \cdot q' + 2(m_{3/2}^2 + p^2)(p \cdot q)^2 p \cdot q' \right. \quad (\text{A.8})$$

$$\left. + (p^2 m_{3/2}^2 + (p^2)^2 - 4m_{3/2}^4) q^2 p \cdot q' \right]. \quad (\text{A.9})$$

The other calculations yield a result with the same structure. The decay rates for a two-body decay are finally related to  $\overline{\mathcal{M}^2}$  by

$$\Gamma = \frac{1}{(2\pi)^3} \frac{1}{8m_{3/2}} \overline{\mathcal{M}^2}. \quad (\text{A.10})$$

Evaluating the expressions for the squared matrix element in terms of center-of-mass frame

kinematics yields for the decay rates

$$\Gamma(\psi_{3/2} \rightarrow \gamma\nu) \simeq \frac{1}{32\pi} |U_{\tilde{\gamma}\nu}|^2 \frac{m_{3/2}^2}{M_{\text{P}}^2} \quad (\text{A.11})$$

$$\Gamma(\psi_{3/2} \rightarrow W^\pm l^\mp) \simeq \frac{1}{16\pi} |U_{\tilde{W}\tau}|^2 \frac{m_{3/2}^3}{M_{\text{P}}^2} f\left(\frac{M_W}{m_{3/2}}\right) \quad (\text{A.12})$$

$$\Gamma(\psi_{3/2} \rightarrow Z^0\nu) \simeq \frac{1}{32\pi} |U_{\tilde{Z}\nu}|^2 \frac{m_{3/2}^3}{M_{\text{P}}^2} f\left(\frac{M_Z}{m_{3/2}}\right), \quad (\text{A.13})$$

where the kinematical function  $f(x)$  is defined as

$$f(x) := 1 - \frac{4}{3}x^2 + \frac{1}{3}x^8. \quad (\text{A.14})$$

The factor 2 between the latter two decay rates stems from the two charge-conjugated final states for the  $W$  case. All lepton masses have been neglected in the result.

## Appendix B

# Derivation of the Gamma-Ray Flux Equations

In this appendix, we give a derivation of the equations used in the gamma-ray chapter for the fluxes from dark matter decays in our halo and from dark matter decay at cosmological distances. The propagation of gamma rays in the Milky Way is straightforward, while the extragalactic flux is slightly more complicated due to the signal getting redshifted by the expansion of the Universe.

### B.1 The Halo Contribution

We assume that the dark matter energy density in the Milky Way halo is given by a halo profile  $\rho_{\text{DM}}(\vec{r})$ . The number of photons created in a volume element at  $\vec{r}$  per unit volume and unit time in dark matter decays is then given by

$$dN_{\gamma}^{\text{em}}(\vec{r}) = \Gamma_{3/2} \frac{\rho_{\text{DM}}(\vec{r})}{m_{3/2}} dt d^3r dE. \quad (\text{B.1})$$

If  $\vec{r}$  is the relative position of the volume element from the observer, the observer receives

$$dN_{\gamma}^{\text{rec}} = \frac{1}{4\pi r^2} dN_{\gamma}^{\text{cr}} dS \quad (\text{B.2})$$

$$= \frac{1}{4\pi r^2} \frac{1}{\tau_{3/2} m_{3/2}} \rho_{\text{DM}}(\vec{r}) r^2 \sin\theta dr d\phi d\theta dt dS \quad (\text{B.3})$$

$$= \frac{1}{4\pi} \frac{1}{\tau_{3/2} m_{3/2}} \rho_{\text{DM}}(\vec{r}) dr d\Omega dt dS \quad (\text{B.4})$$

per unit surface  $dS$ . Defining the differential flux as the number of photons received per unit energy, time, solid angle and detector surface,

$$\frac{dJ}{dE} = \frac{d}{dE} \frac{dN_{\gamma}^{\text{rec}}}{dt d\Omega dS}, \quad (\text{B.5})$$

we get for the halo contribution

$$\left[ E^2 \frac{dJ}{dE} \right]_{\text{halo}}(b, l) = \frac{2E^2}{8\pi} \frac{1}{m_{3/2}\tau_{3/2}} \frac{dN_\gamma^{\text{cr}}}{dE} \int_0^\infty dr \rho_{\text{DM}}(r, b, l) \quad (\text{B.6})$$

$$= \frac{2E^2}{m_{3/2}} D_\gamma(b, l) \frac{dN_\gamma^{\text{cr}}}{dE}. \quad (\text{B.7})$$

We get the total flux in any one direction by integrating over the line of sight,

$$D_\gamma(b, l) = \frac{1}{8\pi\tau_{3/2}} \int_0^\infty dr \rho_{\text{DM}}(r, b, l), \quad (\text{B.8})$$

where  $b$  and  $l$  denote latitude and longitude in the Galactic coordinate system, respectively. We define the averaged constant  $\bar{D}_\gamma$  by integrating  $D_\gamma(b, l)$  over the whole sky, excluding the Galactic disk between  $-10^\circ$  and  $+10^\circ$  latitude

$$\bar{D}_\gamma = \frac{1}{8\pi\tau_{3/2}} \left[ \int_0^{2\pi} dl \int_{10\pi/180}^{\pi/2} db \cos b \int_0^\infty dr \rho_{\text{DM}}(r, l, b) \right] \times \left[ \int_0^{2\pi} dl \int_{10\pi/180}^{\pi/2} db \cos b \right]^{-1}, \quad (\text{B.9})$$

and thus the averaged halo contribution

$$\left[ E^2 \frac{dJ}{dE} \right]_{\text{halo}} = \frac{2E^2}{m_{3/2}} \bar{D}_\gamma \frac{dN_\gamma^{\text{cr}}}{dE}. \quad (\text{B.10})$$

## B.2 The Extragalactic Contribution

The number of photons emitted per gravitino decay in a comoving volume element per unit time  $t^{\text{em}}$  is

$$dN_\gamma^{\text{em}} = \Gamma_{3/2} \frac{\rho_{3/2}}{m_{3/2}} dt^{\text{em}} d^3\chi, \quad (\text{B.11})$$

where we assume that the total dark matter energy density in the Universe is approximately equal to the gravitino energy density,  $\rho_{\text{DM}} = \rho_{3/2}$ . Of these, a comoving observer at comoving distance  $\chi$  receives

$$dN_\gamma^{\text{rec}} = \frac{1}{4\pi\chi^2} dN_\gamma^{\text{em}} dS. \quad (\text{B.12})$$

The energy of an emitted photon gets redshifted as it propagates through the expanding Universe and is received with energy

$$E \equiv E^{\text{rec}} = a(t)E^{\text{em}} = \frac{1}{1+z} E^{\text{em}}. \quad (\text{B.13})$$

The flux is then

$$\left[ E^2 \frac{dJ}{dE} \right]_{\text{extra}} = \int_0^\infty d\chi \frac{\rho_{3/2}}{4\pi\tau_{3/2}m_{3/2}} \frac{dN_\gamma}{dE^{\text{em}}}. \quad (\text{B.14})$$

The comoving distance is an unobservable quantity, so we want to transform the integral into one over the redshift. For this, we need the relationship between comoving distance and

redshift. For light, the Robertson-Walker line element is simply

$$0 = ds^2 = -dt^2 + a(t)^2 d\chi^2, \quad (\text{B.15})$$

where we have set the radial coordinates to zero. We now use the relationship

$$\frac{dz}{dt} = -\frac{a_0}{a(t)^2} \dot{a}(t) = -\frac{a_0}{a(z)} H(z). \quad (\text{B.16})$$

Plugging this into the previous equation, we get the relation between comoving distance and redshift

$$d\chi = \frac{1}{a_0} \frac{1}{H(z)} dz. \quad (\text{B.17})$$

To find the dependence of the Hubble parameter on the redshift, we start from the Friedmann equation,

$$H^2 \equiv \left(\frac{\dot{a}}{a}\right)^2 = \frac{8\pi G}{3} \rho_{\text{tot}} - \frac{k}{a^2} + \frac{\Lambda}{3}. \quad (\text{B.18})$$

In a flat Universe, we set  $k = 0$ , and we can neglect the cosmological constant,  $\Lambda = 0$ . We receive gamma rays from low redshifts, where the energy density of the Universe is dominated by matter and dark energy,  $\rho_{\text{tot}} = \rho_M + \rho_\Lambda$ . We know that the energy density scales like

$$\rho = \rho_0 a^{-3(1+w)} = \rho_0 (1+z)^{3(1+w)}. \quad (\text{B.19})$$

For matter, the equation of state is  $p = 0$ , which yields  $w = 0$ , while for dark energy we assume the equation of state  $p = -\rho$ , corresponding to  $w = -1$ . In a matter- and dark energy-dominated Universe, we therefore get from the Friedmann equation Eq. (B.18)

$$H^2(z) = H_0^2 (\Omega_M (1+z)^3 + \Omega_\Lambda). \quad (\text{B.20})$$

Plugging this into the above equation, we get the relation

$$\frac{d\chi}{dz} = \frac{(1+z)^{-3/2}}{a_0 H_0 \sqrt{\Omega_M (1 + \Omega_\Lambda / \Omega_M (1+z)^{-3})}}. \quad (\text{B.21})$$

We can use this relation to convert the integration over comoving distance into an integration over redshift. With this, we finally get the wanted expression for the extragalactic component of the gamma-ray flux,

$$\left[ E^2 \frac{dJ}{dE} \right]_{\text{extra}} = \frac{2E^2}{m_{3/2}} C_\gamma \int_1^\infty d(1+z) \frac{dN_\gamma}{dE^{\text{em}}} [(1+z)E] (1+z)^{-3/2} \left( 1 + \frac{\Omega_\Lambda}{\Omega_M} (1+z)^{-3} \right)^{-1/2}, \quad (\text{B.22})$$

where we have introduced the abbreviation

$$C_\gamma = \frac{\Omega_{3/2} \rho_c}{8\pi \tau_{3/2} H_0 \Omega_M^{1/2}}. \quad (\text{B.23})$$

If the spectrum is monochromatic,  $dN/dE = \delta(E^{\text{em}} - m_{3/2}/2) = \delta((1+z)E - m_{3/2}/2)$ , the redshift integration can be carried out analytically. We first make use of the delta function

identity

$$\delta\left((1+z)E - \frac{m_{3/2}}{2}\right) = \frac{1}{E}\delta\left((1+z) - \frac{m_{3/2}}{2E}\right). \quad (\text{B.24})$$

Plugging this into the above equation for the extragalactic flux, we perform the integration using the delta function. Collecting factors of  $E$  and  $m_{3/2}$ , we get the expression for the extragalactic component in the case of a monochromatic injection spectrum,

$$\left[E^2 \frac{dJ}{dE}\right]_{\text{extra}} = C_\gamma \left(1 + \frac{\Omega_\Lambda}{\Omega_M} \left(\frac{2E}{m_{3/2}}\right)^3\right)^{-1/2} \left(\frac{2E}{m_{3/2}}\right)^{5/2} \theta\left(1 - \frac{2E}{m_{3/2}}\right). \quad (\text{B.25})$$

## Appendix C

# Solution of the Transport Equation

In this appendix, we explicitly solve the diffusion-loss equation from Chapter 7 for the case of positrons and antiprotons. The interstellar flux of charged particles is related to the number density  $f$  by

$$\Phi_X^{\text{IS}}(T) = \frac{v_X(T)}{4\pi} f_X(T). \quad (\text{C.1})$$

The full diffusion equation for the number density of charged particle species  $X$  under the steady-state condition is

$$0 = \frac{\partial}{\partial t} f_X(T, \vec{r}, t) = \nabla[K(T, \vec{r})\nabla f_X(T, \vec{r})] + \frac{\partial}{\partial T}[b(T, \vec{r})f_X(T, \vec{r})] - \nabla[\vec{V}_c(\vec{r})f_X(T, \vec{r})] - 2h\delta(z)\Gamma_{\bar{p}p}^{\text{ann}}(T)f_X(T, \vec{r}) + Q_X(T, \vec{r}). \quad (\text{C.2})$$

We may treat the propagation of positrons and antiprotons as different limits of this equation in which certain terms in the transport equation can be neglected.

### C.1 Solution for Positrons

In the case of positrons, annihilating scatterings in the Galactic disk as well as the effect of the convective wind can be neglected. We therefore have to solve the following limiting case of the diffusion equation:

$$0 = \nabla[K(T, \vec{r})\nabla f(T, \vec{r})] + \frac{\partial}{\partial T}[b(T, \vec{r})f(T, \vec{r})] + Q(T, \vec{r}). \quad (\text{C.3})$$

The diffusion coefficient has the form

$$K(T) = K_0\beta(T)\mathcal{R}^\delta, \quad (\text{C.4})$$

with  $\beta(T) = 1$  for positrons. The energy loss coefficient is given as

$$b(T) = \frac{T^2}{T_0\tau_E}, \quad (\text{C.5})$$

with  $T_0 = 1$  GeV. We expand the number density of positrons in terms of Bessel and sine functions,

$$f_{e^+}(T, r, z) = \sum_{m,n=1}^{\infty} A_{mn}(T) J_0\left(\zeta_n \frac{r}{R}\right) \sin\left(\frac{m\pi}{2L}(z-L)\right), \quad (\text{C.6})$$

where  $\zeta_n$  is the  $n$ th zero of the Bessel function of the first kind  $J_0$ . The boundary conditions are then automatically fulfilled. We also expand the source term in the same manner,

$$Q_{e^+}(T, r, z) = \sum_{m,n=1}^{\infty} Q_{mn}(T) J_0\left(\zeta_n \frac{r}{R}\right) \sin\left(\frac{m\pi}{2L}(z-L)\right). \quad (\text{C.7})$$

The Bessel functions obey the following orthogonality relation:

$$\int_0^R dr r J_0\left(\zeta_i \frac{r}{R}\right) J_0\left(\zeta_j \frac{r}{R}\right) = \frac{1}{2} J_1^2(\zeta_i) R^2 \delta_{ij} \quad (\text{C.8})$$

Using this property, we can invert Eq. (C.7) solve for the expansion coefficients  $Q_{mn}$ ,

$$Q_{mn}(T) = \frac{2}{J_1^2(\zeta_n) R^2 L} \int_0^R dr r \int_{-L}^L dz Q(T, r, z) J_0\left(\zeta_n \frac{r}{R}\right) \sin\left(\frac{m\pi}{2L}(z-L)\right) \quad (\text{C.9})$$

As dictated by the geometry of the problem, we work in cylindrical coordinates where we have  $\nabla^2 = \partial_r^2 + r^{-1}\partial_r + \partial_z^2$ . Plugging this and the explicit form of the diffusion and energy loss coefficients into the differential equation, we get

$$0 = \sum_{m,n=1}^{\infty} \left[ K(T) A_{mn}(T) \left( -\frac{\zeta_n^2}{R^2} - \frac{m^2 \pi^2}{4L^2} \right) + A_{mn}(T) \frac{2T}{T_0 \tau_E} + \frac{T^2}{T_0 \tau_E} \frac{d}{dT} A_{mn}(T) + Q_{mn}(T) \right] J_0\left(\zeta_n \frac{r}{R}\right) \sin\left(\frac{m\pi}{2L}(z-L)\right), \quad (\text{C.10})$$

where we have used the fact that the Bessel function satisfies the differential equation

$$\frac{d^2}{dr^2} J_0\left(\zeta_n \frac{r}{R}\right) + \frac{1}{r} \frac{d}{dr} J_0\left(\zeta_n \frac{r}{R}\right) + \frac{\zeta_n^2}{R^2} J_0\left(\zeta_n \frac{r}{R}\right) = 0. \quad (\text{C.11})$$

By comparing coefficients by order, we obtain the following first-order ordinary differential equation for the expansion coefficients  $A_{mn}$ :

$$\frac{d}{dT} T_0 A_{mn}(T) + \frac{2T_0}{T} A_{mn}(T) - \left( \frac{\zeta_n^2}{R^2} + \frac{m^2 \pi^2}{4L^2} \right) K_0 \tau_E \left( \frac{T}{T_0} \right)^{\delta-2} A_{mn}(T) + \frac{T_0^2 \tau_E}{T^2} Q_{mn}(T) = 0. \quad (\text{C.12})$$

We can solve this equation by introducing the following integrating factor:

$$\begin{aligned} F_{mn}(T) &= \int_0^T dT' \left[ \frac{2T_0}{T'} - \left( \frac{\zeta_n^2}{R^2} + \frac{m^2 \pi^2}{4L^2} \right) K_0 \tau_E \left( \frac{T'}{T_0} \right)^{\delta-2} \right] \\ &= -\ln\left(\frac{T}{T_0}\right)^2 - \left( \frac{\zeta_n^2}{R^2} + \frac{m^2 \pi^2}{4L^2} \right) \frac{K_0 \tau_E}{\delta-1} \left( \frac{T}{T_0} \right)^{\delta-1}. \end{aligned} \quad (\text{C.13})$$

The solution for  $A_{mn}(T)$  is then given by

$$\begin{aligned} A_{mn}(T) &= \exp[-F_{mn}(T)] \int_T^{T_{\max}} dT' \exp[F_{mn}(T')] \frac{\tau_E T_0}{T'^2} Q_{mn}(T') \\ &= \frac{\tau_E T_0}{T^2} \int_T^{T_{\max}} dT' Q_{mn}(T') \\ &\quad \times \exp \left\{ \left( \frac{\zeta_n^2}{R^2} + \frac{m^2 \pi^2}{4L^2} \right) \frac{K_0 \tau_E}{\delta - 1} \left[ \left( \frac{T}{T_0} \right)^{\delta-1} - \left( \frac{T'}{T_0} \right)^{\delta-1} \right] \right\}. \end{aligned} \quad (\text{C.14})$$

For convenience, we can define the coefficients

$$B_{mn}(T, T') = \frac{\tau_E T_0}{T^2} C_{mn} \exp \left\{ \left( \frac{\zeta_n^2}{R^2} + \frac{m^2 \pi^2}{4L^2} \right) \frac{K_0 \tau_E}{\delta - 1} \left[ \left( \frac{T}{T_0} \right)^{\delta-1} - \left( \frac{T'}{T_0} \right)^{\delta-1} \right] \right\}, \quad (\text{C.15})$$

with the geometry of the problem being encoded in the coefficients

$$C_{mn} = \frac{2}{J_1^2(\zeta_n) R^2 L} \int_0^R dr' r' \int_{-L}^L dz' \rho_{\text{DM}}(\vec{r}') J_0 \left( \zeta_n \frac{r'}{R} \right) \sin \left[ \frac{m\pi}{2L} (L - z') \right]. \quad (\text{C.16})$$

The solution for the Green function at the position of the solar system at  $r = r_\odot$ ,  $z = 0$  is then written as

$$G_{e^+}(T, T') = \sum_{m,n=1}^{\infty} B_{mn}(T, T') J_0 \left( \zeta_n \frac{r_\odot}{R} \right) \sin \left( \frac{m\pi}{2} \right). \quad (\text{C.17})$$

The coefficients can now be computed numerically to obtain the results of Chapter 8.

## C.2 Solution for Antiprotons

In the case of antiprotons, energy losses can be neglected due to the high antiproton mass. All other terms have to be taken into account, however. We therefore have to solve the equation

$$0 = \nabla[K(T, \vec{r}) \nabla f(T, \vec{r})] - \nabla[\vec{V}_c(\vec{r}) f(T, \vec{r})] - 2h\delta(z) \Gamma_{\bar{p}p}^{\text{ann}}(T) f(T, \vec{r}) + Q(T, \vec{r}), \quad (\text{C.18})$$

which is considerably more complicated than in the case of positrons. The Galactic wind is directed away from the disk and given by

$$\vec{V}_c(z) = (2\theta(z) - 1) V_C \vec{e}_z, \quad \vec{V}_c(z) \vec{e}_z \equiv V_c(z). \quad (\text{C.19})$$

Working in cylindrical coordinates again, we expand the antiproton number density as

$$f_{\bar{p}}(T, r, z) = \sum_{i=1}^{\infty} f_i(T, z) J_0 \left( \zeta_i \frac{r}{R} \right). \quad (\text{C.20})$$

The source term is expanded in the same way,

$$Q_{\bar{p}}(T, r, z) = \sum_{i=1}^{\infty} Q_i(T, z) J_0 \left( \zeta_i \frac{r}{R} \right), \quad (\text{C.21})$$

which automatically satisfies the boundary condition for  $r = R$ . Using the Bessel orthogonality relation, Eq. (C.8), we can invert this to get

$$Q_i(T, z) = \frac{2}{J_1^2(\zeta_i)R^2} \int_0^R dr r Q(T, r, z) J_0\left(\zeta_i \frac{r}{R}\right). \quad (\text{C.22})$$

Plugging these expansions into the diffusion equation and using again the differential Bessel function identity (C.11), one obtains

$$\begin{aligned} 0 = & \sum_{i=1}^{\infty} \left\{ K(T) J_0\left(\zeta_i \frac{r}{R}\right) \partial_z^2 f_i(T, z) - K(T) J_0\left(\zeta_i \frac{r}{R}\right) \frac{\zeta_i^2}{R^2} f_i(T, z) \right. \\ & - V_c(z) J_0\left(\zeta_i \frac{r}{R}\right) \partial_z f_i(T, z) - 2\delta(z) V_C f_i(T, z) \\ & \left. - 2h\delta(z) \Gamma_{\bar{p}p}^{\text{ann}}(T) J_0\left(\zeta_i \frac{r}{R}\right) f_i(T, z) + J_0\left(\zeta_i \frac{r}{R}\right) Q_i(T, z) \right\}. \end{aligned} \quad (\text{C.23})$$

Comparing the terms by order, the differential equation to be solved is

$$\begin{aligned} Q_i(T, z) = & (2h\Gamma_{\bar{p}p}^{\text{ann}}(T) + 2V_C)\delta(z) f_i(T, z) + V_c(z) \partial_z f_i(T, z) \\ & - K(T) \left( \partial_z^2 f_i(T, z) - \frac{\zeta_i^2}{R^2} f_i(T, z) \right). \end{aligned} \quad (\text{C.24})$$

We transform this into an algebraic equation by performing a Laplace transformation. The equation transforms as follows:

$$\begin{aligned} \int_0^{\infty} dz e^{-sz} Q_i(T, z) = & (h\Gamma_{\bar{p}p}^{\text{ann}}(T) + K(T)s) f_i(T, 0) \\ & + \hat{f}_i(T, s) \left[ -K(T)s^2 + V_C s + K(T) \frac{\zeta_i^2}{R^2} \right], \end{aligned} \quad (\text{C.25})$$

with  $\hat{f}_i(T, s)$  being the Laplace transform of the number density  $f_i(T, z)$ ,

$$\begin{aligned} \hat{f}_i(T, s) = & \int_0^{\infty} dz e^{-sz} f_i(T, z) \\ = & \left[ (h\Gamma_{\bar{p}p}^{\text{ann}}(T) + K(T)s) f_i(T, 0) - \int_0^{\infty} dz e^{-sz} Q_i(T, z) \right] \\ & \times \frac{1}{K(T)} \left[ s^2 - \frac{V_C}{K(T)} s - \frac{\zeta_i^2}{R^2} \right]^{-1}. \end{aligned} \quad (\text{C.26})$$

We now want to transform back to position space by applying the inverse Laplace transformation,

$$f_i(T, z) = \frac{1}{2\pi i} \int_{\gamma-i\infty}^{\gamma+i\infty} ds f_i(T, s) e^{sz}. \quad (\text{C.27})$$

The integral can be solved using the residue theorem. The integrand has simple poles at

$$s = \frac{V_C}{2K(T)} \pm \frac{S_i(T)}{2}, \quad (\text{C.28})$$

where we have defined

$$S_i(T) = \sqrt{\frac{V_C^2}{K(T)^2} + 4\frac{\zeta_i^2}{R^2}}. \quad (\text{C.29})$$

The inverse transformation then yields for the number density

$$\begin{aligned} f_i(T, z) = & \frac{1}{K(T)S_i(T)} \exp\left(\frac{V_C z}{2K(T)}\right) \\ & \times \left\{ \left( h\Gamma_{\bar{p}\bar{p}}^{\text{ann}}(T) + K(T) \left( \frac{V_C}{2K(T)} + \frac{S_i(T)}{2} \right) \right) f_i(T, 0) \right. \\ & - \int_0^\infty dz' Q_i(T, z') \exp\left(-\left(\frac{V_C}{2K(T)} + \frac{S_i(T)}{2}\right)z'\right) \exp\left(\frac{S_i(T)z}{2}\right) \\ & - \left( h\Gamma_{\bar{p}\bar{p}}^{\text{ann}}(T) + K(T) \left( \frac{V_C}{2K(T)} - \frac{S_i(T)}{2} \right) \right) f_i(T, 0) \\ & \left. + \int_0^\infty dz' Q_i(T, z') \exp\left(-\left(\frac{V_C}{2K(T)} - \frac{S_i(T)}{2}\right)z'\right) \exp\left(-\frac{S_i(T)z}{2}\right) \right\} \end{aligned} \quad (\text{C.30})$$

After some algebra, we arrive at the angular dependence of the number density,

$$\begin{aligned} f_i(T, z) = & \frac{1}{K(T)S_i(T)} \exp\left(\frac{V_C z}{2K(T)}\right) \sinh\left(\frac{S_i(T)z}{2}\right) \\ & \times \left\{ 2h\Gamma_{\bar{p}\bar{p}}^{\text{ann}}(T) + V_C + K(T)S_i(T) \coth\left(\frac{S_i(T)z}{2}\right) \right\} f_i(T, 0) \\ & - \frac{2}{KS_i(T)} \int_0^\infty dz' Q_i(T, z') \exp\left(\frac{V_C}{2K}(z - z')\right) \sinh\left(\frac{S_i(T)}{2}(z - z')\right) \end{aligned} \quad (\text{C.31})$$

We observe the antiproton flux in the Galactic disk at  $z = 0$ . This is thus a good time to make use of the boundary condition  $f_i(T, L) = 0$ , which allows us to solve for  $f_i(T, 0)$  in the above equation,

$$\begin{aligned} f_i(T, 0) = & \left[ 2 \int_0^\infty dz' Q_i(T, z') \exp\left(\frac{V_C}{2K}(L - z')\right) \sinh\left(\frac{S_i(T)}{2}(L - z')\right) \right] \\ & \times \left[ \exp\left(\frac{V_C L}{2K(T)}\right) A_i(T) \sinh\left(\frac{S_i(T)L}{2}\right) \right]^{-1} \end{aligned} \quad (\text{C.32})$$

, where we have defined

$$A_i(T) = 2h\Gamma_{\bar{p}\bar{p}}^{\text{ann}}(T) + V_C + K(T)S_i(T) \coth\left(\frac{S_i(T)L}{2}\right). \quad (\text{C.33})$$

The final result for the number density is now

$$f_i(T, z = 0) = \exp\left(-\frac{V_C L}{2K(T)}\right) \frac{y_i(T, L)}{A_i(T) \sinh(S_i(T)L/2)}. \quad (\text{C.34})$$

where  $y_i$  is defined as

$$y_i(T, z) = 2 \int_0^z dz' \exp\left(\frac{V_C}{2K(T)}(z - z')\right) \sinh\left(\frac{S_i(T)}{2}(z - z')\right) Q_i(T, z'). \quad (\text{C.35})$$

and the integration in  $y_i$  is only performed to  $L$  due to the boundary conditions. The Green function for our position in the Galaxy at  $r = r_\odot$ ,  $z = 0$  is then

$$G_{\vec{p}}(T, T') = \sum_{i=1}^{\infty} \exp\left(-\frac{V_C L}{2K(T)}\right) \frac{y_i(T)}{A_i(T) \sinh(S_i(T)L/2)} J_0\left(\zeta_i \frac{r_\odot}{R}\right) \delta(T - T'). \quad (\text{C.36})$$

We can now solve for the expansion coefficients numerically.

# Acknowledgements

First and foremost, I would like to thank my parents for their enduring support over the past quarter century, material, moral and otherwise, without which my studies would not have been possible, and for which I am deeply grateful.

I also thank my many colleagues from DESY and the University of Hamburg for a very enjoyable year, a nice personal atmosphere and stimulating conversations. In particular, I thank Laura Covi and Michael Greife for a very pleasant collaboration and interesting discussions.

Furthermore, I am grateful to Prof. Dr. Joachim Bartels for agreeing to co-supervise this thesis, thereby making it possible for me to work in the DESY theory group in the first place.

Many thanks also to Leigh Cressman for proofreading the English and for understanding that I devoted so much time to physics lately.

Finally, it is a pleasure to thank Alejandro Ibarra for taking a chance on me and accepting me as his student, for proposing this fascinating subject and for doing an outstanding job advising me during the past year.

# Bibliography

- [1] Gerard Jungman, Marc Kamionkowski, and Kim Griest. Supersymmetric dark matter. *Phys. Rept.*, 267:195–373, 1996.
- [2] Gianfranco Bertone, Dan Hooper, and Joseph Silk. Particle dark matter: Evidence, candidates and constraints. *Phys. Rept.*, 405:279–390, 2005.
- [3] Wilfried Buchmuller, Laura Covi, Koichi Hamaguchi, Alejandro Ibarra, and Tsutomu Yanagida. Gravitino dark matter in R-parity breaking vacua. *JHEP*, 03:037, 2007.
- [4] Heinz Pagels and Joel R. Primack. Supersymmetry, Cosmology and New TeV Physics. *Phys. Rev. Lett.*, 48:223, 1982.
- [5] Alejandro Ibarra and David Tran. Gamma-Ray Spectrum from Gravitino Dark Matter Decay. *Phys. Rev. Lett.*, 100:061301, 2008.
- [6] Alejandro Ibarra and David Tran. Antimatter Signatures of Gravitino Dark Matter Decay. *JCAP accepted*, 2008.
- [7] Manuel Drees. An introduction to supersymmetry. 1996.
- [8] E. Cremmer, S. Ferrara, L. Girardello, and Antoine Van Proeyen. Yang-Mills Theories with Local Supersymmetry: Lagrangian, Transformation Laws and SuperHiggs Effect. *Nucl. Phys.*, B212:413, 1983.
- [9] D. G. Cerdeno and C. Munoz. An introduction to supergravity. Prepared for 6th Hellenic School and Workshop on Elementary Particle Physics:, Corfu, Greece, 6-26 Sep 1998.
- [10] M. Bolz, A. Brandenburg, and W. Buchmuller. Thermal production of gravitinos. *Nucl. Phys.*, B606:518–544, 2001.
- [11] A. D. Sakharov. Violation of CP Invariance, c Asymmetry, and Baryon Asymmetry of the Universe. *Pisma Zh. Eksp. Teor. Fiz.*, 5:32–35, 1967.
- [12] M. Fukugita and T. Yanagida. Baryogenesis Without Grand Unification. *Phys. Lett.*, B174:45, 1986.
- [13] W. Buchmuller, R. D. Peccei, and T. Yanagida. Leptogenesis as the origin of matter. *Ann. Rev. Nucl. Part. Sci.*, 55:311–355, 2005.
- [14] W. Buchmuller, P. Di Bari, and M. Plumacher. Leptogenesis for pedestrians. *Ann. Phys.*, 315:305–351, 2005.

- [15] Sacha Davidson and Alejandro Ibarra. A lower bound on the right-handed neutrino mass from leptogenesis. *Phys. Lett.*, B535:25–32, 2002.
- [16] Josef Pradler and Frank Daniel Steffen. Thermal gravitino production and collider tests of leptogenesis. *Phys. Rev.*, D75:023509, 2007.
- [17] Vyacheslav S. Rychkov and Alessandro Strumia. Thermal production of gravitinos. *Phys. Rev.*, D75:075011, 2007.
- [18] D. N. Spergel et al. Wilkinson Microwave Anisotropy Probe (WMAP) three year results: Implications for cosmology. *Astrophys. J. Suppl.*, 170:377, 2007.
- [19] Masahiro Kawasaki, Kazunori Kohri, and Takeo Moroi. Big-bang nucleosynthesis and hadronic decay of long-lived massive particles. *Phys. Rev.*, D71:083502, 2005.
- [20] Maxim Pospelov. Particle physics catalysis of thermal big bang nucleosynthesis. *Phys. Rev. Lett.*, 98:231301, 2007.
- [21] K. Hamaguchi, T. Hatsuda, M. Kamimura, Y. Kino, and T. T. Yanagida. Stau-catalyzed Li-6 production in big-bang nucleosynthesis. *Phys. Lett.*, B650:268–274, 2007.
- [22] Josef Pradler and Frank Daniel Steffen. Constraints on the reheating temperature in gravitino dark matter scenarios. *Phys. Lett.*, B648:224–235, 2007.
- [23] Toru Kanzaki, Masahiro Kawasaki, Kazunori Kohri, and Takeo Moroi. Cosmological constraints on gravitino LSP scenario with sneutrino NLSP. *Phys. Rev.*, D75:025011, 2007.
- [24] J. L. Diaz-Cruz, John R. Ellis, Keith A. Olive, and Yudi Santoso. On the feasibility of a stop NLSP in gravitino dark matter scenarios. *JHEP*, 05:003, 2007.
- [25] Karsten Jedamzik. The cosmic  $6\text{Li}$  and  $7\text{Li}$  problems and BBN with long-lived charged massive particles. *Phys. Rev.*, D77:063524, 2008.
- [26] B. C. Allanach, A. Dedes, and Herbert K. Dreiner. Bounds on R-parity violating couplings at the weak scale and at the GUT scale. *Phys. Rev.*, D60:075014, 1999.
- [27] Bruce A. Campbell, Sacha Davidson, John R. Ellis, and Keith A. Olive. On the baryon, lepton flavor and right-handed electron asymmetries of the universe. *Phys. Lett.*, B297:118–124, 1992.
- [28] W. Fischler, G. F. Giudice, R. G. Leigh, and S. Paban. Constraints on the baryogenesis scale from neutrino masses. *Phys. Lett.*, B258:45–48, 1991.
- [29] Herbert K. Dreiner and Graham G. Ross. Sphaleron erasure of primordial baryogenesis. *Nucl. Phys.*, B410:188–216, 1993.
- [30] G. F. Giudice, A. Notari, M. Raidal, A. Riotto, and A. Strumia. Towards a complete theory of thermal leptogenesis in the SM and MSSM. *Nucl. Phys.*, B685:89–149, 2004.
- [31] Fumihiro Takayama and Masahiro Yamaguchi. Gravitino dark matter without R-parity. *Phys. Lett.*, B485:388–392, 2000.

- [32] Gianfranco Bertone, Wilfried Buchmuller, Laura Covi, and Alejandro Ibarra. Gamma-Rays from Decaying Dark Matter. *JCAP*, 0711:003, 2007.
- [33] S. Lola, P. Osland, and A. R. Raklev. Radiative gravitino decays from R-parity violation. *Phys. Lett.*, B656:83–90, 2007.
- [34] W. Buchmuller and T. Yanagida. Quark lepton mass hierarchies and the baryon asymmetry. *Phys. Lett.*, B445:399–402, 1999.
- [35] Lars Bergstrom, Piero Ullio, and James H. Buckley. Observability of gamma rays from dark matter neutralino annihilations in the Milky Way halo. *Astropart. Phys.*, 9:137–162, 1998.
- [36] Julio F. Navarro, Carlos S. Frenk, and Simon D. M. White. The structure of cold dark matter halos. *Astrophys. J.*, 462:563–575, 1996.
- [37] Ben Moore, Tom Quinn, Fabio Governato, Joachim Stadel, and George Lake. Cold collapse and the core catastrophe. *Mon. Not. Roy. Astron. Soc.*, 310:1147–1152, 1999.
- [38] Torbjorn Sjostrand, Stephen Mrenna, and Peter Skands. PYTHIA 6.4 physics and manual. *JHEP*, 05:026, 2006.
- [39] P. Sreekumar et al. EGRET observations of the extragalactic gamma ray emission. *Astrophys. J.*, 494:523–534, 1998.
- [40] A. W. Strong, I. V. Moskalenko, and O. Reimer. A new determination of the extragalactic diffuse gamma-ray background from EGRET data. *Astrophys. J.*, 613:956–961, 2004.
- [41] Dominik Elsaesser and Karl Mannheim. Supersymmetric dark matter and the extragalactic gamma ray background. *Phys. Rev. Lett.*, 94:171302, 2005.
- [42] F. W. Stecker, S. D. Hunter, and D. A. Kniffen. The Likely Cause of the EGRET GeV Anomaly and its Implications. *Astropart. Phys.*, 29:25–29, 2008.
- [43] S. Rudaz and F. W. Stecker. ON THE OBSERVABILITY OF THE gamma-ray LINE FLUX FROM DARK MATTER ANNIHILATION. *Astrophys. J.*, 368:406, 1991.
- [44] Michael Gustafsson, Erik Lundstrom, Lars Bergstrom, and Joakim Edsjo. Significant gamma lines from inert Higgs dark matter. *Phys. Rev. Lett.*, 99:041301, 2007.
- [45] Junji Hisano, Shigeki Matsumoto, Osamu Saito, and Masato Senami. Heavy Wino-like neutralino dark matter annihilation into antiparticles. *Phys. Rev.*, D73:055004, 2006.
- [46] D. Maurin, F. Donato, R. Taillet, and P. Salati. Cosmic Rays below  $Z=30$  in a diffusion model: new constraints on propagation parameters. *Astrophys. J.*, 555:585–596, 2001.
- [47] T. Delahaye, R. Lineros, F. Donato, N. Fornengo, and P. Salati. Positrons from dark matter annihilation in the galactic halo: theoretical uncertainties. *Phys. Rev.*, D77:063527, 2008.
- [48] L. J. Gleeson and W. I. Axford. Cosmic Rays in the Interplanetary Medium. *Astrophys. J. Lett.*, 149:L115+, September 1967.

- [49] L. J. Gleeson and W. I. Axford. Solar Modulation of Galactic Cosmic Rays. *Astrophys. J.*, 154:1011–+, December 1968.
- [50] J. S. Perko. Solar modulation of galactic antiprotons. *Astron. Astrophys.*, 184:119–121, October 1987.
- [51] S. W. Barwick et al. Measurements of the cosmic-ray positron fraction from 1- GeV to 50-GeV. *Astrophys. J.*, 482:L191–L194, 1997.
- [52] M. Boezio et al. The Cosmic-Ray Electron and Positron Spectra Measured at 1 AU during Solar Minimum Activity. *Astrophys. J.*, 532:653–669, 2000.
- [53] C. Grimani et al. Measurements of the absolute energy spectra of cosmic-ray positrons and electrons above 7-GeV. *Astron. Astrophys.*, 392:287–294, 2002.
- [54] M. Aguilar et al. Cosmic-ray positron fraction measurement from 1-GeV to 30- GeV with AMS-01. *Phys. Lett.*, B646:145–154, 2007.
- [55] Edward A. Baltz and Joakim Edsjo. Positron propagation and fluxes from neutralino annihilation in the halo. *Phys. Rev.*, D59:023511, 1999.
- [56] I. V. Moskalenko and A. W. Strong. Production and propagation of cosmic-ray positrons and electrons. *Astrophys. J.*, 493:694–707, 1998.
- [57] Edward A. Baltz, Joakim Edsjo, Katherine Freese, and Paolo Gondolo. The cosmic ray positron excess and neutralino dark matter. *Phys. Rev.*, D65:063511, 2002.
- [58] P. Picozza et al. PAMELA: A payload for antimatter matter exploration and light-nuclei astrophysics. *Astropart. Phys.*, 27:296–315, 2007.
- [59] F. Barao. AMS: Alpha Magnetic Spectrometer on the International Space Station. *Nucl. Instrum. Meth.*, A535:134–138, 2004.
- [60] S. Orito et al. Precision measurement of cosmic-ray antiproton spectrum. *Phys. Rev. Lett.*, 84:1078–1081, 2000.
- [61] H. Matsunaga et al. Measurement of low-energy cosmic-ray antiprotons at solar minimum. *Phys. Rev. Lett.*, 81:4052–4055, 1998.
- [62] J. W. Mitchell et al. Measurement of 0.25-GeV to 3.2-GeV anti-protons in the cosmic radiation. *Phys. Rev. Lett.*, 76:3057–3060, 1996.
- [63] M. Boezio et al. The cosmic-ray antiproton flux between 0.62-GeV and 3.19- GeV measured near solar minimum activity. *Astrophys. J.*, 487:415–423, 1997.
- [64] M. Boezio et al. The cosmic-ray anti-proton flux between 3-GeV and 49- GeV. *Astrophys. J.*, 561:787–799, 2001.
- [65] L. C. Tan and L. K. Ng. CALCULATION OF THE EQUILIBRIUM ANTI-PROTON SPECTRUM. *J. Phys.*, G9:227–242, 1983.
- [66] F. Donato et al. Anti-protons from spallations of cosmic rays on interstellar matter. *Astrophys. J.*, 563:172–184, 2001.

- [67] Igor V. Moskalenko, Andrew W. Strong, Jonathan F. Ormes, and Marius S. Potgieter. Secondary antiprotons and propagation of cosmic rays in the galaxy and heliosphere. *Astrophys. J.*, 565:280–296, 2002.
- [68] R. Mertig, M. Bohm, and Ansgar Denner. FEYN CALC: Computer algebraic calculation of Feynman amplitudes. *Comput. Phys. Commun.*, 64:345–359, 1991.

# Erklärung

Ich versichere, daß ich diese Arbeit selbständig verfaßt und keine anderen als die angegebenen Hilfsmittel und Quellen benutzt habe. Außerdem bin ich mit einer Ausleihe bzw. Veröffentlichung einverstanden.

Hamburg, 15.06.08,